ABSTRACT

KANG, TAE-HO. Textile-Embedded Sensors for Wearable Physiological Monitoring Systems. (Under the direction of Dr. H. Troy Nagle.)

For long-term physiological monitoring inside or outside a hospital setting, a reliable, wearable monitoring system would be a convenient platform if biomedical sensors are securely placed in appropriate positions. An article of clothing is an attractive platform to implement such a wearable system. It is highly desirable that the sensors be designed and integrated into the garment in an unobtrusive way.

The purpose of the dissertation is to develop textile-embedded biomedical sensors that can be integrated into textile substrates in a seamless manner for long-term ECG and respiration monitoring while normal daily activities including walking, jogging, sleeping, sitting, and other exercise are transpiring. These sensors should provide both a comfortable textile interface and robustness against noise and motion artifacts.

For ECG monitoring, we developed textile-embedded active electrodes that transform high input impedance signals to low impedance versions by employing a voltage follower circuit. The fabric active electrodes include a transducer layer on the top of the nonwoven substrates and a circuit layer on the bottom. The transducer area, signal path and power lines are filled with Ag/AgCl ink by screen printing or hand painting. The electrical components and external wires were attached using adhesive conductive inks and protected by another textile covering layer.

For respiration monitoring, we devised a fabric sensor structure based on double nonwoven substrates. Stretchable and non-stretchable segments of nonwoven fabrics are laterally attached by, for example,

ultra sonic bonding. The stretchable fabrics are employed in belts around the chest and abdomen and respond to breathing effort by changing the sensor's length in the direction of the strain applied. Rectangular plates for a capacitive sensor or an open-rectangular spiral for an inductive sensor is deposited on the non-stretchable fabric portions of the sensors by printing or painting silver ink. Their relative positions change when the stretchable portion activates. Each plate is initially placed so that the conducting areas overlap minimally. As the stretchable portions of the device are exercised, the two plates slide in opposite directions, changing the effective area and hence the capacitance or inductance values. These capacitance or inductance variations are transformed into voltage outputs by electronic circuits individually designed for each sensor. For single and differential modes of operation in the capacitive sensor, various electrode patterns are suggested. For the inductive sensor, various configurations of spirals are presented to form three different types of planar inductive displacement sensors: a single inductor sensor, a transformer-type differential sensor, and an autotransformer-type differential sensor.

In addition to the design based on double substrates, we demonstrate a respiratory inductive sensor based on a single substrate. To form an inductive sensing area, fine magnet wires are stitched on a stretchable nonwoven substrate. The textile substrates supporting the conducting materials are then laminated to stabilize the geometric structure relationships and mechanically protect the sensor.

Finally, we transform these textile-embedded sensors into a wearable human physiology monitoring system. The various elements of the system are described. Finally, we discuss the possibility of using the system for sleep apnea detection and sleep staging.

TEXTILE-EMBEDDED SENSORS FOR WEARABLE PHYSIOLOGICAL MONITORING SYSTEMS

by
TAE-HO KANG

A dissertation submitted to the Graduate Faculty of
North Carolina State University
in partial fulfillment of the
requirements for the Degree of
Doctor of Philosophy

ELECTRICAL ENGINEERING

Raleigh, NC

2006

APPROVED BY:

H. Troy Nagle, PhD, MD
Chair of Advisory Committee

Wesley E. Snyder, PhD

Edward Grant, PhD

Behnam Pourdeyhimi, PhD

Bradley Vaughn, MD

BIOGRAPHY

Tae-Ho Kang was born in 1965 in rural Korea and moved with his family to Taejon in 1976. He earned a Bachelor of Engineering degree in 1987 and a Master of Engineering degree in 1991 from Chungnam National University in Taejon, Republic of Korea. In December 1990, he joined the Systems Engineering Research Institute (SERI) of the Korea Institute of Science and Technology (KIST) as a researcher. There he was promoted to senior researcher in March, 1996. His research during this time focused upon many government and company-funded projects that aimed to develop software for geographic information systems (GIS), intelligent transport systems (ITS), and image processing. Those systems included a car navigation system (CNS), a positioning system for moving vehicles, an integrated helicopter aviation system, an automated visual inspection system, an optimal traveling path extraction system, and a real-time traffic information processing system.

He came to the United States on January 1, 2001, to pursue the Ph.D. degree in the Department of Electrical and Computer Engineering at NC State University. At NC State, he has studied wearable monitoring systems, focusing on biomedical sensor design and fabrication for ECG and respiration monitoring.

His background includes other scholarly pursuits. In 1995, he was a visiting scholar at Cornell University for two months researching GIS. For several years prior to 2001, he taught artificial intelligence at the Hanbat National University, Taejon, Republic of Korea. In the summer of 2001, he joined Samsung Electronics as an intern to develop Windows CE based GIS application software for Samsung's Web Pad.

He also served in the Korean military and was discharged from military service as a communication specialist in January 1989. He is married to Hyun-A Cho and has one son, Bumsik, and one daughter, Jiyeon.

ACKNOWLEDGEMENTS

Sincerest and deepest thanks are extended to my advisor, Dr. H. Troy Nagle, who for five years has supported, advised, mentored and inspired me to achieve success in various research opportunities. He introduced me to a new multidisciplinary research field: electronics-textiles used for the purpose of developing a new category of biomedical sensors. Without his endurance, support and patient instruction I would not have arrived at this moment.

I also offer special thanks to all my committee members. Dr. Grant and Dr. Pourdeyhimi have encouraged and mentored me to investigate electronics-textiles. Both gave me valuable ideas for textile-embedded sensors. Dr. Vaughn inspired me to investigate challenging questions in sleep monitoring systems from both medical and engineering viewpoints. Dr. Snyder did not hesitate to share his time to discuss medical issues, especially heart related problems. Their advice has been and will continue to be invaluable in my professional career.

I would also like to express my thanks to Carey R. Merritt and Burcak Karaguzel. Carey and I have spent much time together designing, fabricating, and testing fabric biomedical sensors. His proactive and positive attitude helped me to overcome difficulties in my research. Likewise, working with Burcak helped me acquire experience in the various principles and disciplines of Textile Engineering.

I also would like to express my appreciation to Steve and his family for their concern and prayers. Special thanks are given to CRIM members including Joe Giallo who showed me kindness in various ways and Korean friends who have studied with me here at N.C. State.

I offer my most profound thanks to my family, in particular my beloved wife Hyun-A, my son Bumsik, and my daughter Jiyeon, who have endured, sacrificed, and encouraged me during my studies. Without their love and support my achievement would mean nothing. Finally I thank my parents for their unwavering love and support.

TABLE OF CONTENTS

Pages

LIST OF TABLES

Pages

Chapter 5. PLANAR INDUCTIVE DISPLACEMENT SENSORS BASED ON SPIRALS AND DOUBLE-SUBSTRATE DESIGNS

LIST OF FIGURES

Pages

Chapter 2. NONWOVEN FABRIC ACTIVE ELECTRODES FOR BIOPOTENTIAL MEASUREMENT DURING NORMAL DAILY ACTIVITY

Chapter 3. CAPACITIVE NONWOVEN FABRIC SENSORS FOR RESPIRATION MONITORING

Chapter 4. A RESPIRATORY INDUCTIVE SENSOR BASED ON A SINGLE STRETCHABLE TEXTILE SUBSTRATE

Chapter 5. PLANAR INDUCTIVE DISPLACEMENT SENSORS BASED ON SPIRALS AND DOUBLE-SUBSTRATE DESIGNS

Chapter 6. A WEARABLE PHYSIOLOGICAL MONITORING SYSTEM BASED ON TEXTILE-EMBEDDED SENSORS AND ITS APPLICATION IN SLEEP MONITORING

Chapter 1

INTRODUCTION

I. OVERVIEW

A health monitoring system has been developed to monitor a wearer anywhere and anytime for health care, disease diagnosis, security, home rehabilitation, and surveillance. Surveillance includes civilian and military applications such as teams of soldiers, emergency rescue units, and law enforcement. Biomedical sensors serve as front-end elements of this wearable health monitoring system, and as such are directly, indirectly or invasively placed into contact with the human body to measure its physiological status, or to provide additional information like geo-location through the use of a GPS system. However, the sensors used in the past have typically been bulky and wired to devices worn on the subject's body. In most cases, bulky biomedical sensors, including respiratory sensors, have been most conveniently attached to the subject's garment. This has most commonly been accomplished by stitching the devices into the wearable health monitoring systems (e.g. LifeShirt® [1], SmartShirt® [2, 3]). This method provides good maintainability since inoperative sensors are easily replaced.

However since the biomedical sensors in [1-3] are not truly integrated into the garment, they often create discomfort for the subject. For more comfort, wearability, and effectiveness of the wearable health monitoring system, a new class of biomedical sensors is required. These sensors must be significantly different from the currently available, conventional, bulky and rigid versions. The most desirable sensor forms for the wearable health monitoring system are fabrics/textiles themselves, *i.e*. textile-based sensors. An alternative, less attractive, method is to embed the sensor and its conditioning circuit into textiles substrates, *i.e*. textile-assembled sensor. Advances in the technology of electronic-textiles (e-textiles) make these possible and hence wearable health monitoring systems have been developed. E-textiles aim to seamlessly integrate electronics, sensors, computing elements,

interconnections, and telemetry into the fabrics that can form clothing, hats, blankets and other textile products. Such integration into fabrics enables direct sensing of various physiological signals through clothes, body accessories like glass and finger rings, and many other products. By hiding obtrusive biomedical sensors and their related interconnections, the wearable health monitoring system based on e-textiles 1) provides a high degree of comfort and wearability to the user, 2) allows free dynamic body movement, and 3) increases durability by protecting integrated sensors and interconnections from separation and malfunction due to daily use.

Since e-textiles enable direct sensing of physiological signals of the subject, the wearable health monitoring system based on e-textiles has several merits. First of all, since clothing is generally worn by a subject, a health monitoring system based on e-textiles can operate continuously [2]. Second, it is possible to monitor the subject on a long-term basis without interrupting their normal daily life. Therefore it may improve the quality of health service, especially in providing prompt urgent care, disease prevention, early diagnosis, long-term disease treatment, and home rehabilitation. However, e-textile based applications still face a number of technical challenges. Examples of these include power sources, computational capacities, and storage capabilities [4]. Additionally, the topological location of sensing elements, signal and power lines, and processing elements are all fixed throughout the lifetime of the application.

II. THE-STATE-OF-ART TEXTILE-BASED SENSORS

The emergence of compliant conductive yarns or threads which are compatible with natural fibers has enabled researchers in e-textiles to integrate electrical components into garments. The conductive yarns or threads are implemented by various methods: yarns combined with conductive metals [5], yarns coated with conductive metals like Carbon Loaded Rubber (CLR), composite stainless steel yarns such as BEKINOX® VN, and fine continuous metal-alloy yarns. The continuous stainless steel yarns can be woven, knitted, and sewn while providing a precise electrical resistance. Cottet *et al*

generated conductive yarns by combining very fine, conductive metals like copper, silver, and gold with natural or human-made fibers and investigated their characteristics [5]. The characteristic impedance lies between 120Ω and 320Ω with an accuracy of ±5% to ±10% and the cutoff frequency for 100 cm long textile lines is below 120 MHz. This is sufficient to enable use as a transmission line carrying signals less than 100 MHz using 20 cm lines of the conductive yarns. To achieve high conductivity for textile substrates, they are woven with silver-coated conductive yarns treated with galvanic or electrochemical deposition of gold or platinum [6].

Such conductive yarns and threads have been utilized 1) for the routing of power lines, data bus, and signal paths on textiles [7], and 2) to form textile antennas for RFID (Radio Frequency IDentification) [6, 8]. They may also be used to form sensing structures and conductive lines by knitting or embroidering processes. Knitted fabric sensors for respiratory monitoring and knitted fabric electrodes for ECG (Electrocardiogram) recording have been developed [9-14].

Since the materials and methods used in knitting and embroidering are compatible with existing textile technology, knitted and embroidered sensors, and their interface conducting lines, can be directly integrated into garments in an unobtrusive way. In the garment, the conductive yarns enable direct sensing of physiological signals. When the yarns are employed as sensing material, they are classified as textile-based sensors, the most desirable fabric sensors for a wearable health monitoring system.

Although knitted fabric sensors provide the comfort required for clothing, they are limited in their ability to sense physiological signals due to their knitted structure. For example, the knitted fabric electrode sensors for ECGs have high skin contact impedance due to their irregular surfaces, and hence introduce high frequency noise [9]. In our experiments with these devices, we have found that they 1) are usually stretchable and this property may adversely affect the quality of signals and 2) can

not provide the spatial resolution and signal-to-noise ratio needed to sense physiological signals like the EEG and EMG. We have also found that, to avoid high frequency noise and signal degradation, other intermediate materials, including membranes or glue, that enhance contact between the electrodes and the body are required. Unfortunately the use of such materials can make the subject uncomfortable during normal daily activities.

Knitted sensors for respiratory sensing also have some technical limitations. They 1) change inductance as well as impedance and 2) express varying hysteresis characteristics due to their inherent structure when the sensors are loaded and then restored [9]. A knitted fabric structure shows nonlinear response, i.e. irregular extension along the axis of applied strain. To avoid this drawback an elastic belt can be combined with the sensor [9]. However, we have found that, even when the sensor is knitted into the elastic belt, variance in inductance and resistance occurs when the sensor stretches and restores. That is, knitted sensors do not behave in a repeatable fashion, even under identical conditions. As a result, measurement parameters including inductance and resistance are difficult to control. In addition, changes in measured inductance along a sensor during extension are nonlinear and irregular. Those deviations limit the utility of the textile-based, knitted sensors in measuring relative respiratory signals.

III. OBJECTIVE

The objective of this study is to develop textile-based biomedical sensors that can measure a subject's vital signs including respiration and ECG during a long-term period while normal daily activities including walking, jogging, sleeping, sitting, and other exercise are transpiring. The new textile-based biomedical sensors are required to satisfy several requirements. First, the textile-based sensor must be integrated into garments in an unobtrusive way so that they can be used as a body-worn sensor for the wearable health monitoring system. If the sensors are fused into clothing in an unobtrusive way and hence hidden from the subject, then the subject behaves normally as if no sensors were attached

to him/her. This is the realization of "wear and forget." Second, the textile-based sensors should be textile-friendly such that they can be fabricated with conventional textile processing technologies including screen printing, sewing, embroidering, and etc. Use of existing textile processing technology is a critical requirement for integrating the sensor onto garment and for enabling cost-effective, mass production. Third, the wearable fabric sensors should be robust in withstanding interference so that they can be used with minimal impact during normal daily activities including walking, jogging, sitting, driving, sleeping, exercising, etc. The wearable fabric sensor will be utilized during normal daily activities at home, or in the office, gym and even battle fields. These environments may introduce interference that is not encountered in laboratory or hospital environments. Under such circumstances, the sensor should be capable of discriminating the signal of choice from the interference.

Our research has focused on two main vital signs, respiration and electrocardiogram (ECG), to be captured using textile-based sensors during normal daily activities. The ECG signal is an important diagnostic tool in assessment of cardiac function. The normal activity of the heart results in a regular heart beat that can vary in response to many factors. The QRS complex in the ECG signal reflects the electrical activity within the heart during a ventricular contraction, and the time of its occurrence as well as its shape provide much information about the current state of the heart. Respiration and ECG signals are the underlying vital signs used to analyze sleep disorders, exercise stress, and body status. For example, sleep apnea may be identified if there are no airflows for at least ten seconds. Hypopnea may be also identified if airflow falls markedly but does not stop completely. Those sleep disorders may be identified with heart rate variability through ECG signals.

In this study, we developed fabric active electrodes for ECG signals and various fabric displacement sensors for breathing effort. To develop the textile-based sensors that fulfill the requirements, we utilized nonwoven textiles, silver conductive ink, and screen printing technology. Nonwovens are

selected as a substrate to accommodate sensing elements and electric circuits for respiration and ECG signals. Two different types of nonwovens are combined to form a fabric sensor structure for the respiratory signal measurement. Screen printing technologies and silver conductive ink is utilized to form the sensing area and the conductive lines for signal and power paths. The screen printing technologies can deposit electrical materials on various substrates in a manufacturing environment that allows cost-effective application and high throughput [15].

These textile-based sensors can be transformed into a wearable human physiology monitoring system such that persons with medical conditions will be able to wear clothing to alert them to impending medical emergencies. For example, adults suffering from sleep apnea, and babies susceptible to sudden infant death syndrome (SIDS), will be able to wear electronic pajamas that will monitor them continuously during sleep and signal an alert when their breathing stops.

IV. OUTLINE

Chapter 2 investigates nonwoven fabric active electrodes for ECG signals. Layered fabric active electrodes based on nonwoven substrate are designed and fabricated. The active electrodes are used to measure an ECG with instrumentation circuit during sitting and simulated jogging. The test results are also described.

Chapter 3 addresses a new capacitive nonwoven fabric sensor for respiration measurement. A new fabric sensing structure based on various nonwoven substrates is proposed along with a variable area and splicing parallel palate capacitive sensor. Two types of sensors, single and differential respiratory capacitive fabric sensors, are developed.

Chapter 4 focuses on inductive fabric sensors based on a single substrate. Several factors, such as quality factor and variable resistance, that characterize the inductive sensor based on single substrate

are analyzed. The sensors are fabricated on stretchable nonwoven fabrics. A planar inductive pattern is suggested and tested with the analog circuits.

Chapter 5 examines an inductive respiratory sensor based on two nonwoven substrates. Planar spirals with open center areas are employed for large linear sensing range and better performance. First, a single fabric inductive sensor is designed and tested. Then two differential inductive sensors are presented. Several differential schemes are also achieved by connecting spirals in various ways.

Chapter 6 describes a wearable health monitoring system to demonstrate the capabilities of the newly developed fabric biomedical sensors.

Chapter 7 concludes the dissertation, states the dissertation contributions, and indicates possible future research efforts that could extend the findings of this dissertation.

REFERENCES

[1] M. Coyle, "Ambulatory cardiopulmonary data capture," presented at Microtechnologies in Medicine & Biology 2nd Annual International IEEE-EMB Special Topic Conference on, 2002.

[2] S. Park and S. Jayaraman, "Enhancing the quality of life through wearable technology," *Engineering in Medicine and Biology Magazine, IEEE*, vol. 22, pp. 41-48, 2003.

[3] D. Marculescu, R. Marculescu, Zamora, Stanley-Marbell, K. Park, J. Jung, L. Weber, K. Cottet, Grzyb, Troster, Jones, Martin, and Nakad, "Electronic textiles: a platform for pervasive computing," *Proceedings of the IEEE*, vol. 91, pp. 1993-1994, 2003.

[4] P. S. Stanley-Marbell, D. Marculescu, R. Marculescu, and P. K. Khosla, "Modeling, analysis, and self-management of electronic textiles," *Computers, IEEE Transactions on*, vol. 52, pp. 996-1010, 2003.

[5] D. Cottet, J. Grzyb, T. Kirstein, and G. Troster, "Electrical characterization of textile transmission lines," *Advanced Packaging, IEEE Transactions on [see also Components, Packaging and Manufacturing Technology, Part B: Advanced Packaging, IEEE Transactions on]*, vol. 26, pp. 182-190, 2003.

[6] S. Gimpel, U. Mohring, H. Muller, A. Neudeck, and W. Scheibner, "Textile-Based Electronic Substrate Technology," *Journal of Industrial Textiles*, vol. 33, pp. 179-189, 2004.

[7] E. R. Post, M. Orth, P. R. Russo, and N. Gershenfeld, "E-broidery: Design and fabrication of textile-based computing," *IBM Systems Journal*, vol. 39, pp. 840 - 860, 2000.

[8] W. Weber, R. Glaser, S. Jung, C. Lauterbach, G. Stromberg, and T. Sturm, "Eelctronics in Textiles: The Next Stage in Man Machine Interaction," presented at The 2nd CREST Workshop on Advanced Computing and Communicating Techniques for Wearable Information Playing, Nara, Japan, 2003.

[9] M. Catrysse, R. Puers, C. Hertleer, L. Van Langenhove, H. van Egmond, and D. Matthys, "Towards the integration of textile sensors in a wireless monitoring suit," *Sensors and Actuators A: Physical*, vol. 114, pp. 302-311, 2004.

[10] N. Taccini, G. Loriga, A. Dittmar, and R. Paradiso, "Knitted includes for health monitoring," presented at Engineering in Medicine and Biology Society, 2004. EMBC 2004. Conference Proceedings. 26th Annual International Conference of the, 2004.

[11] R. Paradiso, A. Gemignani, E. P. Scilingo, and D. De Rossi, "Knitted bioclothes for cardiopulmonary monitoring," presented at Engineering in Medicine and Biology Society, 2003. Proceedings of the 25th Annual International Conference of the IEEE, 2003.

[12] R. Wijesiriwardana, K. Mitcham, and T. Dias, "Fibre-meshed transducers based real time wearable physiological information monitoring system," presented at Wearable Computers, 2004. ISWC 2004. Eighth International Symposium on, 2004.

[13] E. P. Scilingo, A. Gemignani, R. Paradiso, N. Taccini, B. Ghelarducci, and D. De Rossi, "Performance evaluation of sensing fabrics for monitoring physiological and biomechanical variables," *Information Technology in Biomedicine, IEEE Transactions on*, vol. 9, pp. 345-352, 2005.

[14] R. Paradiso, G. Loriga, and N. Taccini, "A wearable health care system based on knitted integrated sensors," *Information Technology in Biomedicine, IEEE Transactions on*, vol. 9, pp. 337-344, 2005.

[15] R. Parashkov, E. Becker, T. Riedl, H.-h. Johannes, and W. Kowalsky, "Large Area Electronics Using Printing Methods," *Proceedings of the IEEE*, vol. 93, pp. 1321-1329, 2005.

Chapter 2

NONWOVEN FABRIC ACTIVE ELECTRODES FOR BIOPOTENTIAL MEASUREMENT DURING NORMAL DAILY ACTIVITY

ABSTRACT

In this paper we introduce nonwoven fabric active electrodes that provide the comfort required for clothing while robustly recording physiological data in the presence of body movement. Body movement is responsible for most of the interference during physiological data acquisition in normal daily life. Conductive ink is used to form a transducer layer and conductive lines on nonwoven fabrics. Devices are designed and fabricated using hand and screen printing techniques, devices that are reusable, unobtrusive, and wearable. These nonwoven fabric active electrodes can be easily integrated into clothing for wearable health monitoring applications. Test results indicate that nonwoven textile-based sensors show considerable promise for physiological data acquisition.

I. INTRODUCTION

A. Knitted or Embroidered Textile Electrodes

To capture physiological signals, many researchers are investigating the merits of including sensors in textile garments [1-5]. Since human beings are almost always wearing clothes, sensors in their clothing are always accessible and ready to use in normal daily activities. The most common example of a sensor integrated into garments is textile electrodes. Up to now textile-based electrodes for ECG measurements are commonly achieved by knitting or embroidering conductive yarns. These conductive yarns include composite stainless steel versions, yarns coated with conductive metals, and fine continuous metal yarns made from conductive alloys. In [3], the transducer area for an ECG is achieved by knitting stainless steel yarn for ECG measurements on children in a hospital environment. In [6], transducer areas of electrodes are formed by embroidering biocompatible silver coated fibers to electrically stimuli paralyzed muscles. Even though these conductive fabrics still

retain the comfort required for clothing, it is not practical for such electrodes to be included in wearable health monitoring systems. First, such embroidered or woven/knitted electrodes have high skin contact impedance due to their irregular surfaces, and consequently they introduce high frequency noise. Second, high contact impedance and the resulting high frequency noise limit the ability of such electrodes to pick up physiological signals like EOG, EEG and EMG. Third, to achieve good contact between electrodes and skin, gel or other adhesive materials are necessary. Fourth, pure knitted substrates are stretchable and hence cause variations in skin contact impedance as the body moves due to breathing or physical exertion. Fifth, like other passive electrodes, woven or embroidered electrodes introduce DC offset into front-end electric sensing circuits due to motion artifacts, which frequently result in saturation of the instrumentation system. Finally electrical components are not easily secured and interconnected on woven or knitted textiles.

B. Challenges for Wearable Health Monitoring

For practical use of textile electrodes or other electrodes in normal daily activity as components of wearable health monitoring systems, they should be robust to the interference for which body movement is most responsible. Noise resulting from patient movement is particularly troublesome in ambulatory ECG, EEG, and EMG recordings because the bandwidth of the motion artifact overlaps with the ECG signal bandwidth. The expected interference due to body movement is input offset voltage changes which are usually caused due to skin-electrode-amplifier interface movement and common-mode voltage drifts. Body movement deforms the contact shape between electrodes and skin thereby making the impedance of the two input electrodes different. Combined with the common-mode voltage effects, this difference in contact impedance of two input electrodes introduces a large offset voltage, that is large enough to saturate the voltage-follower amplifier [7].

Since body movement is natural in daily life, the input offset voltage should receive special attention during the design of the ECG system. To remove motion artifact, a firm electrode-skin contact is

required and accomplished through several methods. Use of gel, glue or membrane is the most widely employed method to improve conductivity and hence contact impedance of knitted electrodes [3, 4]. Even though glued electrodes with good skin preparation can reduce the contact impedance, it is not practical for daily use of reusable electrodes embedded in wearable garments. The conductive gel tends to dry out over time. Even with the extra adhesive material, the textile electrode generate high impedance signal and hence following signal lines, commonly achieved with conductive yarns, are weak to the outside interference including physical impact to the lines or mains power-line interference. Active electrodes as a method to match impedance can significantly lessen these interferences.

C. Active Electrodes

The role of the active electrodes is to pick up a biopotential signal while transforming high source impedance to low source impedance. The output impedance of the active electrodes is low enough to avoid the interference of the electrically and mechanically induced noise. Therefore, active electrodes are efficient in preventing 60 Hz power line hum without the traditional anti-noise measures of shielding and input offset voltage control.

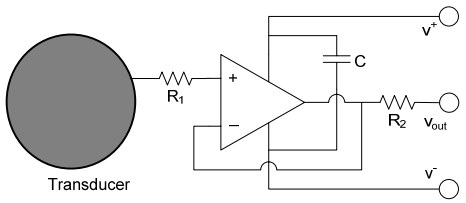

Fig. 1. Schematic diagram for a basic active electrode. (R_1=200kΩ, R_2=50Ω, and C=10nF)

By employing a buffer amplifier (a voltage follower) in the sensor's interface circuitry, one can build "active" electrodes [8, 9]. Fig. 1 shows the fundamental diagram including transducer area, signal and power paths, and electrical components for the basic active electrodes. One op amp having high

input impedance, two resistors and one capacitor are the required electrical components. The operational amplifier (opamp) is in a voltage follower configuration. The voltage follower is placed near the transducer (the electrode).

Regardless of the merit of active electrodes, there has been some reluctance to use them since they require a power supply and the extra power lines also make the fabrication of electrodes more complex. Another drawback in the past is the fact that the prototypes have been implemented on rigid substrates forcing the flat electrodes to be attached to the concave shape of the body using some form of glue adhesive. However, by integrating the electrical components with flexible nonwoven fabrics and incorporating multiple lines and components into the flexible nonwoven clothing, the active electrode can now conform to the contours of the body and hence provide reliable noise-free signals to a wearable health monitoring system.

In this paper we introduced new nonwoven fabric active electrodes that provide comfort for the user while minimizing body movement signal interference in normal daily activities for a wearable health monitoring system.

II. SURVEY ON BIOPOTENTIAL RECORDINGS AND ACTIVE ELECTRODES

A. Front-End Circuits

A common choice of a front-end circuit is an instrumentation amplifier, two coupled input amplifiers following a single differential amplifier, with integrator feed-back for DC suppression because of their high input impedance and high common mode rejection ratio (CMRR) [10-12]. To reject 60 Hz noise, the input common mode voltage is fed back to the right leg of the patient. Since this approach significantly improves common-mode rejection, the driven right leg circuit has become almost standard in biomedical potential recording devices [11, 13].

There are 1) a high electrode offset voltage due to the electrode interface and 2) a DC offset due to unbalanced impedance of the two electrode interfaces. It is strongly desirable to reduce the DC offset at an early stage in the front-end analog circuit to achieve a large gain and an improved signal to noise ratio [7, 14, 15]. In a two-op amp coupled differential input mode with a following single differential amplifier, if higher gain is implemented in the first stage (coupled two op amplifiers), higher CMRR is achieved [10].

DC blocking methods with a serial capacitor were used in [12, 14, 16]. Employing a grounded high pass filter to remove a DC offset at the front-end portion of a circuit should be avoided. This reduces the CMRR of a differential amplifier by converting its differential scheme into a single rail by creating a path to ground before the input stage [12]. To avoid this problem while achieving DC offset suppression, a groundless differential high pass filter [12] was proposed as a front-end circuit. In [16], an ac-coupled amplifier, consisting of a serial capacitor and a bootstrapped operational amplifier, was proposed for simultaneous DC blocking and high gain realization. Another method by Spinelli [15] and Van Rijn et al. [17] to remove DC offset in the input employs integrator feedback within a configuration of three operational amplifiers. In [15], a fully differential amplifier with integrator feedback was proposed as a front-end circuit.

Even with the above improvements, unshielded signal lines between a high impedance signal source and the measurement circuitry will still be prone to introduce 60 HZ power-line interference. In addition, signal artifacts may occur from body, electrode, and/or lead-wire motion. Sometimes this interference lies within the bandwidth of the ECG signal which makes removing it by analog filtering stages difficult.

B. State-of-the-Art Active Electrodes

Various versions of active electrodes have been fabricated [8, 9, 18-22]. Basic active electrodes (see Fig. 1) have been fabricated by *Padmadinata et al*. [18] in a single microelectronic chip using standard bipolar processes. *MettingVanRijn et al*. [19] and *Valchinov* and *Pallikarakis* [20] modified the circuit of [17] by using active electrodes as front-end stages of the amplifier system. In [19], small active electrodes were implemented with thick film technology and standard components. In [20], active electrodes were used in an optical acupuncture system to measure the skin response to laser stimulation. In both [19] and [20], DC suppression and high amplification were achieved.

Degen and *Jackel* presented two different schemes for active electrodes [21, 22]. Reference [10] has revealed that the CMRR of a three op-amp circuit, consisting of an uncoupled (grounded) two op-amp circuit with a following single differential amplifier stage, may be degraded due to misbalanced passive components. However, a high CMRR for this circuit can be achieved by controlling the gain of the single differential amplifier. Based on this, the authors in [21] suggested active electrodes that contain an op-amp connected as a high-gain non-inverting amplifier. The gain of the following differential amplifier was adapted by changing an input resistor by a digital feedback loop to obtain high CMRR. A second active electrode configuration by this group is presented in [22]. This configuration uses a constant-current source to drive the circuit and the voltage across a conducting diode to divide this current between the op-amp's power and output terminals. Only two wires are needed to operate the active electrode, one is for the constant current source and the other for a reference voltage. For DC offset compensation, the reference voltage was controlled by an error feedback loop controlled by an analog integrator or by digital signal processing.

III. NONWOVEN FABRIC ACTIVE ELECTRODES

For fabric active electrodes, a voltage follower circuit was integrated on the nonwoven substrates with a transducer. A simple buffer circuit with minimal components is desirable for fabric substrates due

to difficulties in attaching components. In addition, fewer interconnections will improve the durability of the active electrode circuit.

Although the concept and structure of basic active electrodes are very simple, they bring several advantages if they are implemented on textile substrates and integrated into daily-use garments. By embedding them into the garment, active electrodes will be employed in wearable health monitoring applications that involve body movement such as walking, jogging, and running. We can dramatically reduce the variation effect of skin-electrode contact impedance due to body movement. Because the active electrodes possess low output impedance, they are efficient in preventing environmental interferences like 60 Hz power line hum that is commonly prevalent everywhere, such as at home or at the clinic. In this paper we design and fabricate prototype active electrodes on nonwoven textile substrates to provide a robust way for preventing op-amp saturation from DC offsets due to body movement and external interference for wearable health monitoring systems.

A. Layered Structures of Fabric Active Electrodes.

By closely placing buffer amplifier circuitry (a voltage follower circuitry) and a transducer on textile substrates, we can build "active" fabric electrodes that dramatically reduce the variation effect of skin-electrode contact impedance due to body movement. The active electrodes can be efficiently arranged in a layered structure on a nonwoven fabric substrate. That is, the basic active electrodes shown in Fig. 1 can be implemented on the single nonwoven substrate with two layers: a transducer layer and a circuit layer (see Fig. 2). The circuit layer accommodates electrical components as well as signal and power paths. In this structure, the path between the transducer and op-amp input is extremely short.

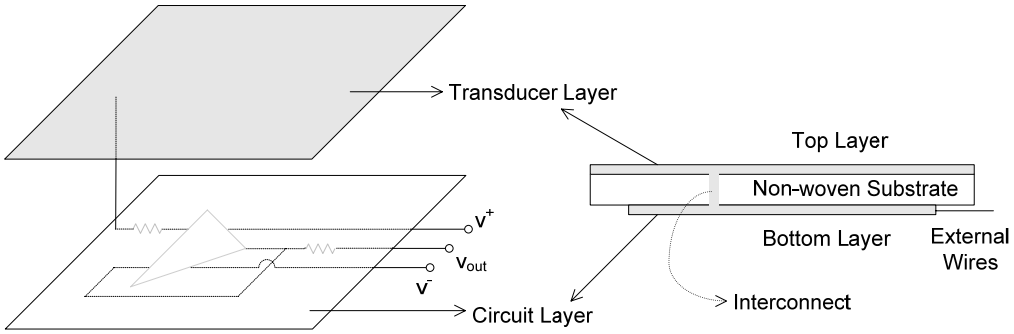

Fig. 2. Two layered basic nonwoven active electrodes on a single substrate. Crossover structure (a via) is required to interconnect between two points on the transducer layer and the circuit layer. Line crossing between ground (v^-) line and op-amp feedback line in the circuit layer do not show up in real circuit configuration. (The bypass capacitor is not shown)

B. Guard Layer

To protect the active electrodes from mechanical interference as well as electric and magnetic interference, we added an extra plate that serves as a dedicated guard/shield layer. The electric circuit is mechanically protected from scratching and bending by sandwiching it between two plates. As shown in Fig. 3, a one-sided conductive plate was added to shield the op-amp's inputs from stray electric fields and capacitive coupling. Adding the conductive layer introduces an unwanted parasitic capacitance between the shield and the electrode's transducer plate. To cancel this capacitive effect, the voltage of the shield and transducer layers should be the same. This is accomplished by connecting the follower's input to the transducer layer and its output to the shield. This is a noise cancellation scheme called the guard method. The voltage across the parasitic capacitor, C_{gt}, appears to be zero because C_{gt} conducts no current. With no current being conducted, no charge transfer can make place to introduce noise into the circuit.

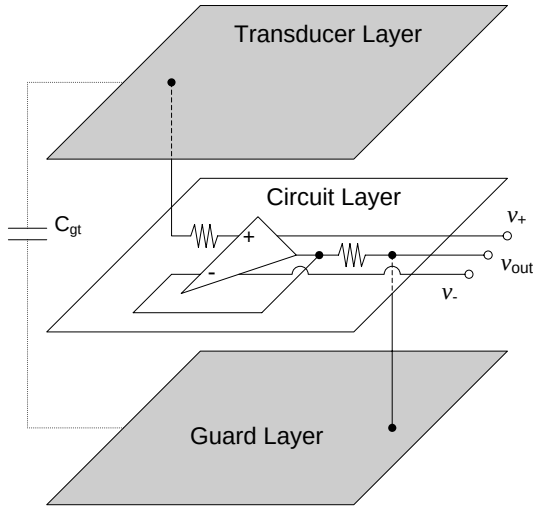

Fig. 3. Schematic diagrams of two-plate active electrodes with the guard layer.

C. Fabrication Methods

To produce the layered fabric active electrodes, we needed processes to form the sensing area (the transducer), conductive lines (electrical signal transport), feed-through interconnects (crossover structures), and adhesive pastes (attachment of the electrical components and wires to the nonwoven textile substrates). First, the forming of the sensor area and the routing of power and signal-transmission lines on the nonwoven textile substrates can be achieved by screen-printing or drawing manually with Ag/AgCl ink. For disposable electrodes (one-time use), silver paste may also be used. Second, the connection between two layers in the same substrate (the top and bottom of the substrate) can be achieved by first punching vias (holes). Next, both layers can be manually re-coated with Ag/AgCl ink so that the ink flows through the vias and touches the ink on the other side. Finally, conductive epoxy or silver paste can be used to attach in fixed positions the electrical components and wires to their respective locations on the fabrics.

IV. EXPERIMENTAL RESULTS

A. Instrumentation

A set of instrument circuits (analog and digital portions) were designed and implemented to measure biopotentials such as the ECG using our active textile electrodes. The analog circuit includes a front-end buffer and a low-pass filter. The digital portion includes a low power micro controller, a flash memory module, and peripheral circuits. Fig. 4 shows the front-end circuit for biopotential measurement using two active electrodes. It also works with three passive electrodes, two of which are for signal input and one of which is for the reference.

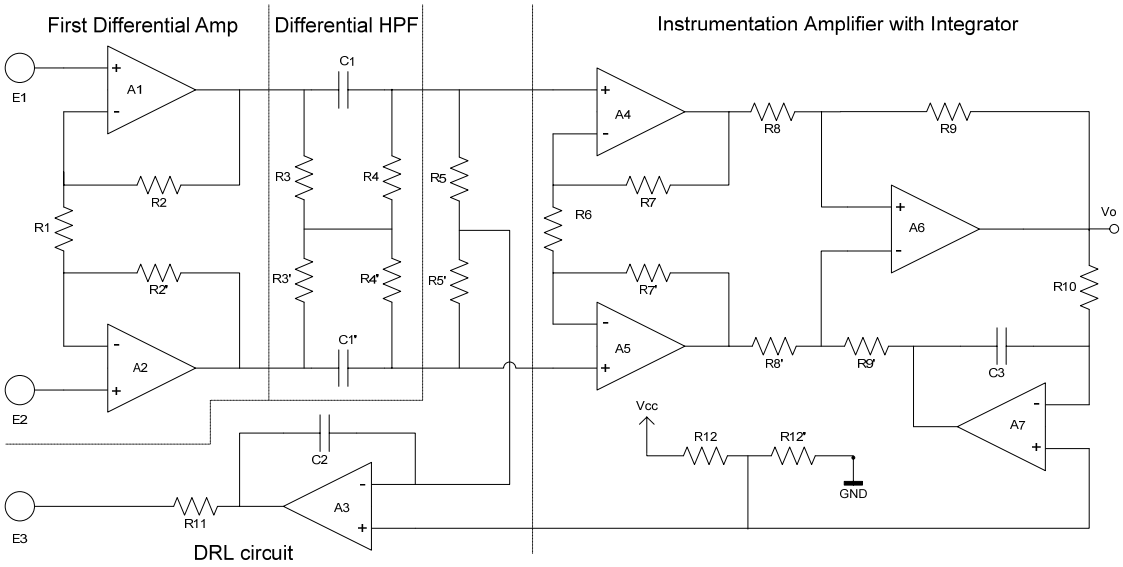

Fig. 4. Schematic diagram of the front-end circuit with single supply for physiological data acquisition using active electrodes. This scheme is a common way to pickup ECG signals except that the differential high pass filter is placed after first differential amplifier [10, 12, 13, 23].

Through the active electrodes, low-output-impedance ECG signals are fed into the first differential amplifier which has a high common-mode-rejection ratio. Even though active electrodes greatly reduce the input offset voltage, the first differential amplifier is designed with low gain (< 10) to avoid circuit saturation. The next stage is a differential high pass filter [12]. Purpose of R5 and R5′ is to detect the common mode input voltage and fed it back to the user's right leg through a driven-

right-leg circuit (DRL) [13]. Then, the signals go into the second differential amplifier that increases the signal to half the full swing range of ADC. The DRL circuit provides an input bias current path and a practical way to reduce common mode input voltage which is one of the sources contributing to DC offset at the front-end op amp. Up to this stage in the circuit, no ground path is needed. Finally, the next stage is the integrator circuit, consisting of A3, R10, and C3. The integrator removes the DC offset by acting like a high pass filter.

The active electrodes start the suppression of DC offset. Any remaining DC offset is further reduced by the differential high pass filter and the integrator circuit respectively. Finally a fourth order Butterworth, Sallen-Key low pass filter was employed to remove high frequency interference (circuit not shown).

In the digital portion, a low powered Atmel® 8Meg microprocessor was used to convert analog signals into digital form in 8-bit resolution. A 16 M Byte flash memory communicates with the processor to store the signal data in real time. Interface software was implemented for the Palm® pilot to display the signals in real time. The whole system including analog and digital circuits can operate under a single power supply.

B. Prototyping the Active Electrodes

To prototype the active fabric electrodes, we chose non-stretchable Evolon® 100 (100 grams per square inch) as the nonwoven substrate and silver filled polymer ink CMI 112-15 was chosen for the conductive lines. TLC272 op amps (8-SOIC or 8-SOP type) with single power supply and SMT-type circuit components (resistors and capacitors) were chosen due to their flat shape and small size.

(a) The transducer layer

(b) The circuit layer with SOIC type op amp

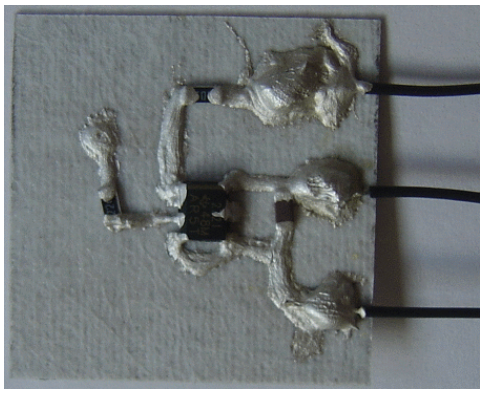

(c) The circuit layer with wire connection

Fig. 5. Images of the hand-printed electrode layer (3 cm × 3cm).

As the first step to fabricate fabric active electrodes, both surfaces of the nonwoven fabrics were treated with insulating material to retard ink penetration. Our preliminary tests show that the ink we selected can penetrate through the fabrics depending on the fabric's thickness resulting in an unwanted short circuit between the conductive inks on both layers. In addition, the treatment may reduce high frequency noise pickup and prevent signal loss due to unevenness in the surface of the fabric.

After the surface treatment, the transducer layer was created by filling the ink on one side of the substrate (Fig. 5(a)) by hand. On the other side, the op amp was attached with super glue and then the signal and power lines are hand printed. Before curing the conductive lines, the resistors and

capacitors were placed in their proper positions. The electrical component attachments to the conductive lines were reinforced by manually redrawing the lines on the electrical components with the ink (Fig. 5(b)). All curing was done at room temperature. After curing, a micro hole was punched to connect the transducer layer with the input of op amp through resistor (R_1). Flexible wires without shielding were connected to the end points of conductive lines for signal, ground and power (Fig. 5(c)). For strong bonding between the electrodes and the wire, the bonding point was soldered. Then the circuit layer was filled with dielectric material to prevent shorts and covered by other stretchable nonwoven fabrics to protect the circuit (Fig. 6(b)). This figure shows the basic active electrode without the guard layer. For the guarded active electrodes, the outside layer of the basic active electrodes was filled with silver ink to form the guard layer as shown in Fig. 7(b). The guard layer was connected through a via to the buffer output (Fig. 7(a)). Similarly the guard layer was covered by other stretchable nonwoven fabrics. Fig. 6(c) shows the completed guarded active electrodes. Finally, one more nonwoven substrate was added to protect the circuit or the guard layer.

Passive electrodes were also fabricated and used as reference electrodes (Fig. 6(a)). Holes were punched and filled with silver ink to make a path between the transducer layer and its back side. After curing the ink, the external wire was attached on the back side of the transducer layer by soldering and painting. Then the back side was covered by other nonwoven fabrics.

(a) Passive electrodes

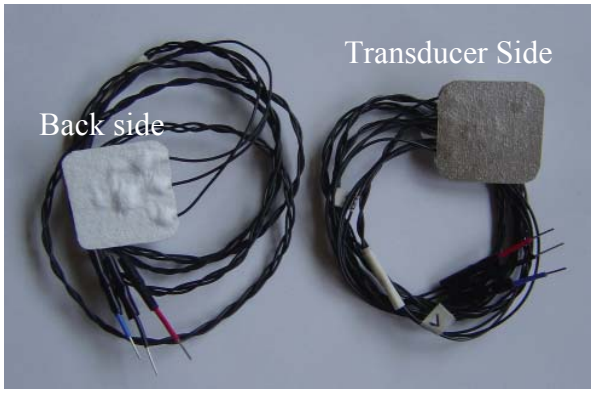

(b) Active electrodes without the guard layer

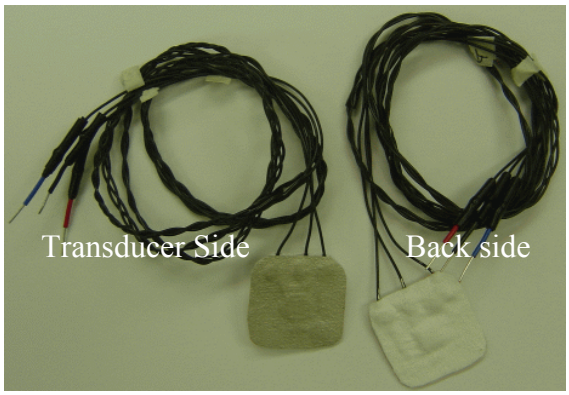

(c) Guarded active electrodes

Fig. 6. Images of completed passive and active hand-printed electrodes.

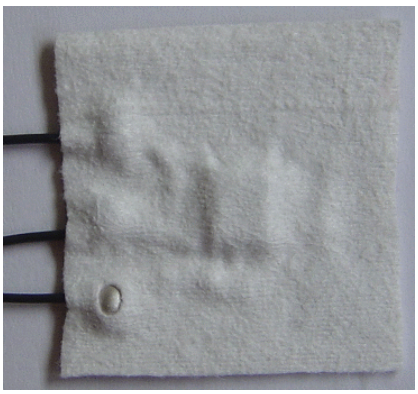

a) Via

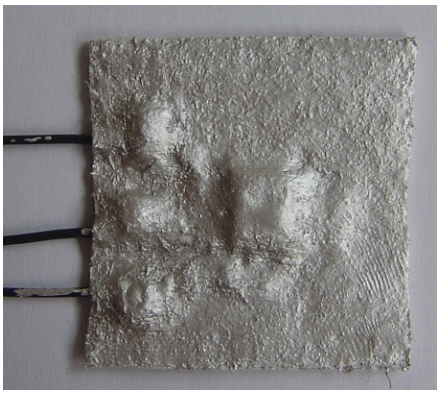

(b) Silver coating

Fig. 7. The silver-ink coated, hand-printed, guard layer.

ECG data were collected using the nonwoven passive electrodes, the nonwoven basic active electrodes, and the nonwoven guarded active electrodes. Fig. 8 shows real ECG signals captured

using nonwoven passive electrodes and nonwoven active electrodes with a subject sitting quietly. There seems to be little difference between the ECG signals captured by the passive and active electrodes and a small amount of high frequency noise can be seen on both signals.

In general, with more activity, more noise creeps into ECG signals. Fig. 9 displays waveforms captured while jogging. Fig. 9a demonstrates the problem of increases noise. The arrows indicate footsteps of the jogger. As the jogger's feet hit the ground, there is peak movement of the electrodes and their connecting wires with respect to the attachment points on the jogger's chest. This generates large negative peaks in the ECG signal. These large artifact signals commonly saturate the high gain amplifiers which are used to transform the mV level output voltages from the passive electrodes to the one-to-five volt level needed for analog to digital conversion. The ECG signals captured by our nonwoven passive electrodes are not saturated due to our use of a multi-stage scheme to remove DC offset in the front-end amplifier circuit. Note that some noise is also present in the ECG signals captured with the nonwoven active electrodes, but is considerably reduced. Overall, the active electrodes show better performance than the passive electrodes when ECG signals are captured during jogging.

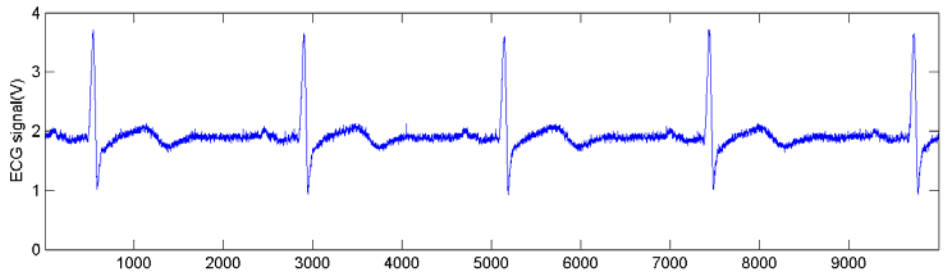

(a) Nonwoven passive electrodes

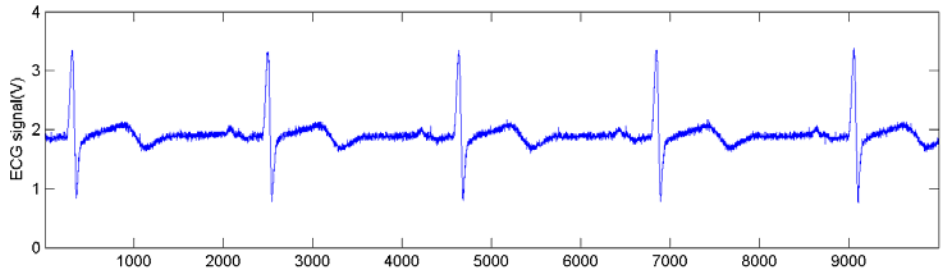

(b) Nonwoven active electrodes

Fig. 8. ECG signals captured with hand-printed nonwoven-fabric electrodes during sitting.

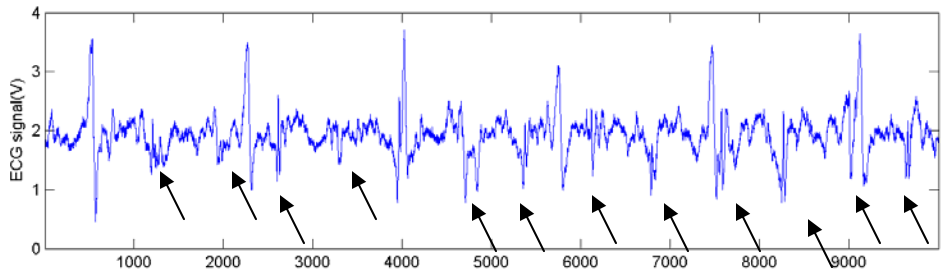

(a) Nonwoven passive electrodes

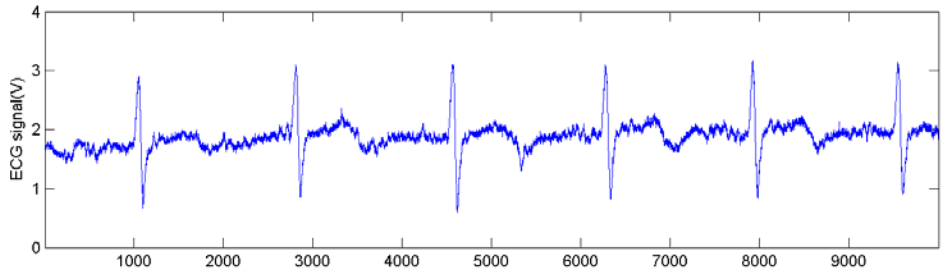

(b) Nonwoven active electrodes

Fig. 9. ECG signals captured with hand-printed nonwoven-fabric electrodes during jogging.

The results for both sitting and jogging using the hand-printed nonwoven fabric guarded active electrodes are shown in Fig. 10. Note that the ECG signals during sitting in Fig. 10a are corrupted when compared to the similar conditions for the passive and active electrodes during sitting in Fig. 8. There may be several reasons for this behavior. One is that the designed guard layer does not in practice achieve the same voltage level as the transducer layer, causing stray electric fields between these two layers. Also, the guarded active electrodes were pressed to the skin of a volunteer subject's chest by a compression belt, so the pressure may have caused unwanted contact between the silver-painted layers of the guard and transducer with the printed signal paths.

During jogging in Fig. 10b, the signal is further degraded when compared to the sitting waveform in Fig. 10a. This follows the same trend as seen in the passive electrodes in Figs. 8a and 9a.

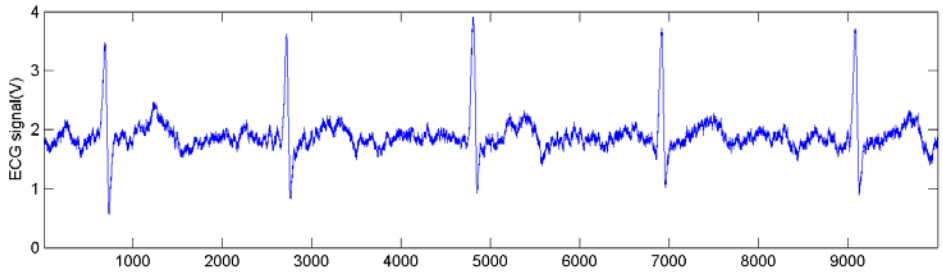

(a) During sitting

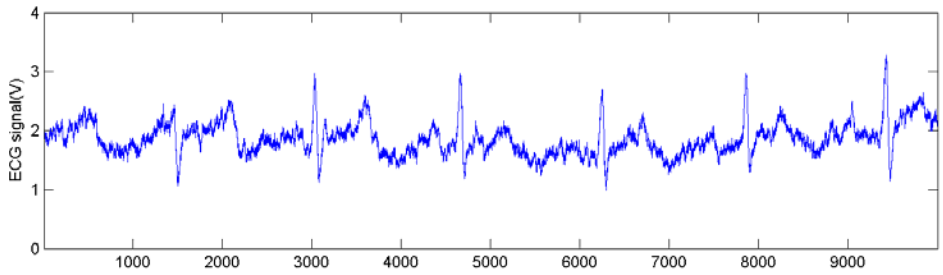

(b) During jogging

Fig. 10. ECG signals captured with hand-printed nonwoven-fabric guarded active electrodes.

C. Screen-Printed Devices

Screen printing is a low-cost, thick film deposition method. A paste containing the desired materials is uniformly spread across specific areas on a substrate which is then cured by thermal processing. Screen printing can be employed to print the signal and power paths needed for electronic circuits on nonwoven textiles [24]. We employ this technology to fabricate active electrodes, examples of which are displayed in Fig. 11.

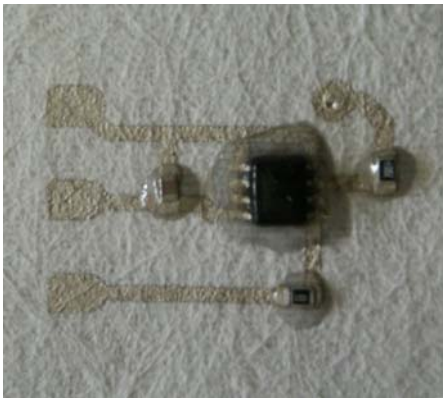

(a) circuit layer

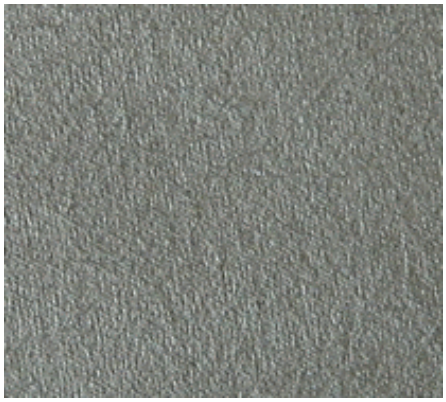

(c) the transducer layer

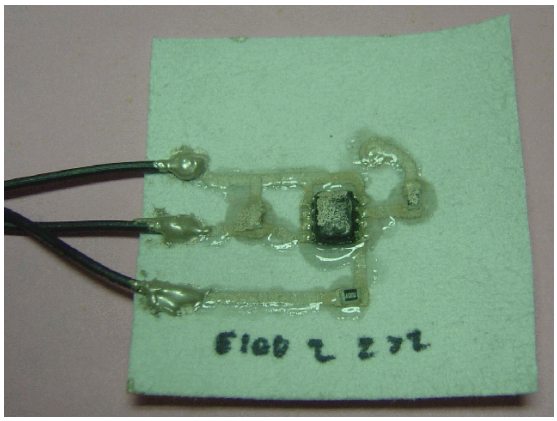

(c) the circuit layer with external wires

Fig. 11. Screen-printed active electrodes. The screen-printed conductive lines and components in (c) are coated with a non-conducting adhesive insulator.

Fig. 12 shows an ECG signal captured during sitting with the screen-printed active electrodes. The electrodes were placed on the skin in the same manner as for Figs. 8, 9, and 10. The screen-printed

electrodes exhibit similar performance as that of the hand-printed versions. To analyze the noise content of the ECG in the screen-printed case, a Fast Fourier Transform (FFT) of the signal was performed as shown in Fig. 13. Note that the ECG signal are free from 60 Hz hum. The screen-printed active electrodes did not introduce high frequency noise which is a common problem in other knitted or embroidered textile electrodes [1-5]. Therefore, we were not forced to use an electrolyte gel or adhesive glue to firmly attach the electrodes to body as is the case in many chronic applications in clinical settings.

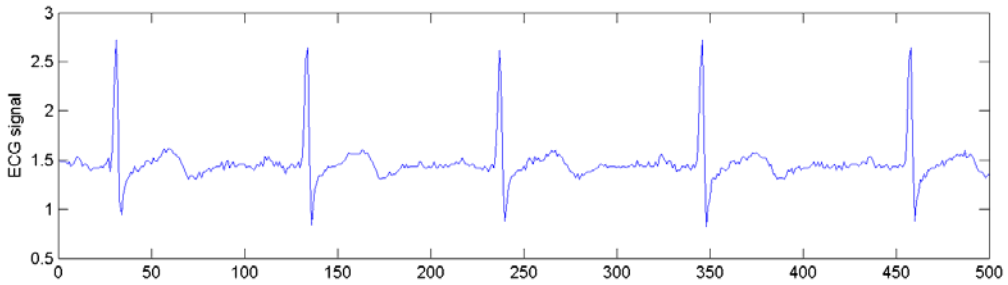

Fig. 12. ECG signals captured with screen-printed active electrodes during sitting.

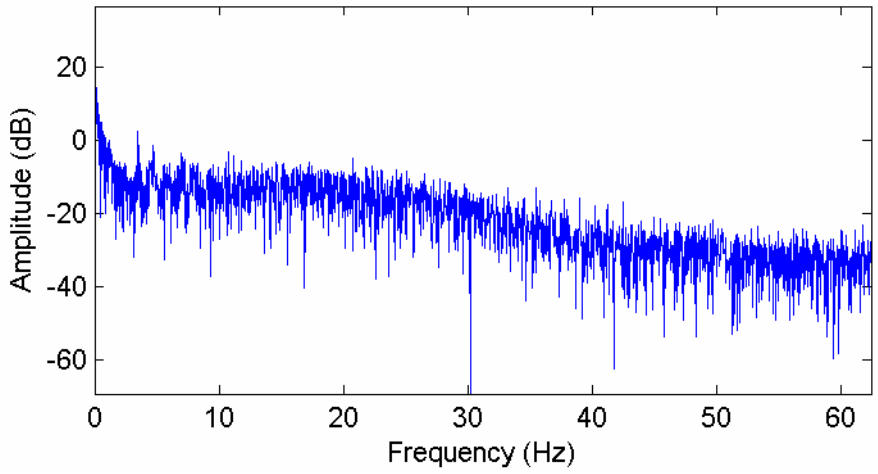

Fig. 13. The FFT of the ECG signals captured for 32 seconds (125 samples per second).

D. Discussion

Since the ECG signals captured with the active electrodes shows show good performance, we can say that silver ink deposited on nonwoven textile substrates is suitable for implementing the electrical circuits. We have demonstrated that nonwovens are suitable substrates to accommodate electrical components and silver printed conductive lines to carry physiological signals and supply power. Even though nonwoven textiles have a relatively rough surface compared to polymer printed circuit boards (PCBs), they do not seem to degrade the signal when the lines printed with silver ink are relatively short (a few millimeters wide and a few centimeters long). This may be due, in part, to nature of physiological signals, typically being at low frequencies of 100 Hz or less. Processing high frequency signals on nonwoven substrates with silver ink may be more problematic [24].

In this study, we attached dry passive electrodes to joggers using a stretchable belt to hold them in place on the jogger's chest. The electrodes must remain in a stable position relative to the jogger's skin layer to avoid motion artifacts in the ECG signals. For nonwoven active electrodes, the pressure applied to the electrode-skin interface by the stretchable belt can be reduced compared to that applied for the passive electrodes. Even with a reduced pressure, the motion-induced noise in the ECG signals was also reduced. In general, all the nonwoven electrodes used in this study conformed well to the shape of the jogger's body and caused no discomfort.

Reducing the pressure on the electrode-skin interface increases the comfort to the user. In addition to decreasing comfort, increased pressure also reduces the durability of the sensor by breaking down the insulation barriers of the circuits we designed and fabricated. When we tested the screen-printed active electrodes, several sets that worked well in benchtop tests actually malfunctioned under pressure applied by the stretchable belt holding them in place while sitting and/or jogging. That never happened with the hand-printed active electrodes. The screen-printed lines were more susceptible to bending and breaking. Thus the design of the electric circuit should be configured to resist and

tolerate bending from the pressure of the stretchable belt. Mechanical barrier with dielectric coating on the printed lines may contribute to protect line broken. Melt blown lamination or dielectric ink printing may be considered.

The lessons learned above have led us to propose changes in our active circuit design to enhance its performance when implemented using screen-printed inks. As shown in Fig. 14, we suggest additional layers be added to our circuit configuration originally shown in Fig. 2, a single shield layer anchored to the reference voltage line and double guard layers connected to the o-amp output. The shield layer anchored to the reference voltage (shown on the left side of Fig. 14) will protect the transducer from outside interference. In addition, the shield layer and the transducer generate a capacitance, C_{gt}. Combined with the skin contact impedance between the body and the transducer, this capacitance will form a low pass filter to reduce input high frequency noise without adding any additional circuit components.

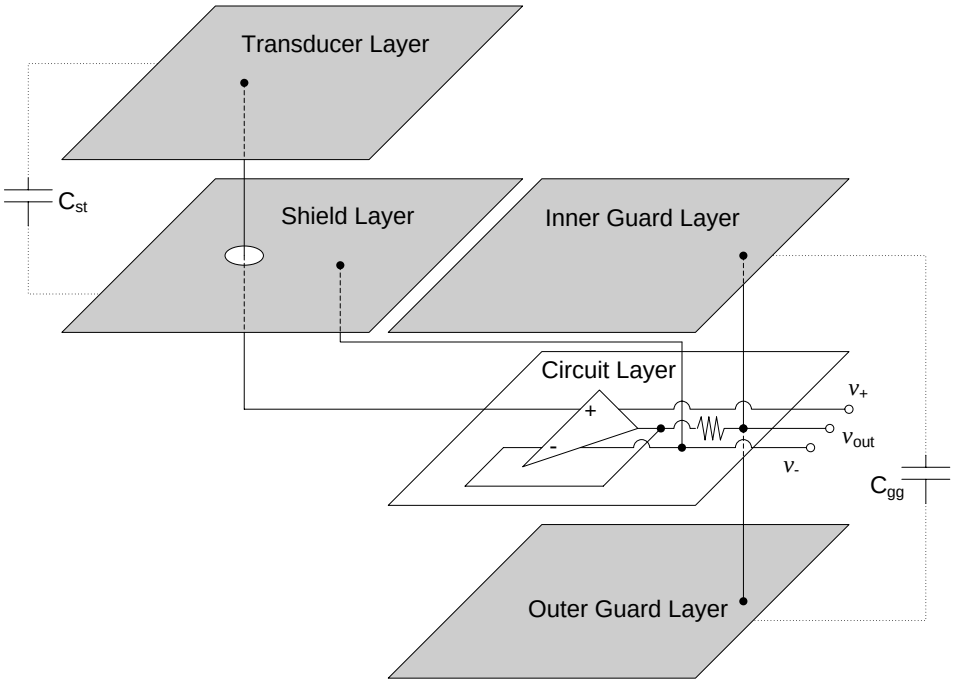

Fig. 14. Schematic layout of shield/guarded circuit of active electrodes.

The double guard layer connected to the op-amp's output is shown on the right side of Fig. 14. These extra plates protect the electric circuit from mechanical as well as electric and magnetic interference. The circuit layer with the two guard layers should be isolated from the pressure of a stretchable belt that holds the transducer on the left side to the jogger's chest. As was the case for our guarded circuit of Fig. 3, the voltage across the parasitic capacitor, C_{gg}, appears to be zero because C_{gg} conducts no current. The shield and/or guard layers isolate the circuit layer to reduce noise pickup.

V. CONCLUSIONS

In this paper we introduced new nonwoven textile electrodes that provide not only the comfort and flexibility required for integration into clothing, but also the robustness against interference during normal daily activity to make them a good candidate from physiological monitoring in active environments. We confirmed that hand-printed and screen-printed electrodes on nonwoven fabrics can capture ECG signals during daily life. In separate tests, we have also confirmed that very weak physiological signal such as the EOG can be measured by using our fabric based electrodes. These nonwoven electrodes have several positive traits. First, the active electrodes are suitable for measuring biopotential signals including the ECG during normal daily activities like jogging, sleeping, walking, and sitting due to their ability to suppress DC offset in a wide variety of settings. Second, the fabric electrodes provide comfortable wearability by integrating the electrical components for active electrodes into flexible nonwoven fabrics. This feature may make the nonwoven active electrodes a prime candidate technology platform for wearable health monitoring applications. In addition, active electrodes based on the flexible nonwoven substrates are easy to trim, shape, and adapt into a variety of body surface contours to measure physiological signals of interest.

To embed the nonwoven fabric active electrodes into a wearable health monitoring system, further study will be needed in improvement the durability of the fabric/electronics interface. For increased durability, mechanical damage must be minimized by protecting the interconnection points for the electrical components and preventing cracks in the conductive lines. In addition, durability requires protection from environmental factors like sweat and moisture.

REFERENCES

[1] J. Coosemans, B. Hermans, and R. Puers, "Integrating wireless ECG monitoring in textiles," *Sensors and Actuators A: Physical*, vol. In Press, Corrected Proof.

[2] E. P. Scilingo, A. Gemignani, R. Paradiso, N. Taccini, B. Ghelarducci, and D. De Rossi, "Performance evaluation of sensing fabrics for monitoring physiological and biomechanical variables," *Information Technology in Biomedicine, IEEE Transactions on*, vol. 9, pp. 345-352, 2005.

[3] M. Catrysse, R. Puers, C. Hertleer, L. Van Langenhove, H. van Egmond, and D. Matthys, "Towards the integration of textile sensors in a wireless monitoring suit," *Sensors and Actuators A: Physical*, vol. 114, pp. 302-311, 2004.

[4] R. Paradiso, G. Loriga, and N. Taccini, "A wearable health care system based on knitted integrated sensors," *Information Technology in Biomedicine, IEEE Transactions on*, vol. 9, pp. 337-344, 2005.

[5] R. Wijesiriwardana, K. Mitcham, and T. Dias, "Fibre-meshed transducers based real time wearable physiological information monitoring system," presented at Wearable Computers, 2004. ISWC 2004. Eighth International Symposium on, 2004.

[6] T. Kirstein, M. Lawrence, and G. Tröster, "Functional Electrical Stimulation (FES) with Smart Textile Electrodes," presented at International Workshop on a new generation of wearable systems for e-health, Pisa, Italy, 2003.

[7] A. C. M. v. Rijn, A. Peper, and C. A. Grimbergen, "High quality recording of bioelectric events. Part 1. Interference reduction, theory and practice," *Medical & Biological Engineering & Computing*, vol. 28, pp. 389 - 397, 1990.

[8] W. H. Ko, "Active electrodes for EEG and evoked potential," presented at Engineering in Medicine and Biology Society, 1998. Proceedings of the 20th Annual International Conference of the IEEE, 1998.

[9] S. Nishimura, Y. Tomita, and T. Horiuchi, "Clinical application of an active electrode using an operational amplifier," *Biomedical Engineering, IEEE Transactions on*, vol. 39, pp. 1096-1099, 1992.

[10] R. Pallas-Areny and J. G. Webster, "Common mode rejection ratio in differential amplifiers," *Instrumentation and Measurement, IEEE Transactions on*, vol. 40, pp. 669-676, 1991.

[11] E. M. Spinelli, N. H. Martinez, and M. A. Mayosky, "A transconductance driven-right-leg circuit," *Biomedical Engineering, IEEE Transactions on*, vol. 46, pp. 1466-1470, 1999.

[12] E. M. Spinelli, R. Pallas-Areny, and M. A. Mayosky, "AC-coupled front-end for biopotential measurements," *Biomedical Engineering, IEEE Transactions on*, vol. 50, pp. 391-395, 2003.

[13] B. B. Winter and J. G. Webster, "Driven-right-leg circuit design," *Biomedical Engineering, IEEE Transactions on*, vol. 30, pp. 62 - 66, 1983.

[14] M. J. Burke and D. T. Gleeson, "A micropower dry-electrode ECG preamplifier," *Biomedical Engineering, IEEE Transactions on*, vol. 47, pp. 155-162, 2000.

[15] E. M. Spinelli, N. Martinez, M. A. Mayosky, and R. Pallas-Areny, "A novel fully differential biopotential amplifier with DC suppression," *Biomedical Engineering, IEEE Transactions on*, vol. 51, pp. 1444-1448, 2004.

[16] R. Pallas-Areny, J. Colominas, and J. Rosell, "An improved buffer for bioelectric signals," *Biomedical Engineering, IEEE Transactions on*, vol. 36, pp. 490-493, 1989.

[17] A. C. M. v. Rijn, A. Peper, and C. A. Grimberge, "Amplifiers for bioelectric events: A design with a minimal number of parts," *Medical & Biological Engineering & Computing*, vol. 32, pp. 305 - 310, 1994.

[18] F. Z. Padmadinata, J. J. Veerhoek, G. J. A. van Dijk, and J. H. Huijsing, "Microelectronic skin electrode," *Sensors and Actuators B: Chemical*, vol. 1, pp. 491-494, 1990.

[19] A. C. MettingVanRijn, A. P. Kuiper, T. E. Dankers, and C. A. Grimbergen, "Low-cost active electrode improves the resolution in biopotential recordings," presented at Engineering in Medicine and Biology Society, 1996. Bridging Disciplines for Biomedicine. Proceedings of the 18th Annual International Conference of the IEEE, 1996.

[20] E. S. Valchinov and N. E. Pallikarakis, "An active electrode for biopotential recording from small localized bio-sources," *BioMedical Engineering OnLine*, vol. 3, 2004.

[21] T. Degen and H. Jackel, "Enhancing interference rejection of preamplified electrodes by automated gain adaption," *Biomedical Engineering, IEEE Transactions on*, vol. 51, pp. 2031-2039, 2004.

[22] T. Degen and H. Jackel, "A Pseudodifferential Amplifier for Bioelectric Events With DC-Offset Compensation Using Two-Wired Amplifying Electrodes," *Biomedical Engineering, IEEE Transactions on*, vol. 53, pp. 300-310, 2006.

[23] E. M. Spinelli, N. H. Martinez, and M. A. Mayosky, "A single supply biopotential amplifier," *Medical Engineering & Physics*, vol. 23, pp. 235-238, 2001.

[24] C. R. Merritt, T.-H. Kang, B. Karaguzel, J. Wilson, P. D. Franzon, B. Pourdeyhimi, H. T. Nagle, and E. Grant, "Electrical Characterization of Transmission Lines on Nonwoven Textile Substrates," presented at Materials Research Society 2005 Spring Meeting, Symposium H, Paper H4.7, San Francisco, 2005.

Chapter 3

CAPACITIVE NONWOVEN FABRIC SENSORS FOR RESPIRATION MONITORING

ABSTRACT

In this paper we propose a novel design of a capacitive displacement sensor based on nonwoven fabric substrates. For the sensor, a unique fabric structure was devised using laterally connected one-dimensionally stretchable and non-stretchable nonwovens. An area-variable parallel plate capacitor placed on the flexible nonwoven substrates generates capacitance variance by sliding electrodes over each other along the sensor's extension axis. Electrodes can be formed by filling specified areas on the substrate with silver ink by screen printing or by hand. A single capacitive sensor and a differential sensor were designed and implemented to have linear sensing range along the horizontal sensor extension axis. This fabric sensor has significant advantages over sensors fabricated using traditional printed circuit board technologies in that they are less bulky and are conformal in the manner of the garment into which they are integrated.

I. INTRODUCTION

Electronic textiles (e-textiles), an emerging interdisciplinary field of research that encompasses electronics, materials science, and textiles, aims to seamlessly integrate electronic circuits, sensors, computing element, and communication into multi-functional textile products [1]. By utilizing textile substrates and processes, such as sewing, weaving, embroidering, laminating, and screen printing, e-textiles provide techniques whereby sensors can be fabricated on flexible substrates that can be directly integrated into garments. This approach has significant advantages over sensors fabricated using traditional printed circuits board technologies in that they are less bulky and are conformal in the manner of the garment into which they are integrated [2].

The literature shows that researchers have been active in attempting to integrate sensing elements and associated circuitry into textiles [3-7]. For example, researchers have fabricated strain gauge sensors from polypyrrole (PPy) coated Lycra® fabrics for human posture and gesture detection[3], or from carbon filled rubber (CFR) coated Lycra® fabrics for respiration monitoring [4]. These fabrics then became threads to form a sensor within a textile substrate. And, although these strain sensors did exhibit piezoresistive properties when stretched, the sensor exhibited undesirable characteristics such as inconsistent loading and unloading properties, which can be attributed to knitted structure of the Lycra® fabrics. This is a quality control issue. The "Respibelt" [6] is another example of a sensor system fashioned by a knitting fabrication process. The "Respibelt" is Lycra® substrate within which the sensing element is formed by incorporating a stainless steel yarn. The Lycra® provides compliance and the stainless steel provides the variation in electrical properties [6]. Extending and contracting the knitting structure alters both the impedance and inductance characteristics simultaneously. Experimentations with the sensors based on Lycra® substrates indicated that it was difficult to control and interpret the parameters that are intended to measure the relative variation of breathing. In addition, the researchers found that by using a substrate formed by knitting that it is difficult to form complex sensor patterns. It was further found that any additional processes required to integrate these sensors on a garment after the formation of the knitted structure (like sewing semi-metalized or metal conductive yarns to complete circuits) was time consuming and error prone.

In this paper we propose a novel design of a capacitive sensor, one based on a nonwoven textile substrate. This capacitive sensor can be: (1) directly integrated into clothing, and (2) can measure change in length in one-dimension. The two design characteristics noted are seen as being the key to fabricating a wearable sensor system for respiration monitoring. A successful sensor system is achieved by consistent quality control, both in the fabrication of the nonwoven fabric substrate and in the formation of the sensor and circuitry using screen printed conductive inks.

II. THE CAPACITIVE DISPLACEMENT FABRIC SENSOR

Capacitive sensors are widely used in industrial processes. They use different constructions to measure different parameters: e.g., position, angular speed, liquid level, and pressure [8, 9]. A basic parallel plate capacitor consists of two electric conductors separated by a dielectric. If fringe effects are neglected, the capacitance of a parallel plate capacitor is given by:

$$C = \frac{\varepsilon A}{d} = \frac{\varepsilon_0 \varepsilon_r A}{d} \quad \text{Farads} \tag{1}$$

where, A is the plate area, d is the plate spacing, ε is permittivity, ε_0 = 8.854pF/m is the dielectric constant for vacuum, and ε_r is a relative dielectric constant. Any variation of the geometrical arrangement, or of the dielectric characteristic of the conductors, results in variations in capacitance. The parallel plate capacitive sensors are easy to design and can easily be integrated on nonwoven textiles with good accuracy and resolution.

A. Structure of the Capacitive Fabric Sensor

A displacement sensor based on a variable parallel-plate capacitive and a nonwoven fabric substrate was designed and developed. Fig. 1 shows the construction of the fabric sensor. The compliant (stretchable) and non-compliant (non-stretchable) nonwoven substrates, that are integral parts of the design of the capacitive sensor, were designed to be attached to fixed and moving plates in a way that the completed assembly forms a capacitive sensor. That is, the stretchable fabrics respond to, for example volume changes, with an associated change of sensor length. Electrodes are formed on the non-stretchable fabric using a screen printing process and conductive ink. The conducting rectangles on the non-stretching fabric are the capacitor plates. The relative position of the two plates of the fabricated capacitor sensor changes when the sensor stretches, i.e., due to displacement changes. The capacitor plates are designed such that the conductors overlap. When stretching occurs, the plates move in opposite directions, thereby changing the effective area and hence the capacitance value.

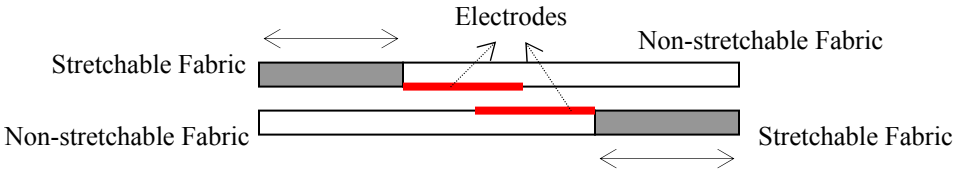

(a) Side view

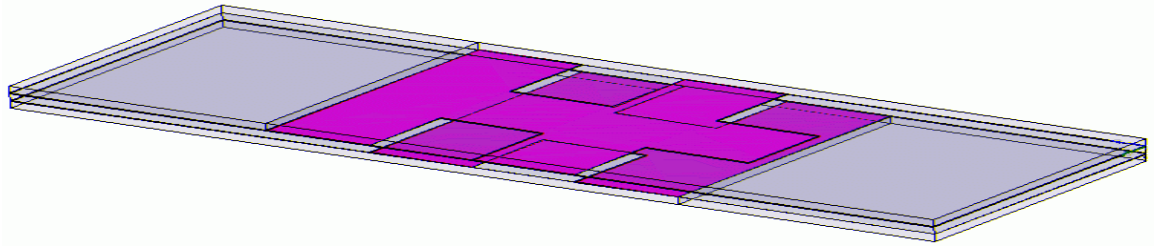

(b) 3D view

Fig. 1. Schematic diagram of the textile-based capacitor sensor.

Fig. 2 shows an example of the dimensions of each sensor electrode and the relative position of each with the sensor extension applied in the horizontal direction. Fig. 2(a) shows the sensor in its equilibrium position and Fig. 2(b) shows the sensor when it is fully stretched. By designing a capacitive sensor based on the interaction of stretchable and non-stretchable fabrics, the overlap of the two electrodes becomes a function of the geometry of the sensor electrodes and stretched length of the sensor. The design of this capacitive sensor differs from other capacitive sensors in that capacitance is based on the relative motion of two plates sliding in opposite directions simultaneously, not one fixed plate and one moving plate as is the more common design.

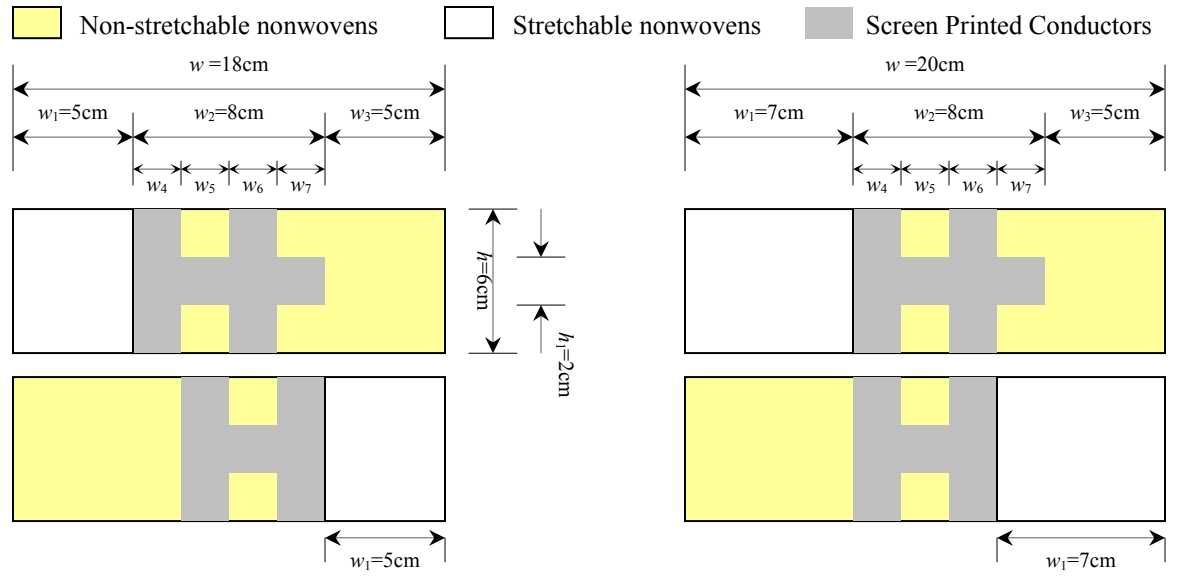

(a) Sensor in the equilibrium position (b) Sensor fully stretched 2cm (40%) horizontally

Fig. 2. The geometric arrangement of the capacitive sensor electrodes.

B. Variations in Capacitance

The capacitor sensor is designed to ensure the capacitance between the two electrodes increases linearly as the sensor stretches, due to the increase in the overlap area of the two plates. Assume that the sensor can be stretched to 40% of its original length at rest, then the dimensions (w_4 and w_6) of each vertical bar of the electrodes should kept to 40% of the length of the stretchable area to ensure linear variations in capacitance. Also, to ensure continuity, the dimensions (w_5 and w_7) between each vertical bar should keep to 40% of the stretchable length. If the dimension (w_1) of the stretchable nonwoven fabrics is 5cm when in the equilibrium position, then the length of the vertical bars and their spaces should be equal to 2 cm. If the sensor does not meet these specifications, the variation in capacitance variance will not be linear. As the length of the sensor increases beyond 40% there will be interference from the vertical bars of the plates of the electrode.

The fabric capacitive sensor has been designed to ensure that the overlap of the conductive area A_{var} varies linearly with the stretched length, within the limits of minimum duplicated area A_{min} and

maximum duplicated area A_{max}. The formulas for calculating the conductive area of the sensor and the sensor limits are given by:

$$\begin{aligned} A_{var} &= (N+1)w_4h_1 + Nw'(h-h_1) \\ A_{min} &= (N+1)w_4h_1 \\ A_{max} &= (N+1)w_4h_1 + Nw_4(h-h_1) \end{aligned} \tag{2}$$

where, N indicates the number of the conductive vertical bar in sensing area, and w' is the maximum stretched length of the sensor. The width of vertical bars and their spaces are assumed to be equal. Because the overlapped conductive areas increase linearly along the axis that the sensor is being stretched, the variations in linear capacitance resulting from the changes in conductive areas in equation 2 are as follows:

$$\begin{aligned} C_{var} &= \frac{\varepsilon A_{var}}{d} = \frac{\varepsilon\{(N+1)w_4h_1 + Nw'(h-h_1)\}}{d} \\ C_{min} &= \frac{\varepsilon A_{min}}{d} = \frac{\varepsilon(N+1)w_4h_1}{d} \\ C_{max} &= \frac{\varepsilon A_{max}}{d} = \frac{\varepsilon\{(N+1)w_4h_1 + Nw_4(h-h_1)\}}{d} \end{aligned} \tag{3}$$

where, ε is the permittivity of the intermediate material and d is the distance between two substrates. The variation in capacitance depends only on the change in the length of the sensor along the axis of stretch and on the number of the conductive elements, or bars, in the sensing region. The sensor generates minimum capacitance when the sensor is in its equilibrium position. The dimension of the conductive bars (h_1), orthogonal to the axis of stretch, ensures minimum capacitance regardless of the stretched length of the sensor. Only the dimensions in the axis of stretch (w) change the capacitance by altering the areas of the conductive elements, one relative to the other, on the non-stretchable fabric.

C. Sensitivity and Sensing Range

The sensitivity of the capacitive sensor along the expanded length is given by

$$\text{Sensitivity} = \frac{\partial C_{\text{var}}}{\partial w'} = \frac{N(h - h_1)}{d} \tag{4}$$

As the number of the vertical bars increases, the capacitance change increases. However, because of the nature of the design of this sensor, an increase in the number of the vertical bars results in a corresponding reduction of the width of the vertical bars. Based on the design philosophy outlined in Section ***B***; an increase in the number of conducting elements (bars) results in a corresponding limit being placed on the range of sensing along the axis of stretch. Put simply, if four vertical bars are placed on the given sensor, then the sensitivity will be doubled while the sensing range will be halved. So, a design compromise will have to be made between the linear sensing range and the rate of variation in capacitance if the dimension of the sensor is limited. Sensitivity is also related to the height (h_1) of the horizontal bar. If we decrease the height, then the sensitivity increases. However, a minimum capacitance is required if the capacitor is used as a component in an oscillator circuit. Once again a design compromise between minimum capacitance and sensitivity has to be made.

D. Modified Electrodes

The sensor design in Fig. 2 does not perform well in simulations due to the presence of fringe electric fields. Also, the performance of the sensors is degraded by misalignment of the two electrodes. Since the nonwoven substrates are quite flexible, the two substrates layers tend to misalign, generating unexpected capacitance. Misalignment may also occur during the fabrication stage. By modifying the top plate electrode pattern, the effects of sensor misalignment can be minimized. Fig. 3 shows the original and modified electrode patterns. The electrode pattern on the top plate (Fig. 3 left image) is taller and its shape is different. In the new design, we remove the horizontal bar area, $w_7 \times h_1$ of the Fig. 2 while making the h' size two times the size of h. The height of the horizontal bar in the top plate should be two times the horizontal bar in the other. Changing the design does not affect the generated overlap between the two electrodes.

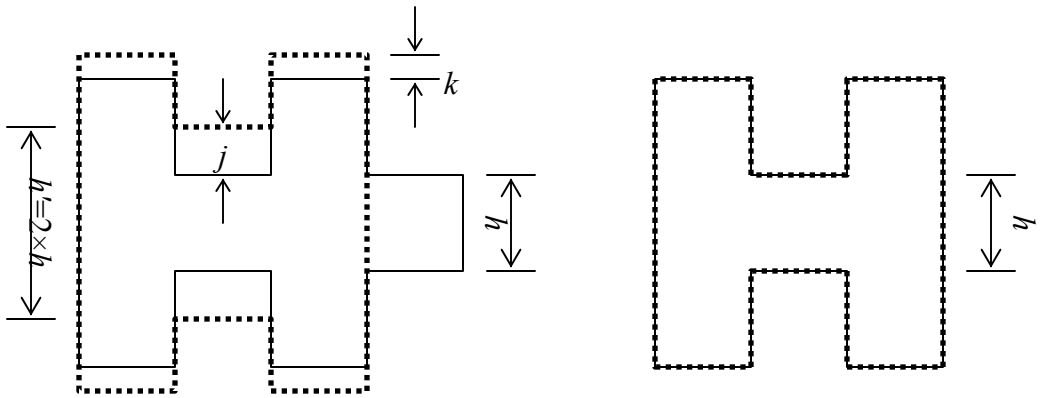

(a) Top plate (b) Bottom plate

Fig. 3. The modified electrode patterns of the capacitive sensor; original design (solid lines), modified electrodes (dotted lines).

The vertical bars are elongated vertically by length 2*k*. All the areas enlarged by *j* or *k* provide a margin to allow the other electrode's misalignment. In the modified design, misalignment does not change the overlap between the two electrodes (see Fig. 4). The smaller value of *j* and *k* determines the maximal amount of misalignment if the sensor is to maintain linear sensitivity.

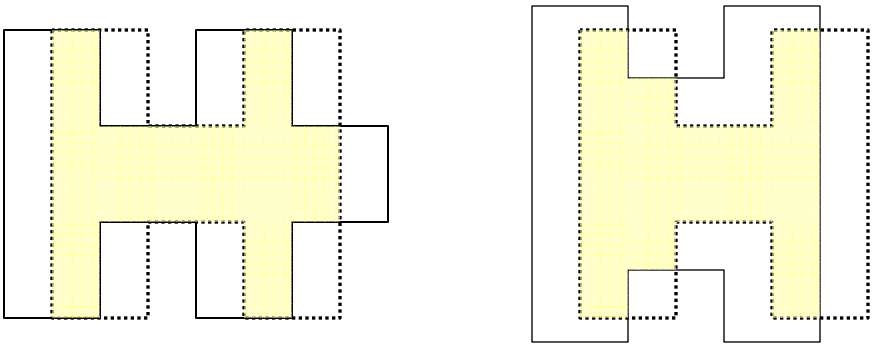

(a) Overlap between the two electrodes (yellow area) with no misalignment. No change in the overlapping areas.

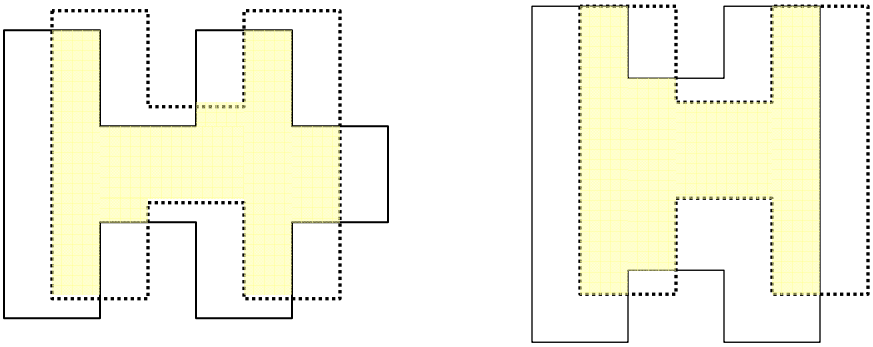

(b) Overlap between two electrodes with misalignment. Changes occur in the overlapping areas.

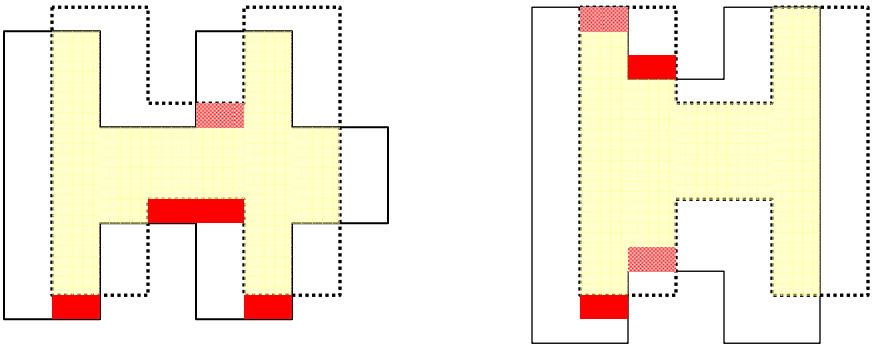

(c) Analysis of changes in the overlapping areas due to misalignment. Solid red rectangles indicate the losses in overlapped area and cross-hatched red rectangles show increases in the overlapped area. In left image for the original design, the losses and increases in area are not equal. In right image for the modified design, misalignment does not change the amount of overlapped area.

Fig. 4. Changes of overlap between the two electrodes due to misalignment in the original design (left) and the modified design (right). The dotted lines are for the top electrode; the solid, the bottom.

Even though the overlapped area in the modified design is unchanged regardless of any misalignment smaller than *j* and *k*, variations in alignment generate variations in total capacitance due to fringe effects. To minimize these fringe effects, we insert extra shield plates to isolate the electrodes within the plane of the nonwoven substrates. Fig. 5 shows the final design of electrodes with planar outside shielding plates. The design allows a maximum displacement of 5 mm in the direction orthogonal to the strain applied. Even with these changes in the design, the sensor's capacitance and sensitivity are still governed by equations (3) and (4), respectively.

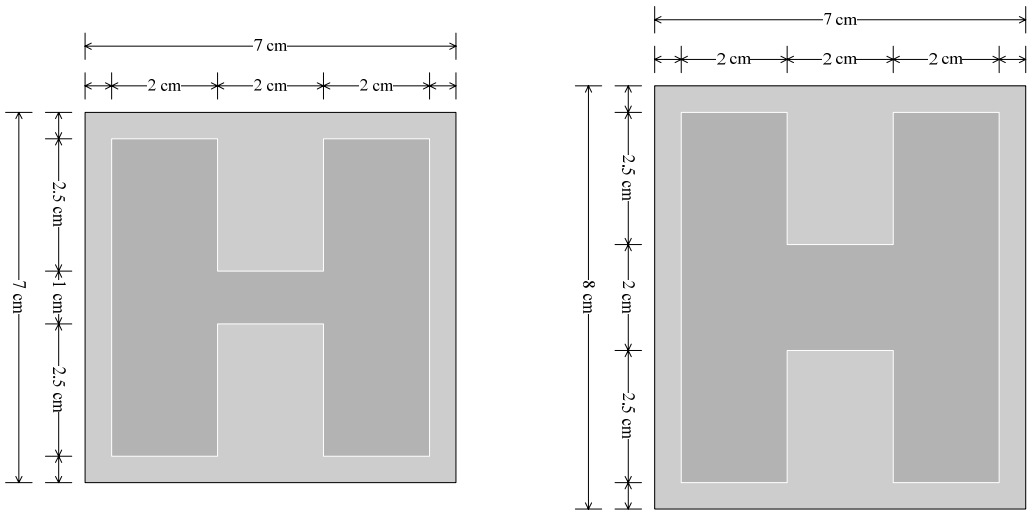

Fig. 5. The modified electrode patterns with planar shield plate. Dark rectangular areas indicate electrodes on the top side and light gray rectangular areas represent a shield on the back side to reduce fringe-field effects and isolate the electrodes from stray electric fields. Note that the dimensions are changed compared with Fig. 2 so that the overlapped areas between the two electrodes are reduced.

E. Characteristics

The fabric-based capacitive sensor has some useful features. First, the sensor gives repeatable and consistent data. That is, the sensor generates the same capacitance at a given stretched length, irregardless of whether the applied load is increasing (stretching) or decreasing (contracting) along the axis of stretch. Second, we can design the capacitive strain gauge sensor, one that generates less capacitance as the sensor stretches, using the similar conductor patterns. By mirroring the conductor on the top substrate with horizontal direction at the same place in Figure 2(a), the sensor electrodes

line up and thereby generate a maximum capacitance. However, when the sensor stretches there will be a resulting decrease in capacitance due to the decreasing area of two electrodes. Finally, we can also utilize the variation in stretched length to make a pressure sensor. Breathing will stretch this sensor as a function of the air volume change in the chest cavity, and compress the distance between the electrodes at the same time. As such, breathing pressure can be correlated to variation in capacitance. By utilizing the variation in stretched length along with the variation in the distance between the electrodes, which are both caused by the variation of pressure caused by breathing, we can double the variation in capacitance. This is due to the fact that variation in capacitance is governed by the conductive area and the distance between two conductive layers.

III. THE DIFFERENTIAL CAPAICTIVE FABRIC DISPLACEMENT SENSOR

To reduce potential static interference effects in fabric-based capacitive sensor (perhaps due to moisture, substrate shrinkage, and the like), a differential capacitive sensor was designed. In this design, the differential capacitor consists of two variable capacitors arranged such that they give the same variation in capacitance regardless of which direction they move, one relative to the other [8]. For example, in Fig. 6, if a top conductor (a pickup plate) moves laterally with respect to the two rectangular electrodes below (a) or the v ramp electrodes below (b), then the capacitance of each conductor varies equally whether it moves to the right or to the left. The capacitive sensor having rectangular-type electrodes has linear sensibility along the sensor extension due to a linear duplicated area change. However, in comparatively large flexible fabric substrate, it is difficult to keep the plate-to-plate distances, between the pickup plate and the electrode E1 and between the pickup plate and the electrode E2, always equal due to bending and tilting. This may cause unbalanced differential capacitance variance. In the capacitive sensor having V-pattern electrodes, the distance difference between the pickup plate and two electrodes may be better than the former capacitive sensor. However the capacitance variance is not linear along the sensor's extension axis.

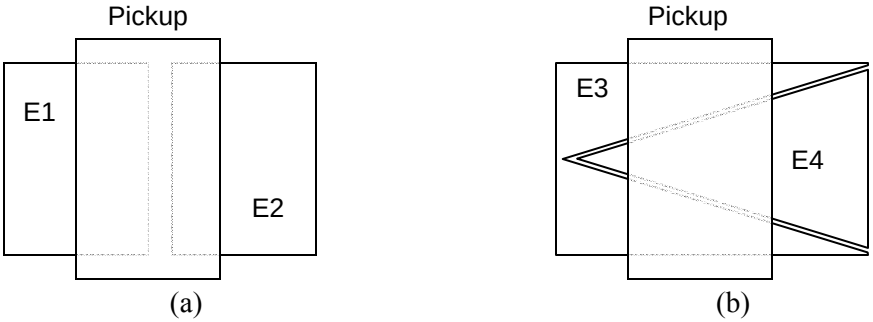

Fig. 6. Area-variable differential capacitive sensors using three electrodes (top view) [6].

A. Design of a Differential Sensor

Fig. 7 shows an example of a differential capacitive sensor design, one based on using nonwoven fabric substrates. In this design two comb electrodes combine to cancel out static interference effects. Even though the comb electrode pattern means a sacrifice the sensing range (approximately half of that obtained from a purely lateral pattern sensor), the sensitivity experienced by this new design will be almost twice that of the lateral pattern sensor based on the same dimensions.

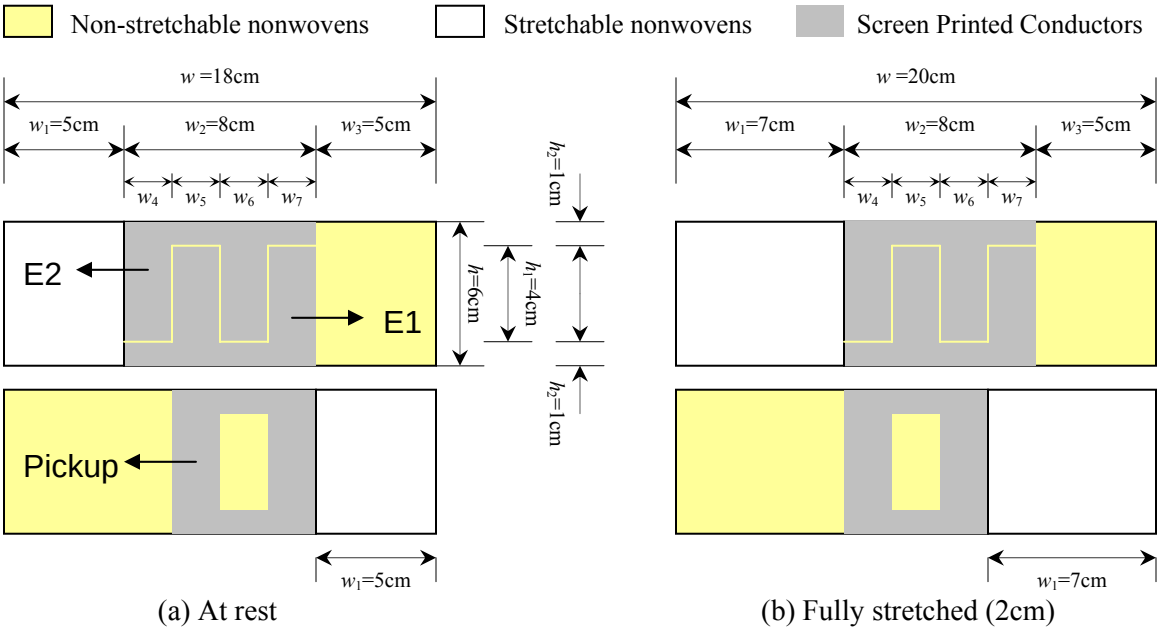

(a) At rest (b) Fully stretched (2cm)

Fig. 7. The design example of the new differential capacitive respiratory sensor.

The overlapped conductor areas between pickup plate and each electrode E1 and E2 are

$$A_{E1} = (N+1)w_4h_2 + N(w_4 - w')h_1 \quad \text{and} \quad A_{E2} = (N+1)w_4h_2 + Nw'h_1 \tag{5}$$

where, w' is the pure stretched length of the sensor. The overlapped areas change between minimum and maximum ($A_{\min}$ and $A_{\max}$) which are given by

$$A_{\min} = (N+1)w_4h_2 \quad \text{and} \quad A_{\max} = (N+1)w_4h_2 + Nw_4h_1 \tag{6}$$

Hence, the capacitances C1 and C2 are

$$C1 = \frac{\varepsilon\{(N+1)w_4h_2 + N(w_4 - w')h_1\}}{d} \quad \text{and} \quad C2 = \frac{\varepsilon\{(N+1)w_4h_2 + Nw'h_1\}}{d} \tag{7}$$

where, d is distance between two conductive plates. Also, the minimum and maximum capacitances are given by

$$C_{\min} = \frac{\varepsilon\{(N+1)w_4h_2\}}{d} \quad \text{and} \quad C_{\max} = \frac{\varepsilon\{(N+1)w_4h_2 + Nw_4h_1\}}{d} \tag{8}$$

Electrode E1 has maximum capacitance while electrode E2 has minimum capacitance in the equilibrium state, i.e., at rest. As the sensor stretches, the capacitances change in opposite direction. If the sensor stretches fully, then electrode E2 with pickup plate has maximum capacitance while electrode E1 with pickup plate has minimum capacitance. The sensitivity of each sensor is

$$\text{Sensitivity for } C1 = \frac{\partial C1}{\partial w'} = \frac{-Nh_1}{d} \text{ and, Sensitivity for } C2 = \frac{\partial C2}{\partial w'} = \frac{Nh_1}{d} \tag{9}$$

As shown in the sensitivity equation (9), as the sensor is stretched the capacitance change is exactly the same for each capacitive sensor but in opposite direction. This is indicated by the sign change in equation (9).

B. Correction of Misalignment Effect

The designed differential sensor may suffer from unwanted changes of overlapped areas in two electrodes since the vertically deviated pickup electrodes affect differently as shown in Fig. 8. To reduce the effect of deviation from unwanted direction, that is orthogonal direction to the stretched

direction, the pickup electrodes are modified. The two horizontal bars of the pickup electrode are expanded toward both up and down by the amount of a given value (h_5) as shown in right image of Fig. 8(a). Two inside vertical bars in the bottom two electrodes are reduced and increased by the value, respectively. Length of h_3 and h_4 should be equal and size of h_5 should be equal to or greater than h_3 and h_4. The maximal amount of misalignment is determined by length of h_3 and h_4.

As shown in Fig. 8(a), overlapped areas between the pickup electrode and each bottom electrodes in the modified design are equal to those of the original design. The increased and decreased overlapped areas due to the misalignment are always same within the maximally allowable amount of misalignment of the pickup electrode in the modified design but not in the original design as shown in Fig. 8 (c). Fig. 9 shows the final design of electrodes with planar outside shielding plates for the differential sensor. The modified differential sensor's capacitances and linearity are still determined by equation (7) and (9), respectively.

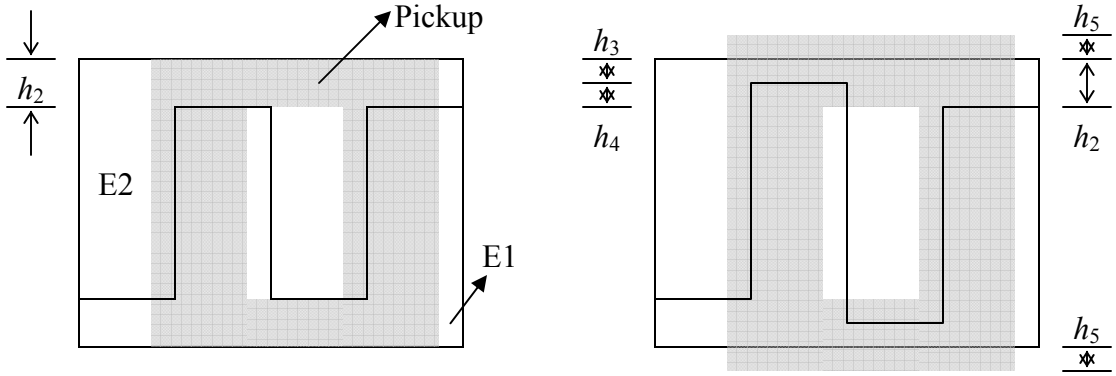

(a) Original pickup electrode pattern (left) and modified pattern (right)

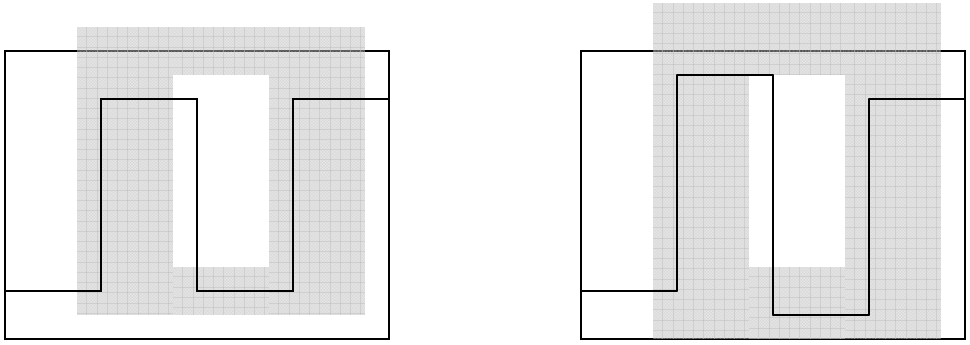

(b) The deviated pickup in the original pattern (left) and in the modified pattern (right)

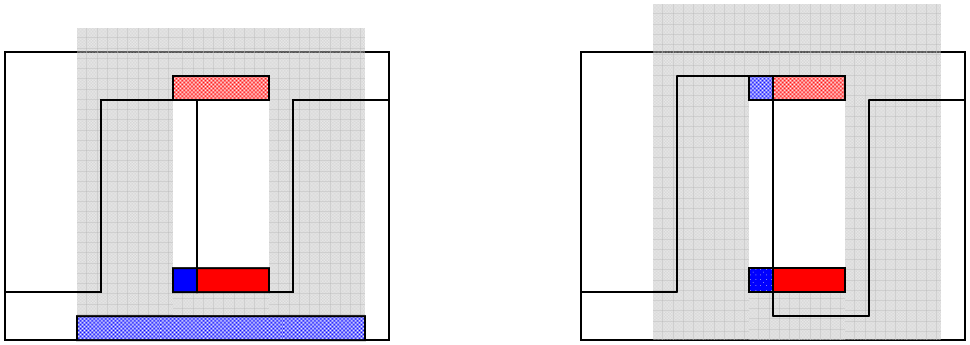

(c) Overlapped area changes due to misalignment. The solid blue areas and dotted blue areas are increased and decreased area in electrode E1 respectively. The solid red areas and dotted red areas are increased and decreased area in electrode E2 respectively.

Fig. 8. Schematic diagrams of the modified electrode patterns for the differential sensor.

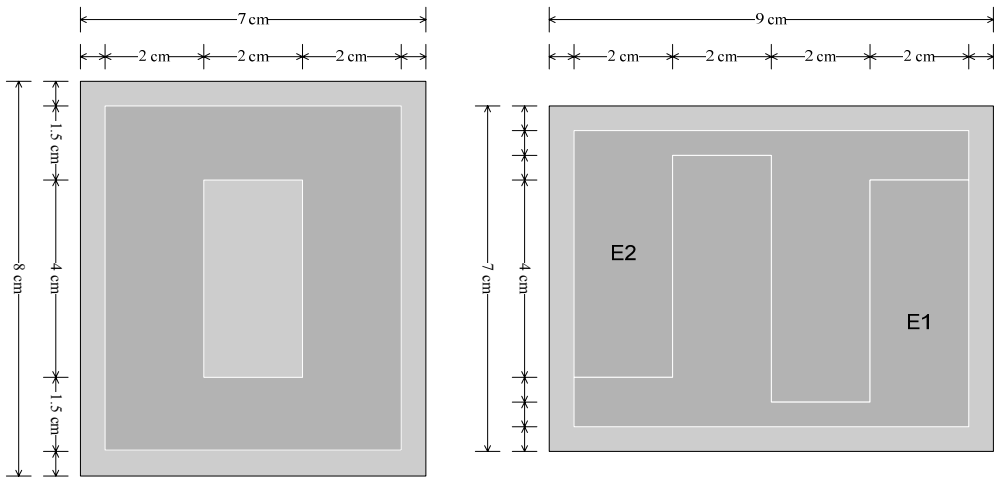

Fig. 9. The modified electrode patterns with planar shield plate for the differential sensor. Dark and light gray rectangles indicate top-side electrodes and back-side shield to reduce the back-plane fringe-field effect and prevent the electrodes from stray electric field, respectively.

IV. SIMULATION RESULTS

In this section, single and differential capacitive sensors were simulated using Q3D Extractor® software from the AnSoft® Corporation for evaluation of performance. This software extracts RLC parameters for a 3D sensor design and gives an equivalent circuit model. Throughout the simulations, we assumed that the depth of printed conductive plates was 200 μm and the distance between two conductive plates was 1.8 mm.

A. Single Capacitive Sensor

First, two designs, original (Fig. 2) and modified (Fig. 5), in the single capacitive sensor were simulated to evaluate performance. In the simulation a capacitance value was extracted for every 1 mm variation. Fig. 10 shows the simulation results. The simulation results show that the capacitance in both designs increased in a near linear fashion as the sensor was stretched. Note that the sensor with the original electrode pattern generates more capacitance but less sensitivity with sensor extension. Two possible reasons for this behavior are: 1) the modified sensor has less overlapped areas between two electrodes and hence less ability to adapt for misalignment of two electrodes, and 2)

the original sensor may experience more back-plane field coupling effects. When the original sensor is fully stretched, the overlapped conductive areas are more than twice the case when the sensor is in its equilibrium position (at rest). However, the capacitance of the sensor when fully stretched is less than twice the capacitance of the sensor at rest. This is due to the fringe, or back-plane, effect. The back-plane effect can be seen by examining the charge distribution images as shown in Fig. 11. The charge distributions of the back sides that do not face with the other conductor are uneven and different according to the relative position of each electrode.

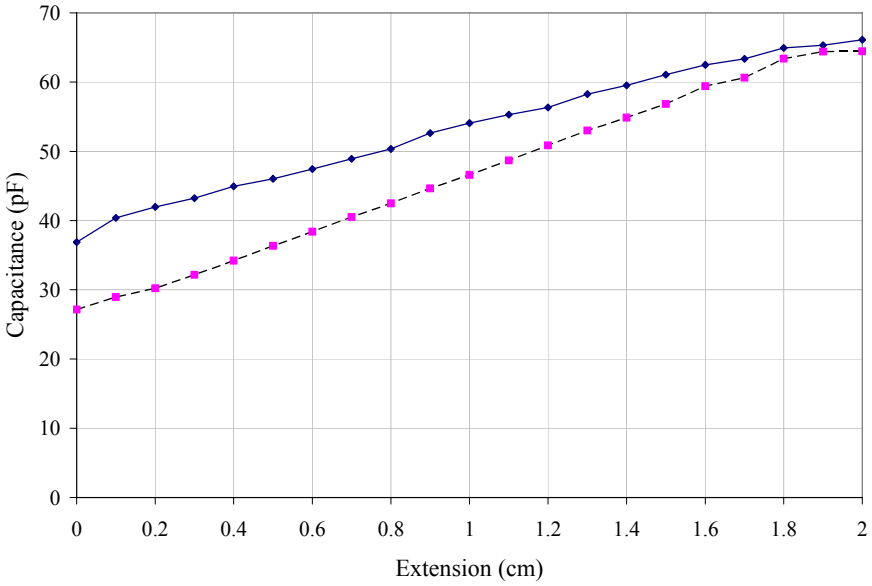

Fig. 10. Simulation results for capacitance variation along with extension of the sensor. Solid and dashed lines indicate capacitance variance of the original and modified designs, respectively. In this simulation, the modified design did not include the shield plates.

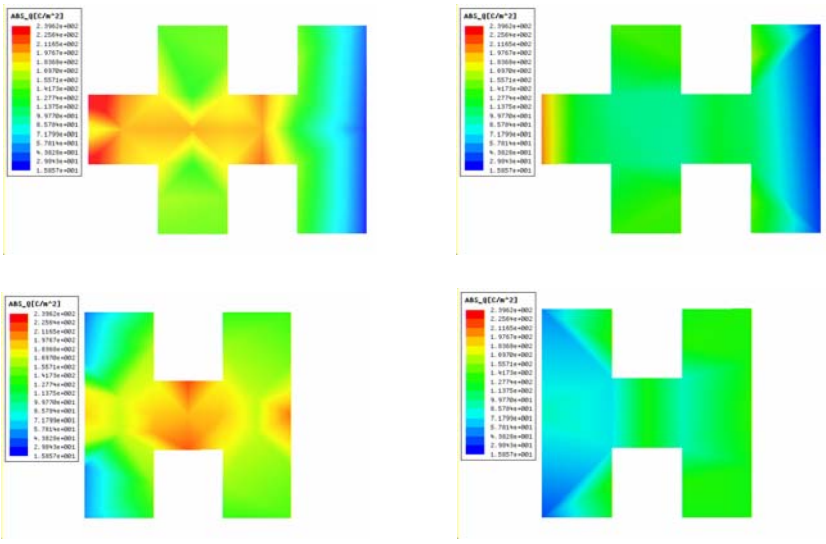

(a)

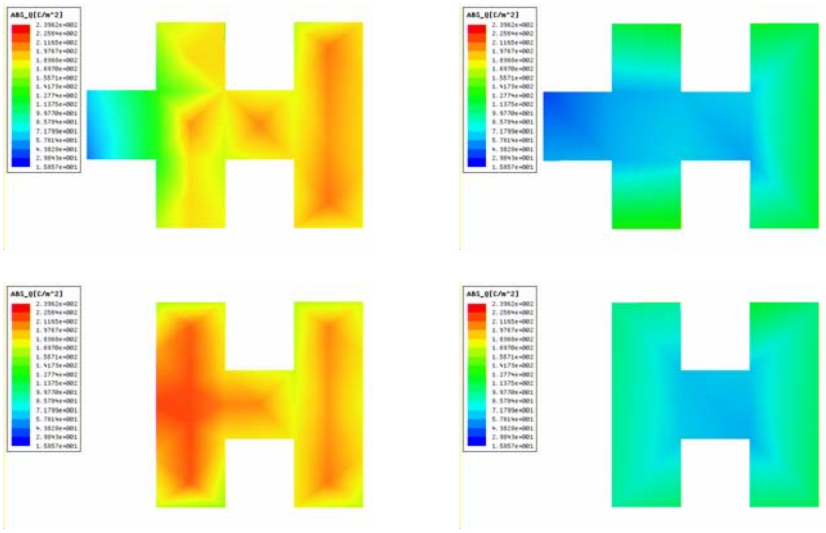

(b)

Fig. 11. Simulation results for charge distributions on the electrodes with the original design of the single capacitive sensor (a) at rest and (b) at fully stretched status. The left images show the charge distribution on the sides faced with the other conductor while the right images indicate the charge distribution in the back sides of the conductor.

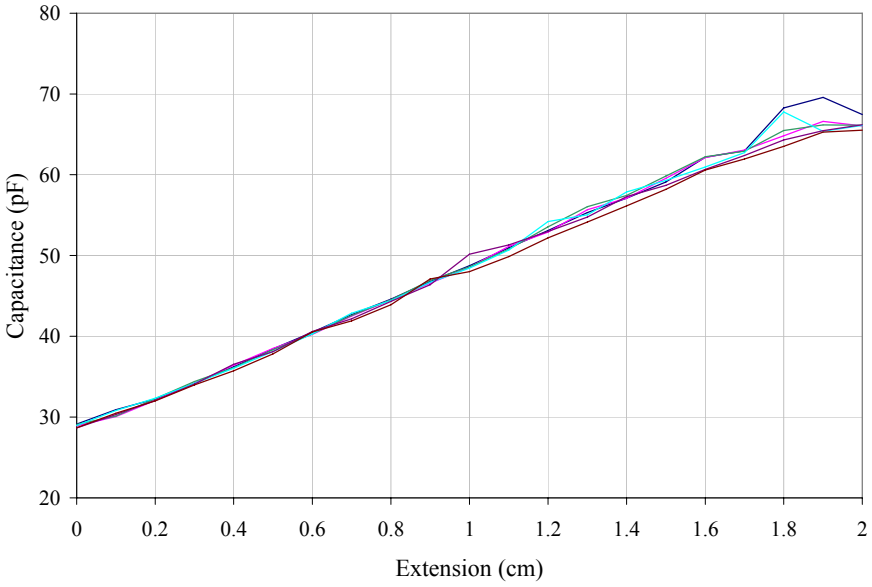

(a)

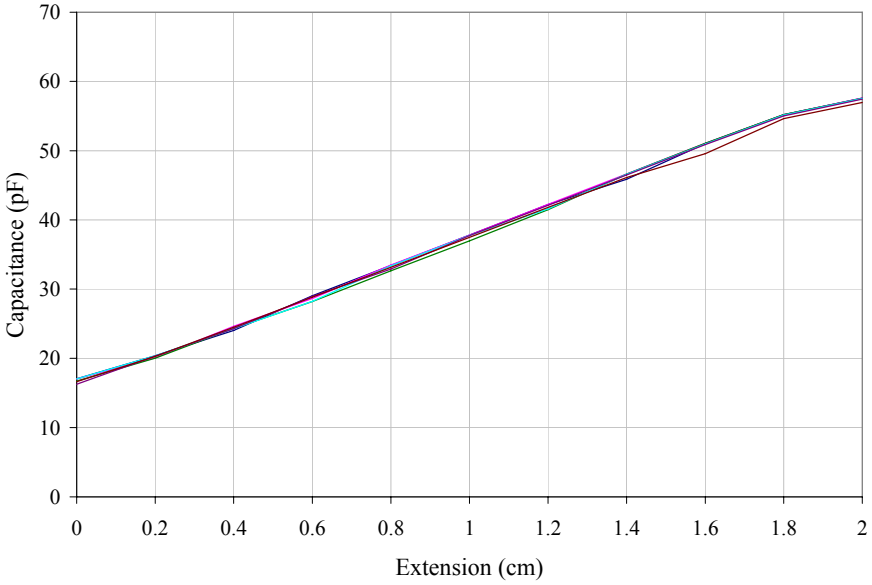

(b)

Fig. 12. Capacitance variance of the modified single capacitive sensor along misalignment between the two electrodes (a) without a shield and (b) with the shield plates. Each of the six lines indicates the capacitance variance when the vertical misalignment of the two electrodes is 0, 1, 2, 3, 4, and 5 mm, respectively.

Fig. 12 shows capacitance variance along different misalignments between the two electrodes in the modified single capacitive sensor. The sensor with the shield plates generates less capacitance by reducing back plane effects and has less offset of capacitance along misalignment of the two

electrodes. In Fig. 12 (a), increasing offset in extension intervals more than 1 cm may be due to an increasing back plane effect. In Fig 12 (b), the max offset is 1.487 pF and this level of misalignment is probably at the computational accuracy of the algorithm. Fig. 13 shows capacitance variance along different gaps between the two electrodes in the modified single capacitive sensor.

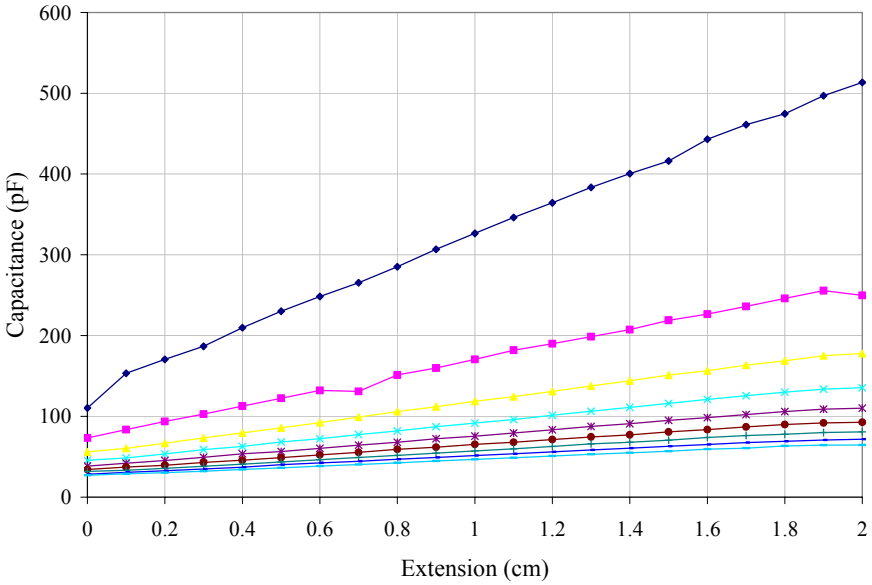

Fig. 13. Capacitance variance of the modified single capacitive sensor along different gaps between the two electrodes. From the top, each line indicates the capacitance variance when the gap is 0.2, 0.4, 0.6, 0.8, 1.0, 1.2, 1.4, 1.6, and 1.8 mm, respectively.

B. Differential Capacitive Sensor

Two differential capacitive sensors, the original (Fig. 7) and the modified design (Fig. 9) were also simulated. Fig. 14 shows the simulation results of the original and modified differential capacitive sensors without shield plates along sensor extension. The capacitance in both designs increases and decreases same amount but in opposite directions. Note that there is a non-linearity at the ends of the plots. This is probably caused by the back-plane effect. In addition, the sensor with the modified design generates more capacitance. The pickup electrode of modified design is wider than two other electrodes and generates more fringe fields.

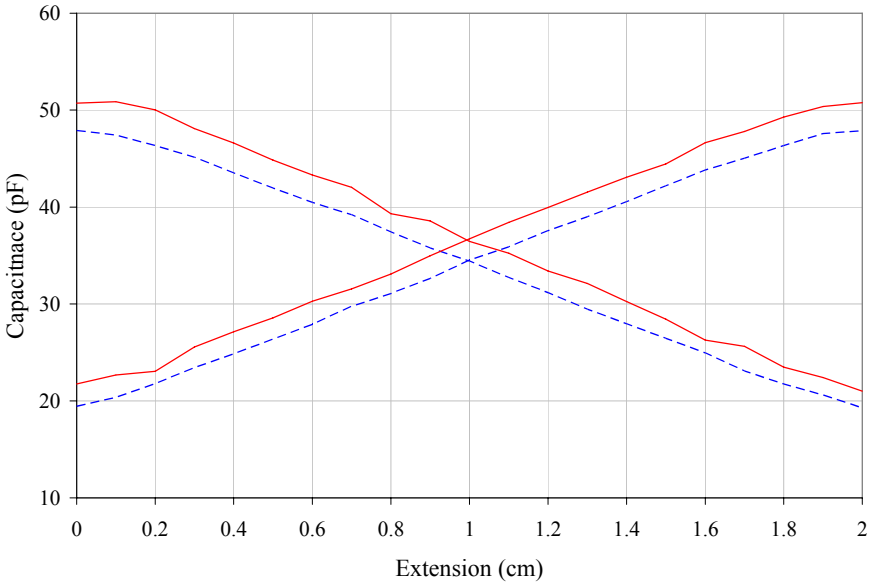

Fig. 14. Simulation results for capacitance variance of the differential capacitive sensor with sensor extension. Dashed and solid lines indicate the capacitance variance of the original and modified design without the shield plates, respectively.

Fig. 15 shows the capacitance variance of the modified design with changes in the vertical misalignment of two substrates. There seems to be little difference in capacitance C2 (between the pickup and E2 of Fig. 9) along with the misalignment, with and without the shield plates. With misalignment, the pickup electrodes move up toward electrode E2 which does not affect to capacitance C2. If the misalignments are 4 mm (the line with the rectangular markers in Fig. 15 (a)) and 5 mm (the line with triangle markers in Fig. 15 (a)), the back-plane effect is reduced and hence capacitance C1 is smaller than the capacitance obtained at the other misalignment (0, 1, 2, and 3 mm cases). As shown in Fig 15 (b), this difference can be mitigated by employing shield plates.

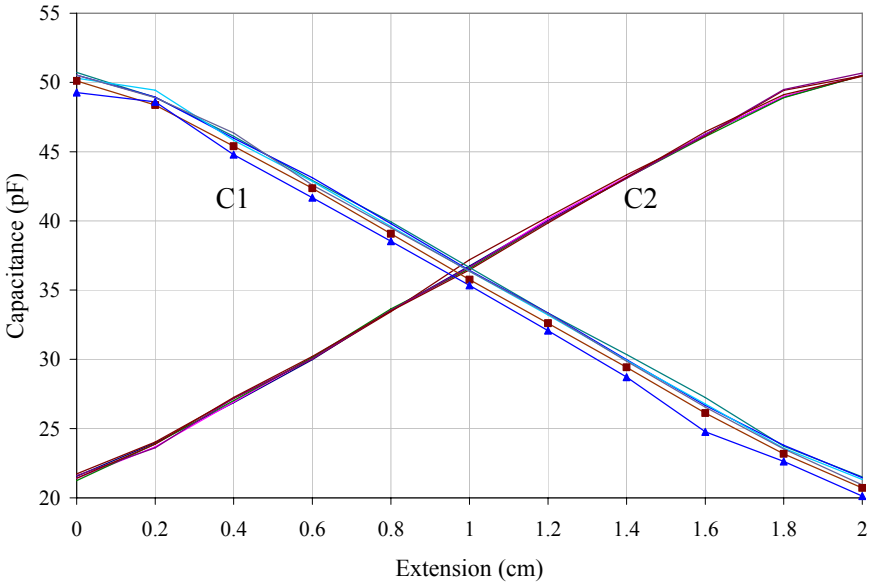

(a)

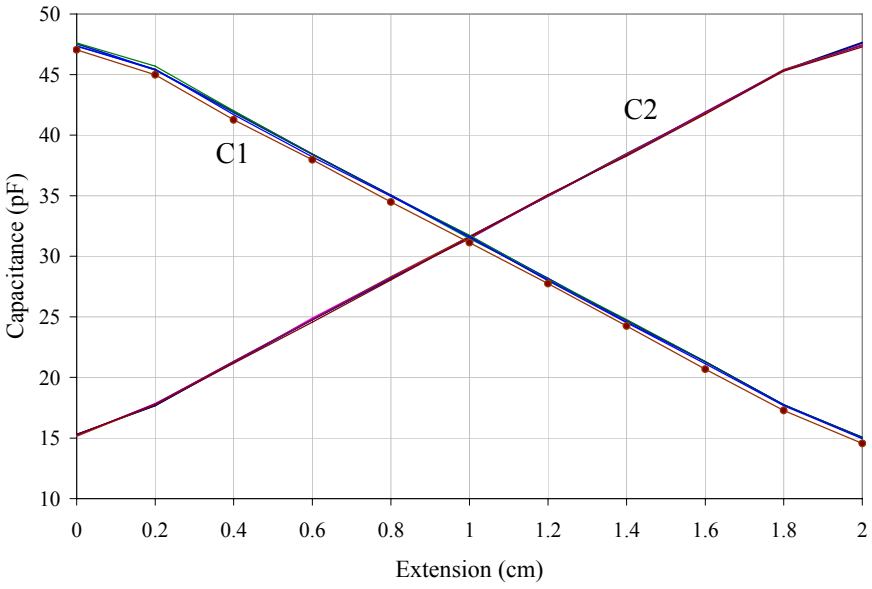

(b)

Fig. 15. Simulation results for capacitance variance of the differential capacitive sensor with vertical misalignment (a) without a shield and (b) with the shield plates. Each of the six lines indicates the capacitance variance when the vertical misalignment of the two electrodes is 0, 1, 2, 3, 4, and 5 mm, respectively.

V. EXPERIMENTAL RESULTS

In this section, we presented experimental results for the modified single and differential capacitive sensors.

A. Instrumentation

To detect capacitive variance with changes in sensor extension, different analog circuits are required for the single and differential capacitive sensor configurations. Fig. 16 shows a functional block diagram to capture the respiratory signal using the single capacitive sensor.

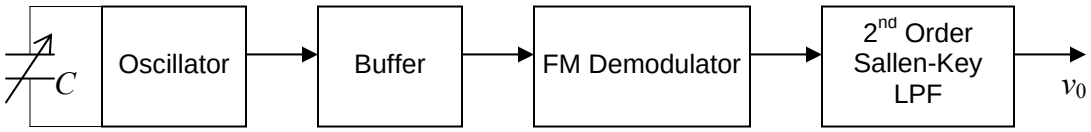

Fig. 16. Functional block diagram to detect capacitance variance for the single capacitive sensor.

Capacitance variance is converted into a frequency shift or pulse width change. For frequency shifting, we employed an R-C oscillator circuit that includes CMOS 7555 timer as shown Fig. 17 [8]. Frequency of an oscillating output signal is determined by 1/RC.

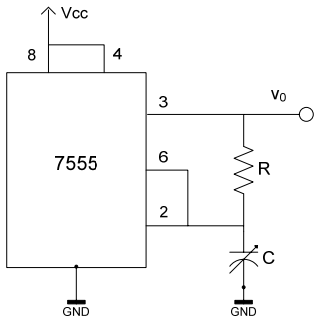

Fig. 17. RC Oscillator Circuit with a CMOS timer (7555).

After the RC oscillator, a buffer amplifier was employed to isolate the oscillator from the load so that the frequency would be more stable. The frequency shift was detected by a FM demodulator and then the detected signals were low pass filtered.

For the differential capacitive sensor, capacitance variance can be determined by the ratio between the two variable capacitors. The steps in signal detection are presented in the function diagram of Fig. 18. In the first step, the circuit of Fig. 19 generates output signals whose amplitudes are controlled by two capacitances of the differential sensor. In the next step in Fig. 18, the output of the op amp is amplified and then supplied to an envelop-detector circuit (a half wave rectifier) to extract amplitude of the ac signals being generated by the sensor. Then a differential amplifier compares the envelope signal with a reference voltage. Finally the output of the differential amplifier is low-pass filtered using a 2nd order Sallen-Key filter.

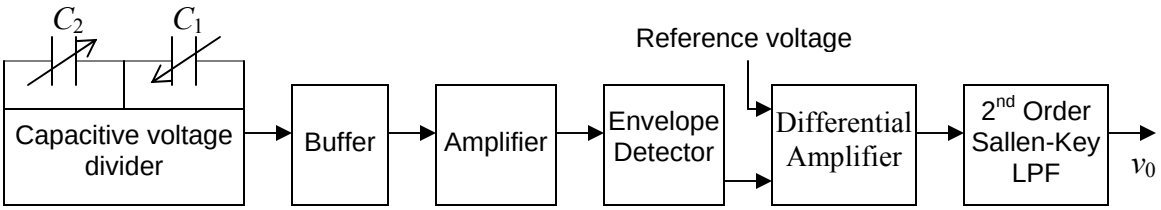

Fig. 18. Functional block diagram to detect capacitance variance for the differential capacitive sensor.

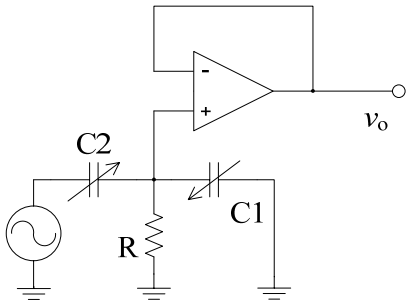

Fig. 19. Analog circuit to detect variations in capacitors C1 and C2 of the differential sensor.

B. Fabrication of prototype fabric capacitive sensors

To demonstrate proof-of-concept, prototype capacitive sensors for the modified designs of Fig. 5 and 9 were built without shield plates using stretchable and non-stretchable nonwoven textiles. To attach the stretchable and non-stretchable nonwovens laterally and seamlessly, we bonded them using an ultrasonic machine. To ensure compatibility with ultrasonic bonding, both the stretchable and non-stretchable nonwoven fabrics must possess similar material properties. In this experiment, a non-stretchable, nonwoven fabric (Evolon®, 70% PET and 30% Nylon) was attached to a stretchable version of the same fabric, processed in a manner to make it extendable in one dimension [10].

The prototype sensors were fabricated by first screen printing silver inks onto the nonwoven substrates and then cutting out the electrode patterns into the desired shapes. The electrodes were then glued onto non-stretchable bands of the same fabric. External wires were attached using conductive epoxy. The bands of non-stretchable and stretchable nonwoven substrates then were assembled to form the sensors as shown in Fig. 20.

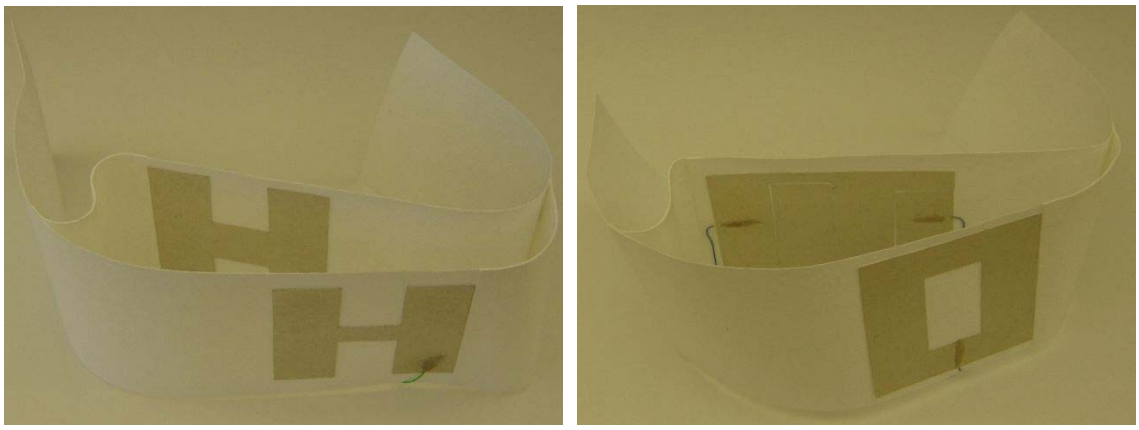

(a) (b)

Fig. 20. Prototype capacitive sensors without shielding plates: (a) single and (b) differential designs.

C. Experimental Results

For the prototypes, capacitance variances were measured using B+K PRECISON® Digital LCR meter model 875B. Fig. 21 shows the results for the single sensor, measured by increasing overlapped areas between the two electrodes in increments of 1 mm along the stretchable axis. Note that the graph pattern is very similar to the pattern in Fig. 12 (a), but with more variation at extensions of under 1.5 mm.

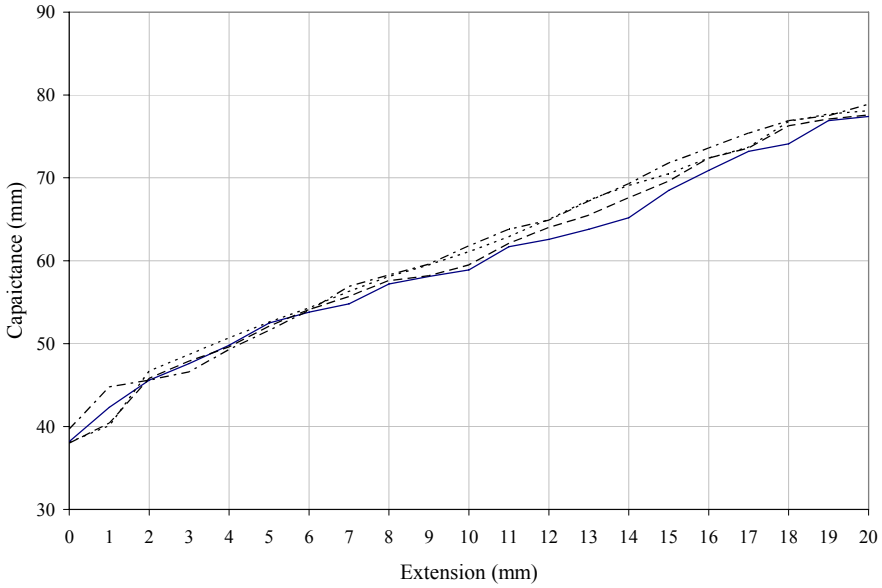

Fig. 21. Experimental measurements of capacitance variance of the single capacitive. The solid, dashed, dotted and dot-dashed lines indicate the capacitance variance when the vertical misalignment is 0, 1, 2, and 3 mm, respectively.

Fig. 22 shows the experimental RC oscillator output when the sensor was at rest (2 mm stretched, the two electrodes are minimally overlapped without pressure) and fully stretched (2 cm stretched, the two electrodes are maximally overlapped with pressure). This oscillation signal drives the FM demodulator of Fig. 16.

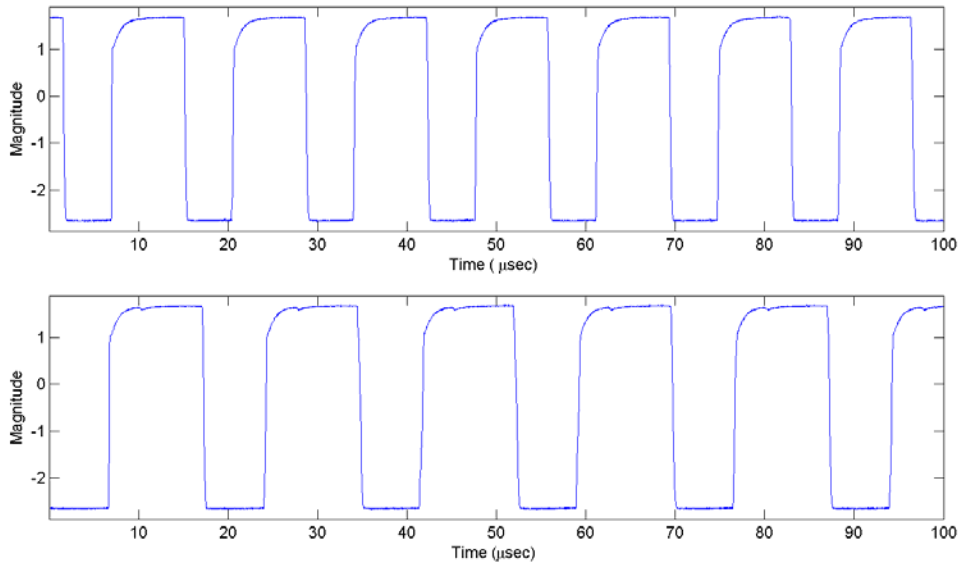

Fig. 22. Experimental RC oscillator outputs when the sensor is at rest (top) and stretched fully (bottom).

Finally, we tested the single capacitor prototype by stretching it approximately 1 cm across the chest of a subject at a controlled rate representative of respiratory signals as shown in Fig 22.

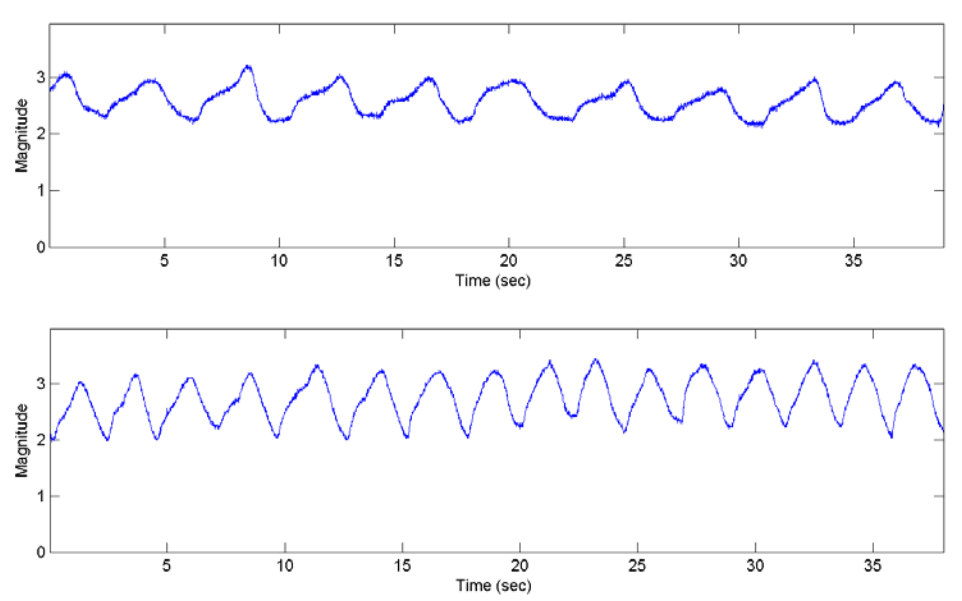

Fig. 23. Detector output magnitude (volts) versus time (seconds) for respiratory-type signals at (a) 14 breaths/min and (b) 25 breaths/min. The positive and negative peaks represent the transitions from inspiration to expiration, and vice versa.

VI. CONCLUSIONS

Nonwoven fabric sensors using single capacitors and differential capacitors to measure the respiratory signals have been designed, simulated, and tested. Prototype sensors were fabricated via screen printing and a combination of stretchable and non-stretchable fabric segments. Respiratory signals were captured with the single capacitive sensor and a simple detection circuit. The computer simulations as well as the experimental measurements show the feasibility the concept. The proposed fabric capacitive sensors work well and can be integrated into garments. Future work includes the fabrication of the sensor using other textile processing techniques and substrates.

REFERENCES

[1] P. S. Stanley-Marbell, D. Marculescu, R. Marculescu, and P. K. Khosla, "Modeling, analysis, and self-management of electronic textiles," *Computers, IEEE Transactions on*, vol. 52, pp. 996-1010, 2003.

[2] C. R. Merritt, B. Karaguzel, T.-H. Kang, J. Wilson, P. D. Franzon, B. Pourdeyhimi, H. T. Nagle, and E. Grant, "Electrical Characterization of Transmission Lines on Nonwoven Textile Substrates," presented at Materials Research Society 2005 Spring Meeting, Symposium H, Paper H4.7, San Francisco, 2005.

[3] E. P. Scilingo, F. Lorussi, A. Mazzoldi, and D. De Rossi, "Strain-sensing fabrics for wearable kinaesthetic-like systems," *Sensors Journal, IEEE*, vol. 3, pp. 460-467, 2003.

[4] R. Paradiso, G. Loriga, and N. Taccini, "A wearable health care system based on knitted integrated sensors," *Information Technology in Biomedicine, IEEE Transactions on*, vol. 9, pp. 337-344, 2005.

[5] E. R. Post, M. Orth, P. R. Russo, and N. Gershenfeld, "E-broidery: Design and fabrication of textile-based computing," *IBM Systems Journal*, vol. 39, pp. 840 - 860, 2000.

[6] M. Catrysse, R. Puers, C. Hertleer, L. Van Langenhove, H. van Egmond, and D. Matthys, "Towards the integration of textile sensors in a wireless monitoring suit," *Sensors and Actuators A: Physical*, vol. 114, pp. 302-311, 2004.

[7] F. Lorussi, E. P. Scilingo, M. Tesconi, A. Tognetti, and D. De Rossi, "Strain sensing fabric for hand posture and gesture monitoring," *Information Technology in Biomedicine, IEEE Transactions on*, vol. 9, pp. 372-381, 2005.

[8] L. K. Baxter, *CAPACITIVE SENSORS: Design and Applications*. Piscataway, NJ: IEEE PRESS, 1997.

[9] R. Pallas-Areny and J. G. Webster, *SENSORS AND SIGNAL CONDITIONING*: JOHN WILEY & SONS, INC., 1991.

[10] Personal communication, Dr. Behnam Pourdeyhimi, Director, Nonwovens Cooperative Research Center, NC State University.

Chapter 4

A RESPIRATORY INDUCTIVE SENSOR BASED ON A SINGLE STRETCHABLE TEXTILE SUBSTRATE

ABSTRACT

For long-term physiological monitoring in health care and surveillance, biomedical sensors may be integrated into garments in an unobtrusive way. To demonstrate the process, we have integrated respiratory inductive sensors into stretchable textile substrates for respiration monitoring. Two methods, stitching fine magnet wires and screen printing silver ink, can be employed to form a conductive path for the inductive sensors. The textile substrates supporting the conducting materials are then laminated to stabilize the geometric structure relationships and mechanically protect the sensor. To quantify electrical and mechanical properties, the inductive respiratory sensors were first fabricated on single nonwoven textile substrates with their inductor patterns stitched onto the substrates using fine magnet wires. For screen-printed conductive lines, we discuss several factors to be considered, and tested several hand-painted prototypes for proof of feasibility. A portable data acquisition unit was designed and constructed to record and display the respiratory signals obtained.

I. INTRODUCTION

An inductor is a passive element that resists changes in current in an electric circuit. Detection of variation of inductance is widely used to sense such metrics as position variation, proximity, and so on. For non-invasive respiratory monitoring, inductive sensors have been employed since the 1970's. A commercialized inductive breathing sensor, called the "Respitrace," is used to evaluate breathing function and diagnose sleep apnea and sleep staging in hospitals and sleep clinics [1, 2]. Respiratory inductive plethysmography (RIP) usually uses a self-inductance measure that is based on the cross-sectional area changes that occur in the rib cage (RC) and abdominal (AB) compartments during a respiratory cycle [3]. In [3], the author's simulated a Zigzag type of an inductive sensor. The authors

show that the relationship between the self-inductance of the sensor and its area depends on both the cross-section and the pattern of the inductor. To ensure that the measurement of respiratory signals was precise, at least two data acquisition points (one on the rib cage and one on the abdomen,) were required for the RIP calibration. In [4], the following formula was used:

$$\Delta V_T(t) = \alpha \Delta RC(t) + \beta \Delta AB(t) \quad (1)$$

where, $\Delta V_T(t)$ is changes in tidal volume and $\Delta RC(t)$ and $\Delta AB(t)$ are RIP ribcage and abdomen signals. Calibration coefficients, α and β are estimated by applying the method of least squares to the recorded signals.

There have been strong demands for an inconspicuous wearable system for a long-term physiological monitoring during normal daily activity. Since an article of clothing is the best platform to implement such a system, the sensor designed for this task is required to be integrated into the garment in an unobtrusive way. Recent researches on wearable textile sensors show possibility [5, 6]. In [5], piezoresistive properties of Lycra® fabrics coated with carbon loaded rubber (CLR) was directly integrated into garment for respiration monitoring. A stainless steel yarn was integrated into a Lycra® substrate to form a sensing element for respiration monitoring [6].

In order to integrate an inductive sensor into clothing, conductors must be fabricated on or into textile substrates. If that conductor is to be used as a sensing element, e.g., an inductive breathing sensor, then the electrical properties of the conductor (its resistance, capacitance, and inductance), must be stabilized. In this paper, we present a method to directly embed an inductive sensor on fabrics for respiration monitoring.

II. METHODS AND MATERIALS

For detection of inductive variation during body volume changes due to breathing effort, conducting materials with a certain layout may be integrated into the stretchable fabrics to form an inductive sensor. Available conductors include hard wires, flexible conductive yarns, and conducting inks. Conductive wires and/or yarns may be inserted into textile fabrics by conventional textile processes like stitching, sewing, and embroidering technologies [7] while conductive inks may be deposited using screen printing technology [8, 9]. In this research, fine magnet wires were stitched into and silver ink was screen-printed onto nonwoven textiles to create inductive fabric respiratory sensors.

After the conductive sensing materials are integrated into textile substrates, a lamination process is employed to stabilize the devices. Lamination firmly fixes the conductor on a textile substrate so that its geometric pattern will reflect the substrate's physical position and sense variations in shape during elongation. Second, lamination makes screen-printed conductive lines on stretchable textile substrates robust against broken lines or cracks by holding the ink in place in the plane of the substrate. Third, another reason to laminate the sensor is to mechanically protect the conductive lines from daily use including washing and scratching. Fourth, the physical properties of the laminated layer can be used to control the stretchability of the sensor. Fifth, it insulates the screen-printed conductive lines and protects them from electrical short circuits. Finally, the lamination layer can be implemented with biocompatible materials to reduce skin irritability. The lamination material used in this study was thermoplastic polyurethane (TPU, 100 gsm) deposited by a meltblown procedure having fine fibers (diameter of 5 μm) with very fine pores.

III. A PLANAR INDUCTIVE PATTERN

In this work, we focused on sensor designs employing a single-layer fabric substrate. Avoiding the use of multiple layers can reduce manufacturing costs so we consider only planar structures. Planar inductors can include spiral, zigzag, meander and solenoid type patterns. Fig. 1 displays these basic

geometric shapes. In these designs, inductance depends on the geometric layout of conductive lines and hence inductance variance depends on the relative change in these patterns caused by the application of strain. The pattern of a one-plate sensor should be optimized such that the variation of the sensor's total inductance is maximized in a limited dimension during stretching.

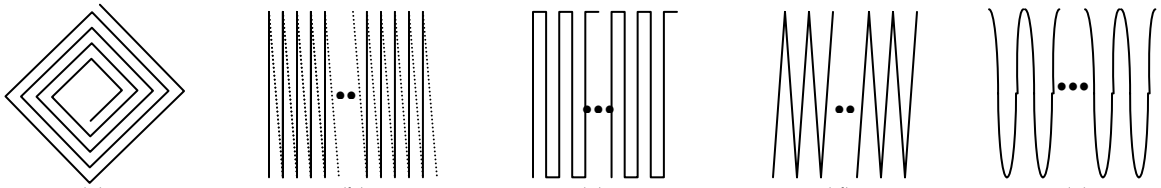

Fig. 1. Basic geometric layout of the conductor for magnetic induction in single-plate sensor. (a) Spiral, (b) solenoid type (conductors on both sides), (c) meander type, (d) zigzag type, and (e) sinusoid type.

In addition to a planar structure, stiffness is another factor that limits the geometric pattern formed on a stretchable substrate. Solid conducting materials such as wires increase the stiffness of stretchable substrates; these conductors may be broken as the geometry of the sensors is distorted during use. If conductive lines are oriented along the direction which strain is applied, they dramatically alter the stiffness of the fabric in the direction. Inductor patterns produced with screen-printed conductive ink are easily breakable if they are oriented in the direction of the applied strain. Thus, it is desirable that no lines be oriented along the direction in which strain is applied. In addition to the orientation of the conductive lines, the line density also impacts the stiffness of the elastic substrates.

Considering the geometric patterns and stiffness constraints mentioned above, we have concluded that two prime candidates for investigation are a zigzag pattern near right-angle corners and a modified meander pattern in which horizontal lines are replaced with skewed lines.

IV. DESIGN CONSIDERATIONS FOR PRINTED LINES ON TEXTILE SUBSTRATES

Screen printing is an attractive alternative to stitching because of potential cost savings in the manufacturing process. In [8], electrical characteristics of screen-printed conductive lines on various nonwoven substrates were explored through DC resistance measurements as well as Time Domain Reflectometry (TDR). The test results showed that screen printing is suited for depositing transmission lines onto nonwoven fabrics.

Inductors screen printed onto a flexible nonwoven substrate can be used as a component of an LC filter, transformer, and voltage controlled oscillator, or as an inductive sensor integrated into a garment. When employing screen printed conductive lines on textile substrates for the inductors, there are a number of factors that must be considered. These include the inductor's quality factor, line resistivity, surface roughness, and conductor integrity.

A. Inductance and Quality Factor

To make a fabric-based inductor practical and valuable, the quality factor Q of the inductor must be high enough so that the inductor will give a high voltage response. The Q of an inductor is a figure of merit that indicates how closely the characteristics of the component come to those of an ideal component. For example, a low-quality inductor in an LC tank circuit generates relatively weaker peak-to-peak oscillatory signals on the deviated frequency. In the worst case, the low-quality inductor may fail to oscillate the tank circuit. Fig. 2 shows equivalent circuit of an inductive sensor where *Z* is impedance of the inductor.

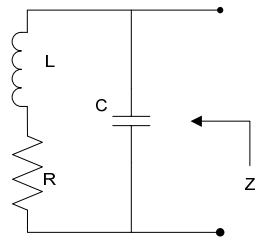

$$Z = \frac{R + j\omega L}{-\omega^2 CL + j\omega CR + 1}$$

Fig. 2. Equivalent circuit of the inductive sensors.

The quality factor of an inductor is characterized by its Q value which is defined as [10]

$$Q = 2\pi \cdot \frac{\text{energy stored}}{\text{energy loss in one oscillation cycle}} \tag{2}$$

Then, the quality factor, Q_{inductor} is given by

$$Q_{\text{inductor}} = \frac{R_p}{wL} = \frac{wL}{R} \tag{3}$$

where R_p is an equivalent parallel resistance. So, to obtain a high quality factor for the inductor, the serial resistance needs to be minimized (maximize equivalent parallel resistance) and the inductance needs to be maximized. In this research, the screen printed planar inductors have relatively low inductance due to the planar nature of the geometry of the inductor while having relatively high serial impedance. Even though it is acceptable for inductive sensing, their use in a transformer and a LC filter may be limited without improvement.

B. Line Resistivity

When a printed conductive straight line is modeled as a flat wire having depth (t), width (w), and length (l), the dc resistance of the conductor is calculated using:

$$R_{dc} = \frac{\rho l}{A}(\Omega) \tag{4}$$

where, ρ is the resistivity and A is the cross-sectional area (t × w). The frequency corrected resistance of the straight rectangular wire is found with:

$$R = \frac{K_C R_S l}{2.0(w+t)} \quad (\Omega) \tag{5}$$

where R_S is surface resistivity (sheet resistivity) and K_C is a current crowding factor [9]. If $1.0 \le w/t \le 100.0$, K_C can be represented with less than 0.5 % error as follows:

$$K_C = 1.048312 + 0.21768001\ln(w/t) + 0.77176189e^{-w/t} \tag{6}$$

R_S is the skin effect resistance and described by:

$$R_S = \frac{1.0}{\sigma\delta} = \sqrt{\frac{\pi f \mu}{\sigma}} (\Omega / \text{square}) \text{ with } \delta = \frac{1}{\sqrt{\omega\mu\sigma}} = \text{skin depth and } \sigma = \text{conductivi ty} \quad (7)$$

The skin depth is the depth at which the current density is reduced to e^{-1}. This can also be thought of as the equivalent thickness of a conductor at dc having the same resistance. Thus, equation (5) represents an increase in resistance with frequency due to the skin effect. Therefore to achieve a high quality factor, the serial impedance needs to be reduced. This is done by increasing the depth or the width of printed conductive line for both the dc-driven or ac-driven circuits. In a limited dimension, increase of line widths may cause to reduce a number of lines and hence lower inductance, we need to compromise between a quality factor and inductance. In addition, to avoid the skin effect, a low frequency ac signal is preferred to drive and pickup an inductive sensor signal.

C. Surface Roughness

The uneven surface of nonwoven fabrics can make the surface of the conductor rough, and rough edges and surfaces of conductors increase conductor losses. In [11], an approximate formula was described to estimate conductor losses caused by line roughness:

$$\alpha_c = \alpha_{c,0} \left\{ 1.0 + \frac{2.0}{\pi} \tan^{-1} \left[1.4 \left(\frac{\Delta}{\delta} \right) \right] \right\} \quad (8)$$

where, $a_{c,0}$ is the conductor losses calculated for perfectly smooth conductor, Δ is the rms surface roughness, and δ is the skin depth. For the research in this paper, this formula indicates that nonwoven fabrics with a very smooth surface are desirable. If the use of a rough surface is unavoidable, then the surface should be treated by a smoothing process to obtain a better inductor quality factor.

D. Conductor Integrity

Screen printing on nonwoven textile substrates reduces the compliance of the substrate due to the conductive ink altering the stiffness properties. Assuming that there is a perfect bond existing

between the printed conductor and nonwoven fabric, broken lines can be expected when the compliant nonwoven substrate is stretched beyond a specific limit. Thus, there is a limit to the strain that can be applied to the sensor to avoid causing damage to the conductor integrity.

Preliminary tests were conducted on devices made by hand-drawing the conductive lines on stretchable substrates. These tests showed that, at the beginning of the application of strain, the resistance of the inductor increased linearly as the nonwoven substrate elongated over a 3 mm range. At 3 mm of stretch, the resistance almost doubled. The mechanism of resistance change may be due to minute cracks in the printed conductor. Changes in conductor resistance cause changes in the Q of the inductor in (3). These resistance changes will cause signal distortions such as frequency shifts and peak-to-peak amplitude changes away from the designed operating point for the detection circuit.

A continued increase in the strain applied to the sensor beyond its operational limit causes larger cracks to appear in the conductive line, resulting in open circuits. Once these large cracks begin to appear in the conductive lines, the resistance values change randomly from the minimum values to infinity. It is clear that the screen printed line is subject to damage in the direction in which it is being stretched. Preliminary tests on hand-printed conductive lines show that lines oriented at near 90º to the direction of the applied strain are more robust when subjected to large increases in strain. Therefore, when designing inductive sensors based on screen printed lines and compliant nonwoven substrates, care must be taken in deciding the geometry of the conductive lines in relation to the direction of the applied strain.

Other preliminary tests with the printed inductor showed that the dense zigzag patterns (Fig. 1d) are very resistant to line breaks but generate the least inductance. The reason for this is that the angle between neighboring straight lines is very acute (the lines are oriented nearly 90º relative to the direction of the applied strain). At the peaks of the structure where the lines reverse directions, the

conductive lines overlap somewhat, shortening the current path and thus reducing the inductance. The meander pattern (Fig. 1c) also generated a very low inductance and the horizontal portions of the lines frequently disconnected with increasing strain. The solenoid pattern (Fig. 1b) generates higher inductance compared to the zigzag and meander layouts, but it has patterns on both sides of the substrate and is more difficult to fabricate.

V. EXPERIMENTAL RESULTS AND DISCUSSION

A. Instrumentation

Body volume changes due to breathing effort cause inductance variance in the respiratory inductive sensor. Inductance can be detected in a various ways. For example, inductance variance results in a frequency shift through an oscillator circuit [6, 12]. Then frequency variation due to breathing effort can be changed into voltage output through FM demodulation implemented using a phased-locked loop [12], X-OR phase comparator [6], and a frequency-voltage converter.

For this sensor, we employed a Colpitts oscillator in which variations in sensor inductance generates a frequency shift [12]. The resonant frequency of the Colpitts oscillator as shown in Fig. 4 is determined by

$$f_{osc} = \left(2\pi \sqrt{L\left(\frac{C_1 C_2}{C_1 + C_2} \right)} \right)^{-1} \tag{9}$$

For frequency stability, relatively high capacitance is required to ensure that parasitic capacitance changes have minimal impact. The output of the oscillator drives a buffer to isolate the oscillator from the load to improve stability. Then, the frequency shift is detected by either a FM demodulator implemented using a phased-locked loop, or phase comparison with a given reference signal. In phase comparison method, an exclusive-OR phase comparator (Phase comparator 1 of CD74HC7046 chip, Texas Instrument®) was employed to generate the difference between the Colpitts oscillator

output and the reference signal. The signals are amplified using a differential amplifier after the signal was low pass filtered with fourth order low-pass Sallen-Key filter.

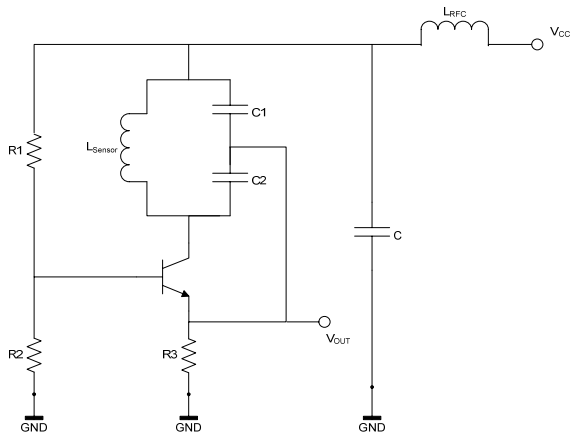

Fig. 3. The Colpitts oscillator circuit to pickup inductance variance of the sensor.

In the digital portion, a low powered micro controller (Atmel® ATmeg128L) was used to convert analog signals into digital form in 8-bit resolution and store the data in real-time to a local storage (a 16 M Byte flash memory). This system can operate either a stand-alone mode or a client-mode. Interface software was implemented for the Palm® pilot to control and communicate with the processor, display the respiration waveform in real time and collect the signal data for permanent storage. The whole system including analog and digital circuits can operate under a single power supply (3V).

B. Simulation

The planar inductor patterns of Figs. 1c (meander) and 1d (zigzag) were simulated to compare their relative performance. These two basic patterns were modified as shown in Fig. 4. In Fig. 4a the meander layout was changed to employ peaks modeled after those of the zigzag structure to reduce line fractures during stretching. The simulation for each structure was written using Q3D Extractor software from Ansoft® and was executed on a personal computer having 3.0 GHz CPU and 2 GB main memory. The model assumes that each line is composed of many square-shaped segments.

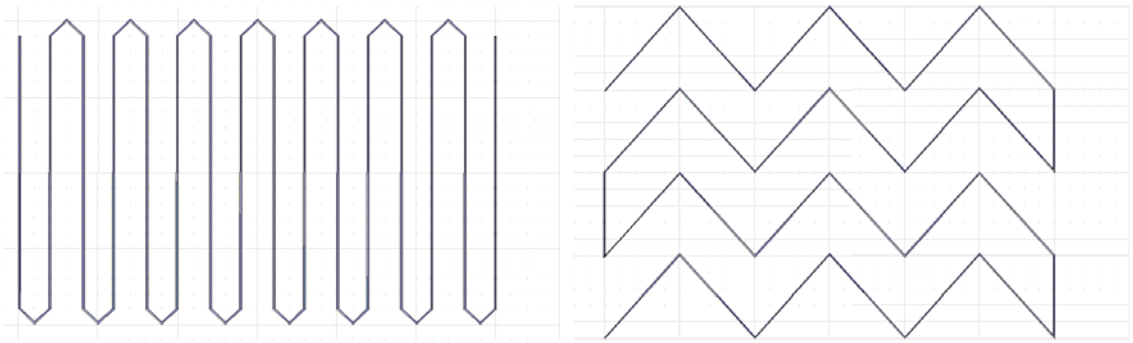

(a) Modified meander pattern (b) Modified zigzag pattern

Fig. 4. Modified patterns for simulation (sensor dimension at rest is 4cm × 6cm).

To simulate the inductance change along sensor extension, we assume several things to make the simulation simple. First, hard conductive lines could not be extended. Second, we assume that the sensor extension may affect uniformly over the whole sensing range regardless of density of conductive lines that may change the stiffness of substrate. Third, the conductive diagonal line keeps its linearity even though the strain is applied. Finally, the vertical lines are robust to the horizontal strain so that no distortion may happen in the vertical lines.

Under these assumptions, applying strain along with horizontal axis (the direction the strain applied) cause shrink the diagonal lines in vertical direction (orthogonal direction to the strain applied), making equal the length of the diagonal lines before and after stretching. In the zigzag pattern, the shrink occurs in both top and bottom areas of the diagonal lines as shown Fig. 5. This reduced distance, Δy were adjusted in the simulation as follows:

$$\Delta y = \frac{y_0 - \sqrt{{y_0}^2 - (2x_0 \cdot \Delta x + \Delta x^2)}}{2} \tag{10}$$

where x_0 and y_0 indicate original sizes in x and y axis, and Δx shows the increment of the diagonal line along horizontal direction due to sensor extension. In the modified meander pattern, the shrink may occur with one direction toward inside at the peaks, but twice Δy.

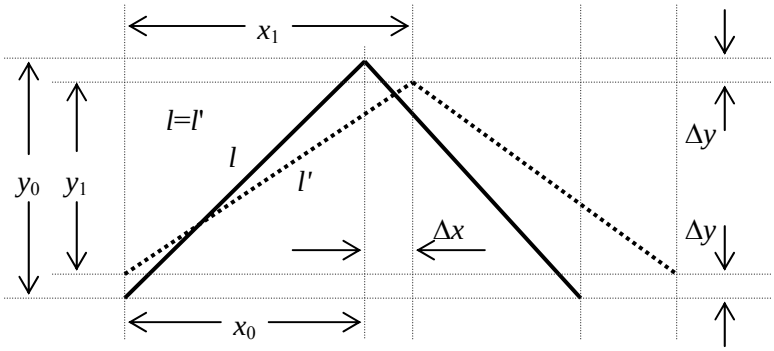

Fig. 5. Line shape changes on a right-angled corner along with sensor extension. Solid and dotted lines indicate original conductive line and transformed line, respectively. (l=l')

Simulation results for inductance variance along with sensor extension shows in Fig. 6. Note that the inductor with the modified meander pattern generates larger inductance and variance.

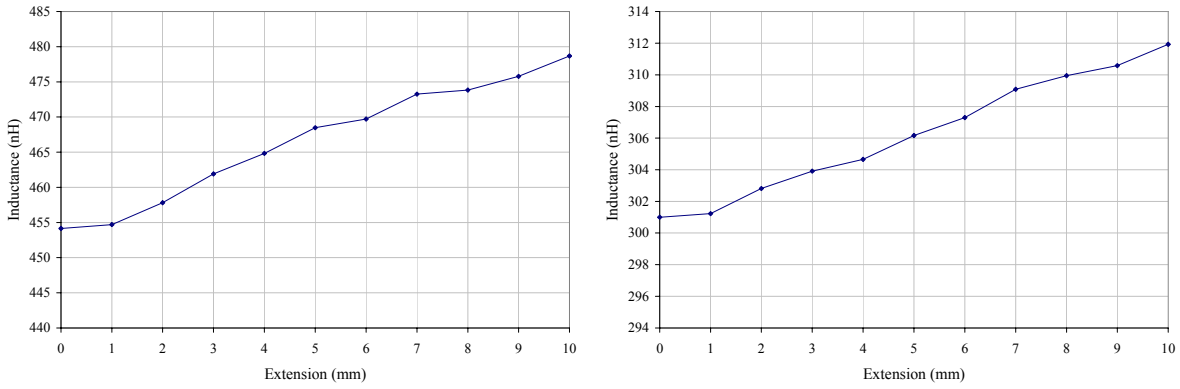

(a) (b)

Fig. 6. Simulation result of inductance variance along with sensor extension for inductors with (a) the modified meander pattern and (b) the modified zigzag pattern.

C. Prototyping the sensors

Fig. 7 shows the formation of stitched fine magnet wires on nonwoven substrates. During testing we noted that samples without lamination were more compliant and easier to stretch. The lamination process makes the structure less compliant and binds the wires tightly into the structure. Even so, the structure still stretches with applied strain if the materials are chosen properly.

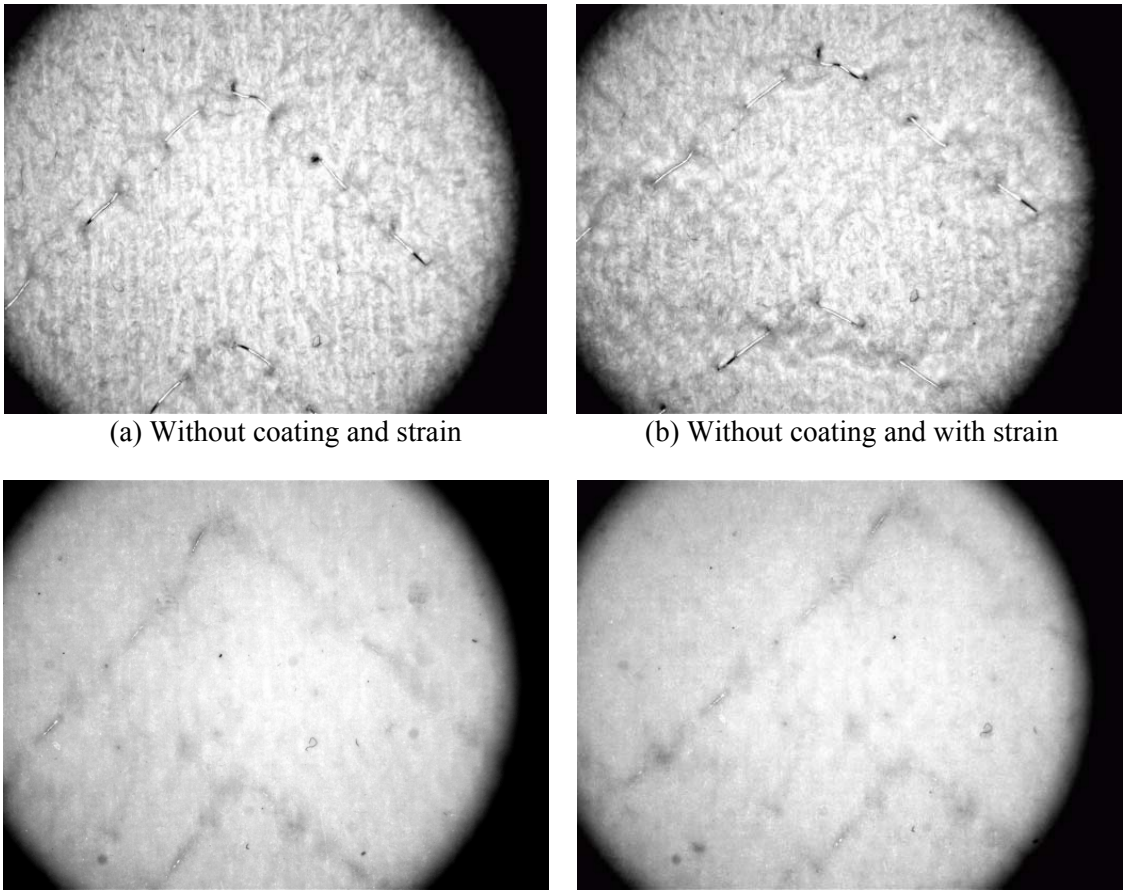

(a) Without coating and strain (b) Without coating and with strain

(c) With coating and without strain (d) With coating and strain

Fig. 7. Formation of stitched pure fine magnet wires before and after lamination.

We also investigated the use of fine, twisted magnetic wires for the structures of Fig. 6. Each fine magnet wire was twisted with a general textile yarn in 500 turns per meter. The fine magnet wires are very brittle in their original form. Twisted yarns are more flexible than the solid wires and make manufacturing more reliable. Finally, a protective coating of TPU was laminated to cover the surface. The final configuration is shown in Fig 8.

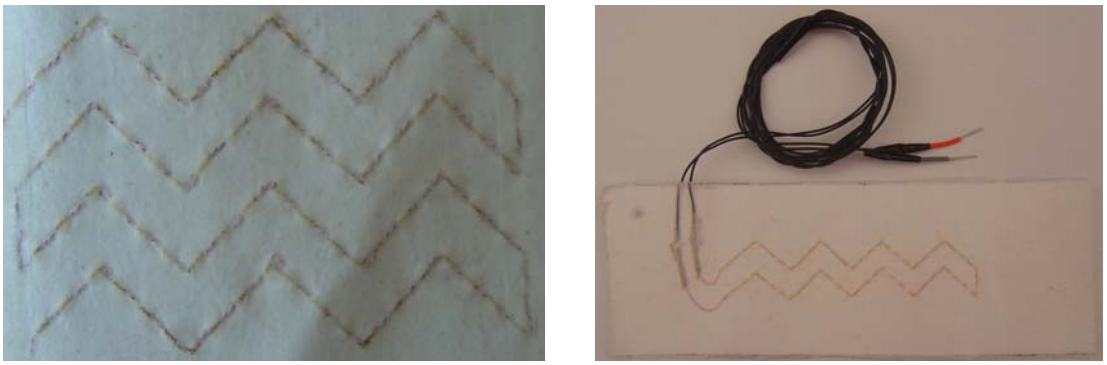

(a) (b)

Fig. 8. Examples of inductive sensors with (a) four lines of zigzag pattern and (b) two lines of zigzag pattern.

D. Experimental results

For respiratory signal detection, two identical inductive sensors were fabricated: one is used as a breathing sensor while the other one is used as a reference sensor. Then, two Colpitts oscillators, one for the breathing sensor and the other for the reference sensor generated two different sensor-dependent sinusoids for phase comparison. Fig. 8 shows simulated breathing signals by stretching and relaxing the sensor by hand.

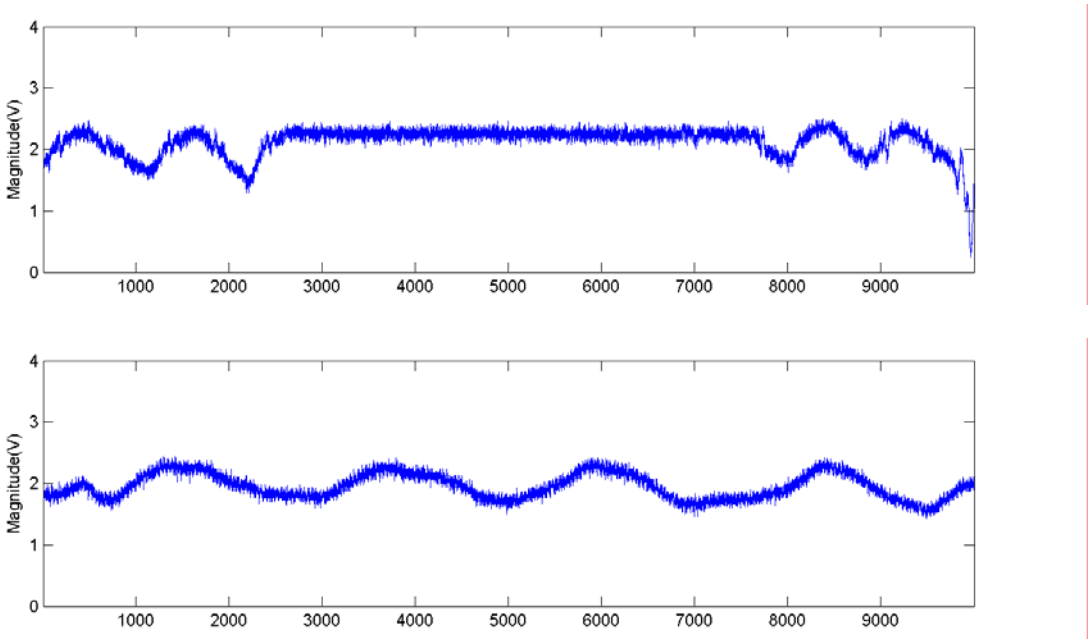

Fig. 9. Simulated breathing signals during 4 seconds (sampling rate is 2500 samples/sec).

The hard wires integrated into textile substrates to form the inductive sensors show almost no changes in resistance along sensor extension. Thus, the frequency and amplitude changes in Colpitts oscillator are caused by inductance changes of the sensor. However screen printed conductive lines may show different characteristics.

E. Discussion

Even though the inductive sensor stitched with hard wire conductive lines shows stretchability, their processing procedure is quite cumbersome. In our preliminary work, the fine magnet wires as well as the twisted fine magnet wires with general textile yarns are not compatible for sewing machines due to its brittleness. To employ automated process like sewing, we may employ composite stainless steel yarns. In [7], attempts were made to sew composite stainless steel yarn onto a fabric substrate to create signal and communication paths.

These simple inductive sensors exhibit low inductance and small variance during operation in secure environmental place. However for inductive sensors to be practical, they are required to be designed to have high inductance and variance along sensor extension to provide reasonable sensitivity. Hence, their performance must be enhanced for use in severe and noisy environments. One effective method is to reduce the return path in which current flows in the opposite direction while increasing the paths that have same current flow direction as shown in Fig. 10. Low inductance results from numerous return paths, which generate relatively strong negative mutual inductances between each line segment.

Another method is to duplicate the pattern providing that it does not increase the stiffness. By using two very closely spaced lines and making current in each flow in same direction, we can increase the total inductance almost by a factor of more than three. For example, the pattern of Fig. 10 can be printed on both sides of textile substrates.

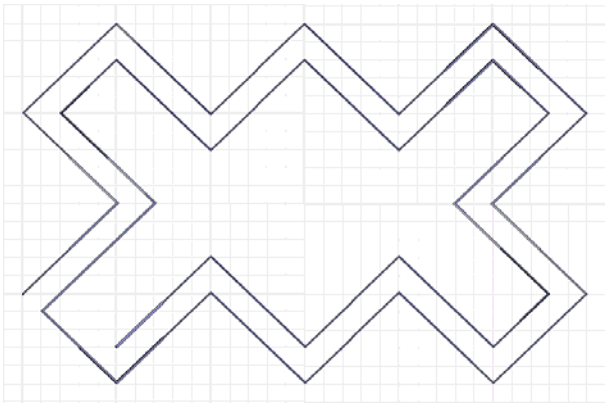

Fig. 10. Modified pattern to increase inductance.

IV. CONCLUSIONS AND FUTURE WORK

The feasibility of building an inductive sensor based on a single planar textile substrate is presented in this paper. Without employing wrinkled stretchable fabrics or Lycra® fabrics, we fabricated inductive sensors on stretchable flat nonwoven substrates. Stitched fine magnet wires serve as the inductive sensing elements by changing their geometric layout when the fabric substrate is stretched. The sensors have a conformal coating to hold the wires in place so that the sensor responds linearly over its operating range. Holding the wires in place guarantees that the sensor will respond to small amounts of applied strain. This method provides a simple sensing structure to detect respiratory signals. These sensors exhibit low inductance and small inductance variance during operation. Hence, their performance must be enhanced for use in severe and noisy environments as discussed in the previous section.

REFERENCES

[1] S. J. Redmond and C. Heneghan, "Cardiorespiratory-based sleep staging in subjects with obstructive sleep apnea," *Biomedical Engineering, IEEE Transactions on*, vol. 53, pp. 485-496, 2006.

[2] K. P. Cohen, W. M. Ladd, D. M. Beams, W. S. Sheers, R. G. Radwin, W. J. Tompkins, and J. G. Webster, "Comparison of impedance and inductance ventilation sensors on adults during

breathing, motion, and simulated airway obstruction," *Biomedical Engineering, IEEE Transactions on*, vol. 44, pp. 555-566, 1997.

[3] P. Martinot-Lagarde, R. Sartene, M. Mathieu, and G. Durand, "What does inductance plethysmography really measure?," *J Appl Physiol*, vol. 64, pp. 1749-1756, 1988.

[4] R. K. Millard, "Key to better qualitative diagnostic calibrations in respiratory inductive plethysmography," *Physiological Measurement*, vol. 23, pp. N1-N8, 2002.

[5] R. Paradiso, G. Loriga, and N. Taccini, "A wearable health care system based on knitted integrated sensors," *Information Technology in Biomedicine, IEEE Transactions on*, vol. 9, pp. 337-344, 2005.

[6] M. Catrysse, R. Puers, C. Hertleer, L. Van Langenhove, H. van Egmond, and D. Matthys, "Towards the integration of textile sensors in a wireless monitoring suit," *Sensors and Actuators A: Physical*, vol. 114, pp. 302-311, 2004.

[7] E. R. Post, M. Orth, P. R. Russo, and N. Gershenfeld, "E-broidery: Design and fabrication of textile-based computing," *IBM Systems Journal*, vol. 39, pp. 840 - 860, 2000.

[8] C. R. Merritt, B. Karaguzel, T.-H. Kang, J. Wilson, P. D. Franzon, B. Pourdeyhimi, H. T. Nagle, and E. Grant, "Electrical Characterization of Transmission Lines on Nonwoven Textile Substrates," presented at Materials Research Society 2005 Spring Meeting, Symposium H, Paper H4.7, San Francisco, 2005.

[9] R. Parashkov, E. Becker, T. Riedl, H.-h. Johannes, and W. Kowalsky, "Large Area Electronics Using Printing Methods," *Proceedings of the IEEE*, vol. 93, pp. 1321-1329, 2005.

[10] C. P. Yue and S. S. Wong, "On-chip spiral inductors with patterned ground shields for Si-based RF ICs," *Solid-State Circuits, IEEE Journal of*, vol. 33, pp. 743-752, 1998.

[11] B. C. Wadell, *Transmission Line Design Handbook*: Artech House, Inc., MA, 1991.

[12] K. P. Cohen, D. Panescu, J. H. Booske, J. G. Webster, and W. J. Tompkins, "Design of an inductive plethysmograph for ventilation measurement," *Physiological Measurement*, vol. 15, pp. 217-229.

Chapter 5

PLANAR INDUCTIVE DISPLACEMENT SENSORS BASED ON SPIRALS AND DOUBLE-SUBSTRATE DESIGNS

ABSTRACT

In this paper, new planar inductive displacement sensors based on open-rectangular spirals are presented. For these new sensors, we use two substrates, each of which is made from stretchable and non-stretchable materials that are laterally attached. Various configurations of spirals are presented to form three different types of planar inductive displacement sensors: a single inductor sensor, a transformer-type differential sensor, and an autotransformer-type differential sensor. In the single inductive sensor, an inductor is created by having two rectangular spiral windings slide one relative to the other, thereby changing their overlapped area and generating linear mutual inductance variances. In a second configuration, a differential inductive sensor is achieved employing three spirals, one (primary coil) of top of the other two (secondary coils). The overlapping areas change in equal amounts but in opposite directions. Finally the autotransformer-type differential inductive sensor includes two inductors which were made of two sets of two interleaved spirals and utilize simultaneously negative and positive mutual coupling between each spiral. The two inductors undergo the same overlapped area changes as the displacement changes while keeping their layout fully symmetrical. In the two inductors, one inductance increases and the other inductance decreases by the same amount while the total inductance of the sensor remains constant, regardless of lateral displacement changes. To show proof of concept, a computer simulation of inductance variations with simple spiral models of the three different inductive sensors is performed. The sensors are built with winding spirals of fine magnet wires on nonwoven textile segments. Then, inductance variances along sensor extension are measured and presented. These inductance variations are transformed into voltage outputs by electronic circuits individually designed for each sensor. Computer simulation and

experimental results with fabricated prototypes show that the differential sensors have wide, quasi-linear sensing ranges.

I. INTRODUCTION

Planar type displacement sensors are frequently employed for measuring changes in parameters such as position, displacement, and stretching of flat surface structures. Such planar sensors should be unobtrusive for the normal operation of the surface being monitored. A piezoelectric-film sensor is a common choice for these measurement due to its flat shape and flexibility [1]. Especially the sensor does not require any external source to pick up the displacement changes. But piezoelectric films are unsuitable for measurements that require a wide sensing range since piezoelectric films operate at the micro-scale when stretched along their planar axis. In applications that require millimeter to centimeter elongation measurements, inductive sensors may be utilized.

In this paper, we suggest planar displacement inductive sensors that have large quasi-linear sensing range while generating high inductance. For these sensors, open-center spiral patterns are utilized to satisfy planar geometry limits. In a preliminary work, we compared the efficiency of the following planar patterns: solenoid, meander, zigzag, and spiral. Based on those results, we chose rectangular spiral patterns for the planar inductors reported here since they generate relatively high self-inductance within a limited space as well as a high mutual coupling coefficient factor when they are stacked together. Planar spiral patterns of this type are widely used in on-chip passive components such as inductors, transformers, VCO components and LC tank components [2-6]. In this study, several configurations of rectangular spirals are presented that use double (stacked) substrates in their design, each of which includes stretchable and non-stretchable materials like nonwoven textiles that are laterally attached. These basic building blocks are configured to become single or differential lateral stretch sensors stretchable along their planar axis.

In the following section we describe a single inductive sensor in which two rectangular spirals slide over each other, changing their overlapped area and generating mutual inductance variances along the stretching axis. In the section III, a differential inductive sensor is summarized. The differential sensor consists of two open-rectangular spirals which are laterally placed in the same substrate and a third spiral that slides over the other two, changing mutual inductances between the third spiral and the others. Another differential inductive sensor is presented in the section IV. Four spirals (two pairs) are interleaved and stacked to achieve the differential mode of operation. Each spiral pair in the differential sensor undergoes the same overlapped area changes and hence same change in mutual inductance is achieve, but in the opposite polarity. In section V, sensing circuitry is described that couples inductance variations in each inductive sensor with useful signal outputs. Section VI describes experiments and their results while Section VII offers conclusions and recommendations for future work.

II. A PLANAR SINGLE INDUCTIVE SENSOR (SIS)

In this section, we present the design of two planar single inductive sensors and explain the behavior of their sensing mechanisms. Experimental results for the single sensor will be presented in section VI.

A. Double Substrate Sensor Structure

The planar single inductive sensor has two substrates, each of which includes stretchable and non-stretchable nonwoven textiles segments that are laterally configured as shown in Fig. 1. Conductors, like fine magnet wires or screen-printed conductive-ink lines, are placed in a rectangular spiral pattern on each of the non-stretchable fabrics to form open-planar inductors. Relative positions of the two planar inductors change when the sensor stretches. Each plate is initially placed so that the inductors minimally overlap [Fig. 1(a)] or maximally overlap [Fig. 1(b)]. As the stretchable portions of the device are activated, each set of plates slides in the opposite direction, changing the effective area and

hence the mutual inductance value between the two, resulting a change in the total inductance value of the sensor. In the sensing structures of Fig. 1(a) and Fig. 1(b), the inductance increase and decrease respectively as the sensor is extended along the horizontal axis. Only the structure of Fig. 1(a) will be employed in the three different types of inductive sensors presented herein.

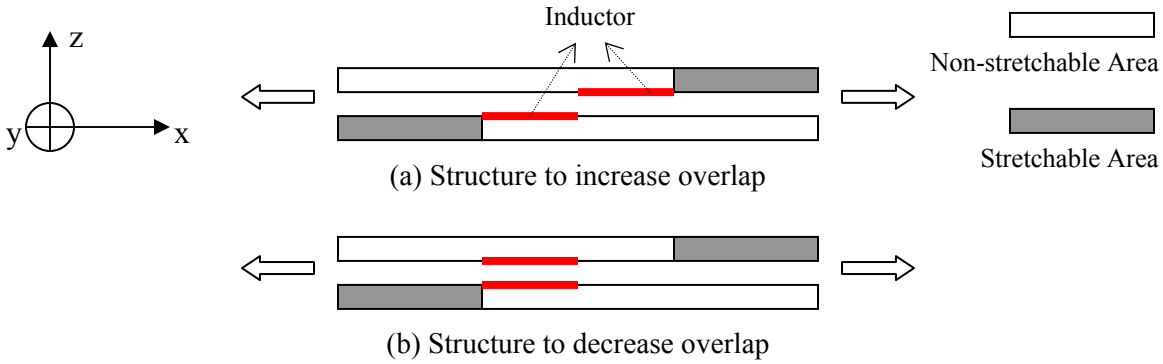

Fig. 1. Substrate structure and relative position of the inductors at rest. (Arrows indicate the directions that sensors expand along the x-axis)

B. Sensing Mechanism

Let's assume that two spirals S_1 and S_2 on each substrate are serially connected so that current in S_1 and S_2 flows in the same direction as shown in Fig. 2 (a). As the sensors stretch, the two rectangular spirals slide over each other, increasing or decreasing the overlap between them depending on the sensor structure as shown in Fig. 1. If two spirals, S_1 and S_2 are equal in pattern and dimension, and hence self-inductance (L_1=L_2=L), then the mutual coupling factor, k between S_1 and S_2 is given by $k = M/\sqrt{L_1 L_2} = M/L$ where M is mutual inductance and k <1. Since the mutual inductance between two spirals is positive, a total inductance value of the sensor, L_{total} is,

$$L_{total} = L_1 + L_2 + 2M = 2(L + M) = 2(1 + k)L \qquad (1.a)$$

Since L is invariant regardless of sensor extension, the inductive variance is only dependant on k (or mutual inductance, M), which is responsible to the sensor position or extension. If we assume that the two inductors do not deviate vertically, the maximum total inductance value of the sensor is achieved when two spirals are stacked vertically and $k \geq 0.9$. The mutual coupling factor decreases as the

overlap decreases and finally falls to a near zero value when there is no overlap at all. Thus the total inductance of the sensor changes from more than 3.8L to about 2L providing high sensitivity and a high inductance value.

If Spirals S_1 and S_2 are serially connected, so that the current flows in S_1 and S_2 are in the opposite direction (see Figure 2(b)), then

$$L_{total} = L_1 + L_2 - 2M = 2(L - M) = 2(1 - k)L \tag{1.b}$$

In this configuration, the minimum inductance is generated when the two spirals are vertically stacked; in this case the mutual inductance is maximized. The total inductance of this sensor will be between 0.2L and 2L.

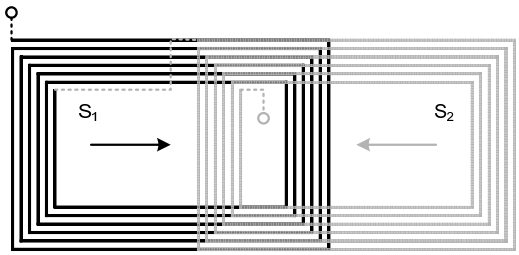

(a) Connection in series enhancement. The current in the two spirals flows in the same direction; the large arrows indict the direction of movement of the spirals if the sensor employs the structure to increase overlap [see Fig 1(a)]. Otherwise the direction is in opposite [see Fig. 1(b)].

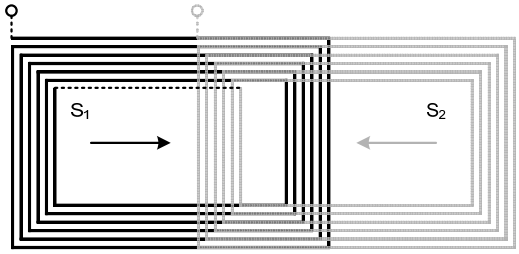

(b) connection in series opposition. The current in the two spirals flows in the opposite direction

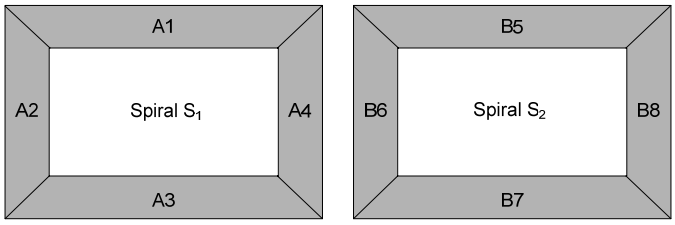

(c) Approximated spirals with the component bars

Fig. 2. Schematic diagrams of stacked spirals for the single inductive sensor (SIS).

C. Equivalent Circuit

Fig. 3 shows an equivalent circuit for the stacked open-rectangular spiral inductive sensor. To maximize the resonance quality factor Q of the planar spiral inductor, high inductance values and low serial resistances are needed. We need to increase the width and depth of the lines to reduce the serial impedance (R_{s1} and R_{s2}), but minimize the width and depth of the lines to reduce size and minimize costs, making this choice an important design parameter. The stray capacitances in each spiral, C_1 and C_2, are invariant regardless of stretching while the coupling capacitance between the two spirals, C_{12} is variable according to their overlapped position. These parasitic capacitances are determined by the lateral dimensions (C_1 and C_2) or vertical dimensions (C_{12}). The magnitude of the parasitic capacitors can be reduced by reducing the line width of the conductors, but this increases the magnitude of the serial resistance values. Specifically, the stray capacitances, C_1 and C_2, are reduced by increasing the line spacing in the spirals. The coupling capacitance, C_{12} can be reduced by placing the two spirals so that the conductive lines overlap minimally. In our experience, these parasitic capacitance values are typically a few pF and thus can be ignored for most applications. Hence, making the conductive lines wider and thicker is the best way to improve performance.

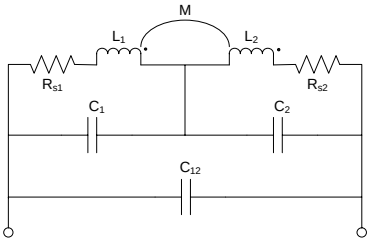

Fig. 3. Equivalent circuit of the single inductive sensor based on two stacked spirals.

D. SIS Simulation

Fig. 4 shows the computer simulation of the sensor's inductance variance when the two spirals are moved laterally. The simulation was written using Q3D Extractor software from Ansoft® and a personal computer having 2.4 GHz CPU and 2 GB main memories. We assumed that the current

flows in the same direction in two spirals in rectangular conductive lines to speed up computing time. The dimensions of each rectangular spiral are 40 mm height and 60 mm width. The width is larger than the height to achieve a wider sensing range. Line width w, line depth t and spacing s between next two lines in the spirals are 400 µm, 200 µm, and 200 µm respectively. The number of turns in the spirals is twelve and the vertical distance between them is assumed to be 2 mm. Fig. 4(a) shows the self inductance of and mutual inductances between each of the open-rectangular spirals. That is, the parameters are measured while the two spirals are disconnected. Fig. 4(b) shows the total inductance of the sensor measured while the two spirals are connected serially.

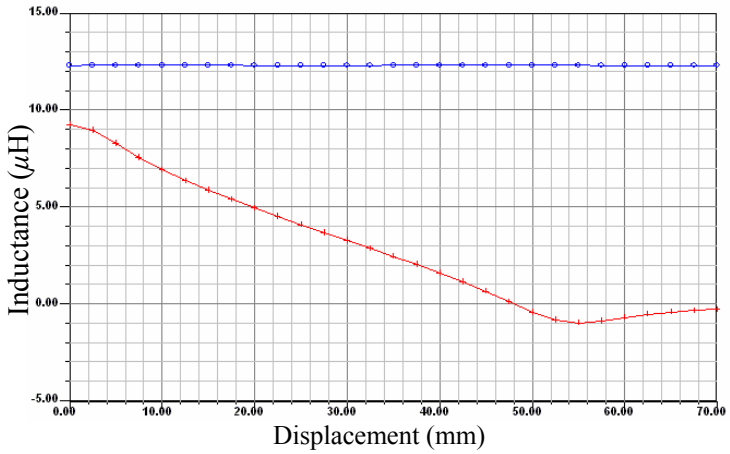

(a) Self and mutual inductance: the upper line indicates self inductance of the spirals (L_1 and L_2) and the bottom line shows the mutual inductance between two spirals (M_{12})

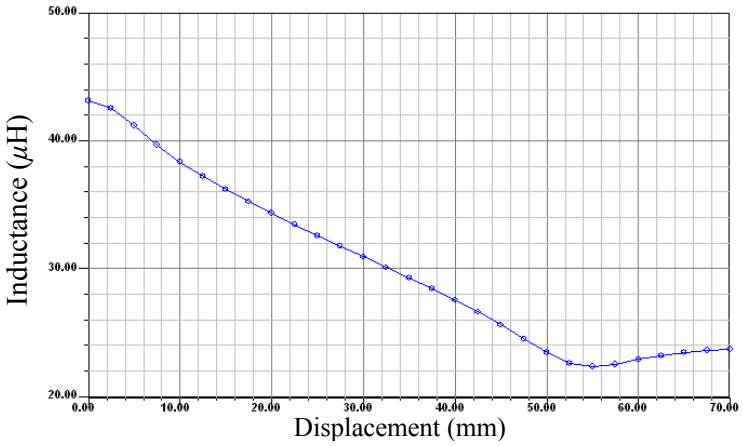

(b) Total inductance variance of the sensor

Fig. 4. Simulation results for inductance variance of the single inductive sensor along with lateral deviation of two spirals; the simulations were performed using Q3D Extractor from Ansoft®.

In Fig. 4, we can observe a linear sensing range from 10 to 50 mm. The longer the horizontal dimension of the spiral, the more linear is the sensing range. Nonlinearity at both extremes in the figure shows that mutual interference between each vertical bar is strong and occurs when the spirals are stacked vertically or are maximally extended.

E. Inductance Variance

In the open-center spiral inductor, the vertical lines do not interfere magnetically with the horizontal lines and vice versa due to their right-angle geometry. Interaction between multiple parallel straight line segments generate comparatively high mutual-inductive coupling in planar geometries. This is true even when two spirals are stacked together. Multiple straight line segments are grouped into a bar (a current sheet) as shown in Fig. 2(c), eight bars interact with each other to generate mutual inductance variations as the sensor geometry changes during operation. The self inductance of and the mutual inductance between each bar are described as follows,

$$M_{i,j} = \begin{bmatrix} L_1 & M_{1,2} & \cdots & M_{1,7} & M_{1,8} \\ M_{1,2} & L_2 & \cdots & M_{2,7} & M_{2,8} \\ \cdots & \cdots & \cdots & \cdots & \cdots \\ M_{1,7} & M_{2,7} & \cdots & L_7 & M_{7,8} \\ M_{1,8} & M_{2,8} & \cdots & M_{7,8} & L_8 \end{bmatrix} \tag{2}$$

Then, the total inductance of the sensor can be described as [2, 7]:

$$\begin{aligned} L_{total} &= \sum_{i=1}^{8} L_i + \sum_{i=1}^{8} \sum_{j=1, j\neq i}^{8} M_{i,j} \\ &= L_1 + L_2 + L_3 + L_4 + L_5 + L_6 + L_7 + L_8 - 2M_{13} - 2M_{57} - 2M_{24} - 2M_{68} + 2M_{15} - 2M_{17} \\ &\quad + 2M_{37} - 2M_{35} + 2M_{26} - 2M_{28} + 2M_{48} - 2M_{46} \\ &= 4L_1 + 4L_2 - 4M_{13} - 4M_{24} + 4M_{15}(\downarrow) - 4M_{17}(\downarrow) + 4M_{26}(\downarrow) - 2M_{28}(\downarrow) - 2M_{46}(\uparrow) \end{aligned} \tag{3}$$

where L_1=L_3=L_5=L_7, L_2=L_4=L_6=L_8, $2M_{13} = 2M_{57}$, $2M_{24} = 2M_{68}$, $M_{15} = M_{37}$, $M_{17} = M_{35}$, $M_{26} = M_{48}$ and $M_{12} = M_{14} = M_{16} = M_{18} = M_{23} = M_{25} = M_{27} = M_{34} = M_{36} = M_{38} = M_{56} = M_{58} = M_{67} = M_{78} = 0$. The up and down arrows indicate increasing and decreasing absolute magnitudes of the mutual inductance,

respectively, when the two spirals are moved along the x-axis. All self inductance values (L_1, L_2, L_3, L_4, L_5, L_6, L_7, L_8) of each bar and all the mutual inductance values (M_{13}, M_{24}, M_{57}, M_{68}) between each set of parallel bars on the same spirals are invariant regardless of sensor extension.

In closely stacked spirals, mutual magnetic coupling between each bar is stronger when they are stacked vertically than when they are placed laterally, even though the self inductance of the planar spiral is determined primarily by its lateral dimensions. M_{15} and M_{37} change during sensor extension while the horizontal bars keep their vertically stacked geometry and thereby contribute mostly to evoke mutual inductance variance. That is, the inductance variance due to sensor extension depends mostly on the mutual inductances M_{15} and M_{37} resulting from the vertically overlapped area of the horizontal bars in the two spirals. M_{17} and M_{35} occur between laterally placed bars. M_{26}, M_{48} and M_{46} are the main factors in degrading the sensor linearity due to bars that transit between a lateral geometry and a stacked geometry. The absolute magnitude of M_{46} rises uniquely as the two spirals are further deviated along the x-axis. Assume that each vertical bar is laterally far away from other vertical bars and the top horizontal bar is far away from the bottom horizontal bars. Then the linear sensing range and sensor linearity are determined mainly by how inductances M_{15} and M_{37} are linearly changed during sensor extension and only partly by how much other mutual inductance terms, since they are dominated by the values of M_{15} and M_{37}.

III. A LATERAL DIFFERENTIAL INDUCTIVE SENSOR (LDIS)

In this section, we present the design of a lateral differential inductive sensor (LDIS) and explain the behavior of its sensing mechanisms. Experimental results for the LDIS will be presented in section VI.

A. Differential Sensors

To improve noise and interference rejection, a differential mode is employed in many common sensing devices [8, 9]. We now describe a differential inductive sensor consisting of two variable inductors so arranged that they undergo the same inductance change, one larger and one smaller, when a target measurement such as position changes. From the differential mode of operation eliminates inductance offsets due to steady-state influences such as humidity, parasite capacitance in the instrumentation electronics, and planar misalignment (displacement) of the rectangular spirals. For cases in which both spirals are perturbed by the same dc effects, subtraction cancels these unwanted influences. So employing the differential mode of operation is highly preferable in noisy environments, especially a wearable health monitoring system for normal daily use.

One of many goals in designing a differential inductive sensor is obtaining symmetry between the two variable inductors so that inductance changes during measurements will have equal magnitudes. We investigated two differential structures based on double substrates and the open-rectangular spiral patterns: 1) an area opposition method in which two variable inductors experience the same changes in spirals' overlapped-areas, but in the opposite directions, and 2) a current flow opposition method in which the differential mode is achieved by forcing positive and negative mutual coupling in the two variable inductors by making the current flows different in the two inductors.

B. LDIS Configuration Based on Three Spirals

Based on the area-opposition method, we present a lateral differential inductive sensor (LDIS) which consists of three spiral inductors. The substrate structure is same as used in the single inductive sensor of section II. Two spiral inductors S_1 and S_2 are laterally placed on one of the two plates. The third spiral plate is stacked on the top of two spirals and is free to move laterally, thus changing overlapped areas and mutual inductances in the opposite directions between the third inductor S_3 and each spiral inductor S_1 and S_2 (M_{13} and M_{23}) as shown in Fig. 5. In a sensor interface circuit, the third

spiral may act as a primary coil while the spirals S_1 and S_2 may act as secondary coils, mimicking a differential transformer.

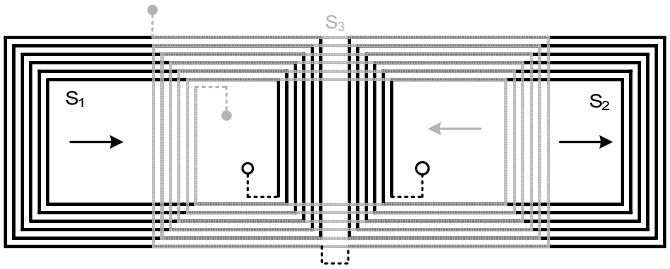

Fig. 5. Geometric layout of the lateral differential inductive sensor (LDIS) based on three spirals.

Fig. 6 shows our simulation results for the mutual inductance changes of the lateral differential sensor when three spirals have same geometry and dimension. Line width, depth and spacing in the spirals are equal to the values used to simulate the single inductive sensor of section II. The two spirals S_1 and S_2 are assumed to be apart 1.0 cm. Structurally, the linear sensing range of this differential sensor is less than that of the single inductive sensor. In addition, the gap between S_1 and S_2 further reduces the linear sensing range. In this lateral differential sensor, coupling parasite capacitances between the third spiral S_3 and each spirals S_1 and S_2 (C_{13} and C_{23}), change differently, specifically in the opposite directions. Generally all differential inductive sensors based on the area-opposition method experience differential changes of parasite capacitance in the two inductors. That is, one rises while the other falls during sensor extension (stretching).

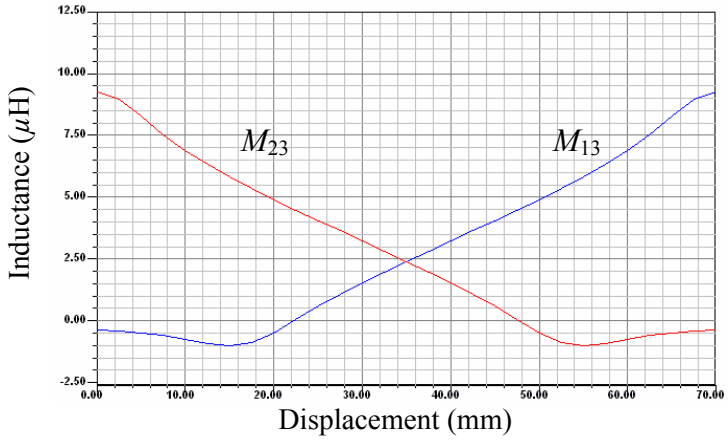

Fig. 6. Mutual inductance variances between the third spiral S3 and the two spirals S1 and S3 in the lateral differential inductive sensor.

IV. A SYMMETRIC DIFFERENTIAL INDUCTIVE SENSOR (SDIS)

To improve the differential characteristics for the sensors presented in the previous section, the two variable inductors should have the same structural geometry and experience the same stimuli such as magnetic inference so that these stimuli affect equally both inductors. Parameters such as parasite capacitance should change equally in the two variable inductors during sensor extension. The influence of moisture and humidity should impact both inductors equally. However, maintaining a constant relative lateral geometry may be difficult for the planar differential inductive sensor if it has wide sensing areas and multiple substrates. Here we present a new symmetric differential inductive sensor in which the two variable inductors are positioned to minimize the problem described above.

A. Geometric Layout

For the symmetric differential inductive sensor, four open-rectangular spirals (two pairs) are employed on two plates (a double substrate) so that each pair is laterally interleaved in each plate. As shown in Fig. 7 (a) and (b), on the bottom plate the black and gray spirals are interleaved and on the top plate the red and orange spirals are interleaved with each other. Then, a set of two spirals, each of which is placed in the different plates and serially connected, forms either an increasing variable inductor (Inductor 1) or a decreasing variable inductor (Inductor 2). In the increasing variable

inductor its inductance increases while in the decreasing variable inductor its inductance decreases by the same amount by utilizing both positive and negative magnetic coupling as the two sets of the two spirals slide over each other. To achieve differential mode simultaneously, the connections should meet a certain condition; for the increasing variable inductor, current flow in one set of two spirals, each of which is placed in the different plates, should be in the same direction while for the decreasing variable inductor current flow in the other set of two spirals should be in the opposite directions.

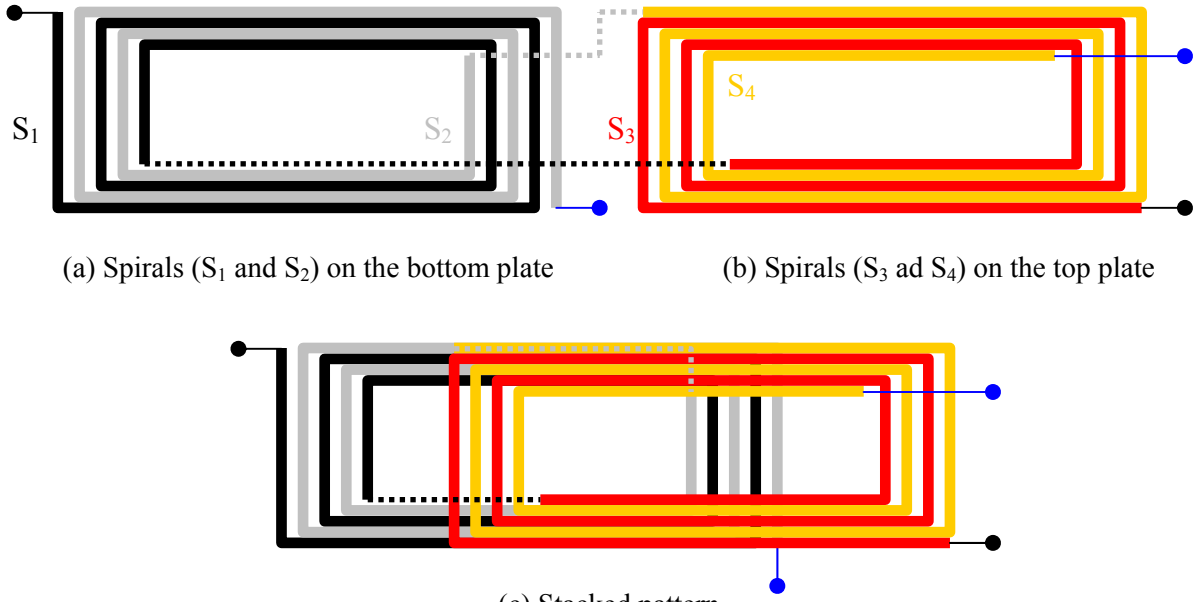

(a) Spirals (S_1 and S_2) on the bottom plate (b) Spirals (S_3 ad S_4) on the top plate

(c) Stacked pattern

Fig. 7. Geometric layouts of the four spirals for the symmetric differential sensor. The dotted lines indicate the connection between the two spirals that become single variable inductor. There are two single variable inductors for the differential sensor.

Fig. 7 shows one of possible configurations of the four spirals for the symmetric differential inductive sensor. The spiral S_1 (black) on the bottom plate is connected to the spiral S_3 (red) on the top plate so that the current flows in the same direction regardless of port assignment of source and sink. On the contrary, the connection between the spiral S_2 and S_4 make the current flows in opposite directions regardless of port assignments of source and sink. That means this differential sensor is port-free if the connection is done as suggested.

If the four spirals are configured to meet the requirement for the symmetric differential inductive sensor, then the current in one of the two spirals (for example, S_2 and S_4 of Fig. 7) in the decreasing inductor flows in the opposite directions with the other three spirals. That is, the current in the spiral S_2 may flow in opposite direction to those of the spirals S_1, S_3, and S_4, or the current in the spiral S_4 may flow in opposite direction to those of the spirals S_1, S_2, and S_3, respectively, depending on the port assignments of source and sink. Either configuration will work as the symmetric differential sensor. Hereinafter we will only assume that the current in the spiral S_2 flows in the opposite direction compared to the current flows in the other spirals S_1, S_3, and S_4.

B. Principles

Let us assume that self inductances of and mutual inductances between the four spirals are presented as L_i and M_{ij}, then there relationship may be expressed as follows:

$$M_{i,j} = \begin{array}{c} \text{Displacement-invariant} \quad \text{Displacement-variant} \\ \left[\begin{array}{cc:cc} L_1 & M_{12} & M_{13} & M_{14} \\ M_{12} & L_2 & M_{23} & M_{24} \\ \hdashline M_{13} & M_{23} & L_3 & M_{34} \\ M_{14} & M_{24} & M_{34} & L_4 \end{array}\right] \\ \text{Displacement-variant} \quad \text{Displacement-invariant} \end{array} \tag{4}$$

The self inductances of four spirals are approximately equal due to their matching geometry and dimensions, i.e. $L_1 = L_2 = L_3 = L_4 = L$. These self inductances are displacement-invariant. The mutual inductance between S_1 and S_2, M_{12}, is negatively coupled since current in S_1 and S_2 flows in opposite directions. The mutual inductance between S_3 and S_4, M_{34}, is positively coupled since current in S_3 and S_4 flows in the same direction. Both M_{12} and M_{34} are displacement-invariant due to fixed relative position of each two spirals while having same absolute magnitude. They cancel each other when we calculate the total inductances of the two variable inductors and the total inductance of the sensor.

As the differential sensor stretches, the two interleaved spirals on the bottom plate change their overlapped area with the two interleaved spirals on the top plate so that the mutual inductances of the four spirals change, thereby changing the output voltage of the sensor. The changes in the mutual inductances between four spirals are different due to the opposing current direction in one of the spirals. The mutual inductances M_{13} and M_{14} are positively coupled since currents in S_1, S_3 and S_4 flow in the same direction, increasing with sensor extension. Mutual inductances M_{23} and M_{24} are negatively coupled since current in S_2 flows in the opposite direction as those in S_3 and S_4. The absolute magnitudes of M_{23} and M_{24} increase along with sensor extension due to the increase of their overlapped areas. That is, M_{13}, M_{14}, M_{23}, and M_{24} are displacement-variant. At the steady state of the symmetric differential sensor, even though the mutual inductances M_{14} and M_{23} have different coupling effects, their absolute values are equal due to the matching geometry of the two spirals. As the displacement increases, M_{14} decreases while M_{23} increases by a similar amount.

By using the segment-based approach method for estimating inductances [2, 7], we can represent the total inductance values of two variable inductors, L_{s1} and L_{s2}, based on the self of and the mutual inductances between the four spirals as follows:

$$\begin{aligned} L_{s1} &= L_1 + L_3 - M_{12} + M_{34} + 2M_{13} - M_{23} + M_{14} = 2(L + M_{13}) \\ L_{s2} &= L_2 + L_4 - M_{12} + M_{34} - 2M_{24} - M_{23} + M_{14} = 2(L - M_{24}) \end{aligned} \tag{5}$$

where $L_1 = L_2 = L_3 = L_4 = L$, $|M_{12}| = |M_{34}|$, $|M_{14}| = |M_{23}|$, and $|M_{13}| = |M_{24}|$ due to the sensor's symmetric geometrical structure. The total inductances of the two variable inductors L_{s1} and L_{s2} are simplified by canceling symmetric positive and negative mutual inductances. The resulting equation (5) is identical to the equation (1) that governs the total inductance of the single inductive sensor. This means that this new differential sensor performs the same function, but will have better noise immunity and stability during operation in challenging environments.

Also we can find the total inductance, L_s, of the differential sensor where the two variable inductors are serially connected as follows:

$$L_s = L_{s1} + L_{s2} + 2M_{s1,s2} = 4L \tag{6}$$

where $M_{s1,s2}$ is zero. Hence, the total inductance of the sensor is always constant as $4L$ regardless of the displacement of the sensor.

C. SDIS Simulation

Now we simulate the performance of this four-spiral differential version of the sensor using the simulation software (previously described in Section II). The following parameters were used in simulating inductance variances versus displacement:

1) The spirals are six turns with 400 μm width, 200 μm height, and 800 μm spacing.
2) A set of two spirals are interleaved with the spacing 200 μm on both the bottom plate and the top plate.
3) The outside dimension of the two interleaved spirals is 60 mm width and 40 mm height.
4) The two interleaved-spirals on the top plate are stacked on the other interleaved spirals on the bottom plate with the vertical distance 2 mm.

First, the simulation was performed without any connections between the spirals on the top plate and the bottom plate. In each spiral, source and sink ports were assigned so that the current in the spiral S_2 flows in the opposite direction with those in the other spirals (S_1, S_3, and S_4). Equation (7) shows resulting self-inductance of and mutual-inductance magnitudes and coupling relationships between each spiral.

$$M_{i,j} = \begin{bmatrix} L_1 & M_{1,2} & M_{1,3} & M_{1,4} \\ M_{1,2} & L_2 & M_{2,3} & M_{2,4} \\ M_{1,3} & M_{2,3} & L_3 & M_{3,4} \\ M_{1,4} & M_{2,4} & M_{3,4} & L_4 \end{bmatrix} = \begin{bmatrix} 3192.2 & -2957.3 & 2320.6 & 2309.8 \\ -2957.3 & 3193.7 & -2310.2 & -2322.2 \\ 2320.6 & -2310.2 & 3185.4 & 2950.9 \\ 2309.8 & -2322.2 & 2950.9 & 3186.0 \end{bmatrix} nH \tag{7}$$

Within rounding errors, we can verify our assumptions that $L_1 \approx L_2 \approx L_3 \approx L_4$, $|M_{12}| \approx |M_{34}|$, $|M_{14}| \approx |M_{23}|$, and $|M_{13}| \approx |M_{24}|$. Since the direction of the current flow in the spiral S_2 is different from that of the other spirals, mutual inductance coupling related to the spiral S_2 are negative. Using the equation (5) and the simulation result of the four separated spirals, we can estimate inductances of two variable inductors that are configured with these four spirals. The estimated inductances are

$$\begin{aligned} L_{s1,\max} &= 2L + 2M_{13} = L_1 + L_3 + 2M_{13} = 3192.2 + 3185.4 + 2 \times 2320.6 = 11018.8\,(nF) \\ L_{s2,\min} &= 2L - 2M_{24} = L_2 + L_4 - 2M_{24} = 3193.7 + 3186.0 - 2 \times 2322.2 = 1735.3\,(nF) \end{aligned} \tag{8}$$

In this case the inductances of the two variable inductors are maximum and minimum, respectively since the absolute magnitude of M_{13} and M_{24} are maxima.

The inductances of the two variable inductors are directly calculated after connecting the each two spiral (S_1, S_3) and (S_2, S_4) to form the increasing and decreasing variable inductors respectively. Source and sink are allocated to the ports of each variable inductor so that the current in the spiral S_2 flows in the opposite direction to those of spirals S_1, S_3, and S_4. The simulation result for the two variable inductors is

$$M_{i,j} = \begin{bmatrix} L_{s1} & M_{s1,2} \\ M_{s1,2} & L_{s2} \end{bmatrix} = \begin{bmatrix} 11041.0 & -9.2872 \\ -9.2872 & 1737.5 \end{bmatrix} nH \tag{9}$$

Note that the mutual inductance between the two variable inductors is very small compared to the self inductances of the two variable inductors (by a factor of 100 to 10,000), and hence can be ignored as expected. The resulting, simulated self inductances of the two variable inductors are almost equal (within 0.1 %) to the inductances of equation (10) which was estimated using equation (5) and equation (7). Hence, equation (5) may be used for most sensor development applications.

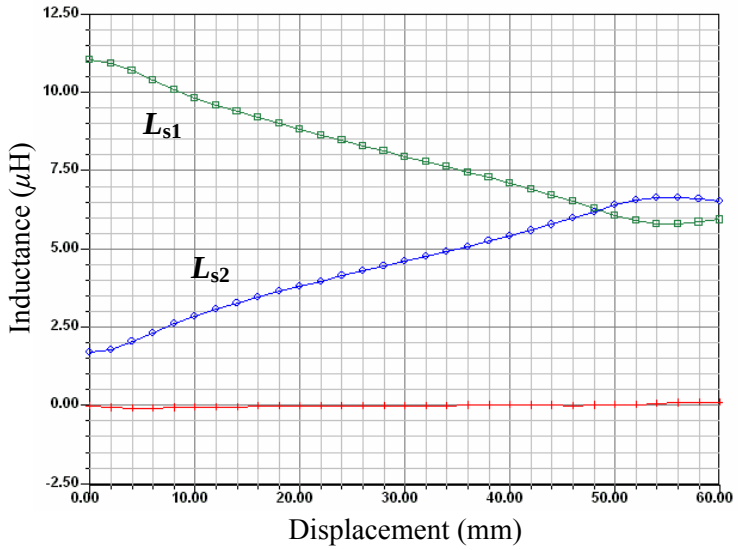

Fig. 8. Simulation results for inductance changes of the two variable inductors in the symmetric differential sensor as the displacement in x-axis increases. A bottom flat line indicates the mutual inductance between the two variable inductors.

Fig. 8 shows the simulation results for the inductance changes versus displacement in x-axis. As was noted in inductive sensor configurations on Fig. 4, this new differential sensor also exhibits nonlinearities at both lateral displacement extremes due to interference between the vertical bars of each spiral. Nevertheless, the simulation shows that there is a large linear sensing range in the middle of the displacement range. We can increase the linear sensing range by increasing the horizontal size of the spirals. As shown in the simulation results, the mutual inductance between the two variable inductors is almost zero regardless of displacement due to the symmetric current flow geometry.

V. SENSING CIRCUITRY

To detect inductance variances, different sensing circuitry is required for each of the three different sensor configurations. As a modulating (or active) device, an inductive sensor is commonly driven by an alternative current or voltage to generate signal (voltage output) that is coupled with inductive parameters. Therefore the sensor's interface circuitry requires an ac voltage or current source. The SIS of Fig. 2 can be inserted into an oscillator circuit, for example a Colpitts oscillator, as a resonant tank component to evaluate inductance variance for displacement measurements. The resonant

frequency of the tank circuit changes as the inductance of the single sensor changes. The measured displacement by the single inductive sensor may have a nonlinear relationship with the inductance changes. In addition, the influence of the surrounding magnetic fields and parasitic inductances and capacitances can also adversely impact the operation of the instrumentation circuit.

The inherent nonlinearity of the measurement method used for the SIS may be improved by employing a differential sensor. The inductance variances in the "lateral differential inductive sensor" shown in Fig. 6 can be measured using circuits developed for linear variable differential transformers (LVDTs). Traditionally, these LVDT structures offer very fine resolution, electrical isolation between the primary and secondary coils, and linearity. The spiral S_3 of Fig. 6 is used as a primary coil while the other two spirals are considered as secondary coils as shown in Fig. 9(a). If an alternating current is applied into the primary coil, voltages are induced in the two secondary coils according to the position of the primary spiral. This configuration of the spirals provides electrical isolation between the primary and secondary coils. However, the transformer dissipates energy in the form of flux leakage and introduces a phase difference between the input excitation and the output sensed output voltages [10]. In addition, for better efficiency, relatively high current flow and high frequency input excitations to the primary coil are required. As usual in LVDTs, when the primary is in the central position as shown in Fig. 10 (a), there is an equal voltage induced into both S_1 and S_2 which add together to generate v_o. However, since their polarity is in opposition, the resulting output voltage is zero. As the primary moves closer to S_1 (and away from S_2), the output sum favors S_1 which is in-phase with the excitation voltage. Conversely, as the primary coil moves closer to S_2 (and away from S_1), the sum favors S_2 (the out-of-phase voltage). The electronics therefore, must detect information about both the phase and magnitude of the output.

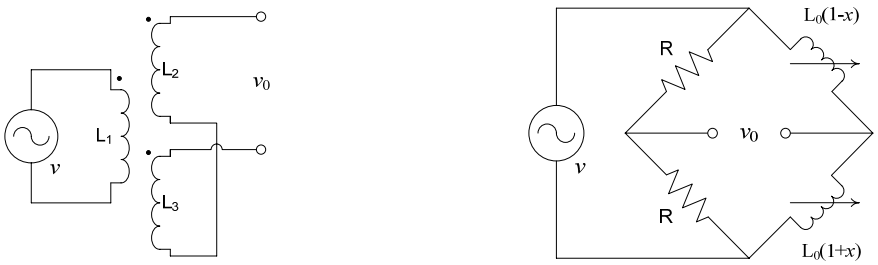

(a) Two-port differential transformer for LDIS (b) Linear ac bridge circuit for SDIS

Fig. 9. Sensing circuitry for differential inductive sensors.

The SDIS structure requires another instrumentation circuit. This configuration may be used as an autotransformer to avoid many of the traditional drawbacks of differential transformers such as flux leakage, unnecessary power consumption, and phase detection errors. In the autotransformer circuit, the two inductors of the sensor can be used as a voltage divider. The SDIS is well suited for this mode of operation. First, as shown in the simulation results of Fig. 8, the mutual inductance between the two sets of inductive spirals is almost zero regardless of the sensor's lateral position. This is true at any distance between two plates if the plates are fabricated in a manner that requires them to keep their flat-plane orientation. Second, the total inductance of each set serially connected spirals is equal to the sum of each inductance measured independently, and therefore is constant regardless of the displacement and distance between two plates. These characteristics allow the symmetric differential inductive sensor to be employed as a voltage divider. Therefore, the output autotransformer type differential sensor can be detected using the well-known linear ac bridge circuit with resistive arms [10] as shown in Fig. 9(b) where the output voltage is as follows:

$$v_o = -v\frac{x}{2} \tag{10}$$

Fig. 10 compares the two sensing configurations displayed in Fig. 9. The output of the LDIS is characterized by magnitude and phase differences as shown in Fig. 10(a) while the voltage output of the symmetric differential inductive sensor is characterized by only its magnitude as shown in Fig. 10(b). Thus Fig. 10(b) is the preferred sensing method. Through its whole effective sensing range,

the output voltage can be identified by magnitude reducing the complexity for the instrumentation circuit.

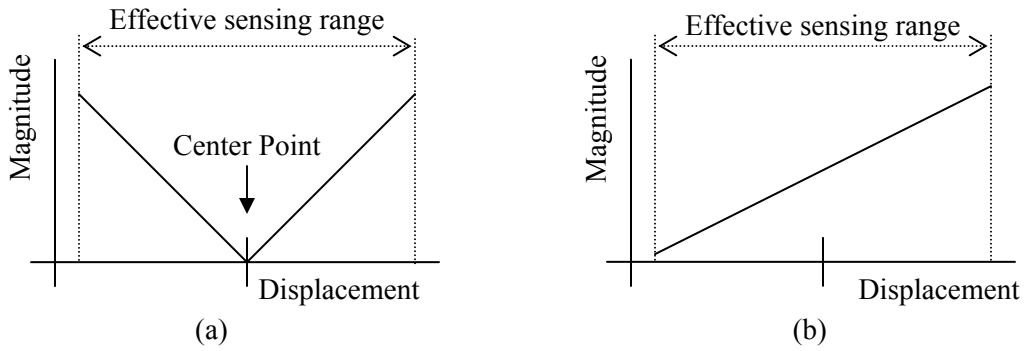

Fig. 10. Comparison voltage outputs in the two differential sensors (a) the lateral differential inductive sensor and (b) the symmetrical differential inductive sensor.

VI. EXPERIMENTAL RESULTS AND DISCUSSION

A. Fabrication

In order to demonstrate proof of concept, a prototype of the inductively coupled structure described in Fig. 1 was first implemented using two different nonwovens, one stretchable and the other not, which are laterally connected using non-toxic glue. For the planar spirals, fine magnet wires (diameter of 90 μm and resistance of 2.868 Ω/meter) were used as shown in Fig. 11.

(a) Single wire winding (two terminals, type α)

(b) Two interleaved wires wound together (four terminals, type β)

Fig. 11. Planar spiral inductors based on fine magnet wires.

After characterization, the inductors of Fig. 11 were then used to construct the sensing structures of Fig. 2 (single inductor sensor, SIS), Fig. 5 (lateral differential inductive sensor, LDIS), and Fig. 7 (symmetric differential inductive sensor, SDIS). Fig. 12 displays a photograph of one of the implementations, that of the SIS of Fig. 2.

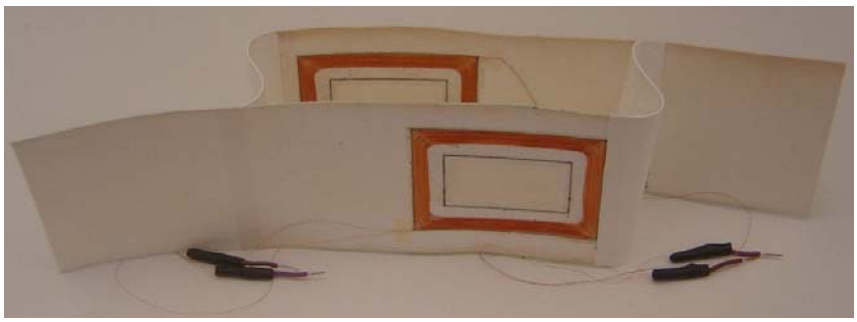

Fig. 12. A prototype sensor for the single inductive sensor (SIS).

B. Inductance measurements

Individual spiral windings of types α and β displayed in Fig. 11 were placed in their respective positions to implement three of the new sensors (Figs. 2, 5, and 7). Measurements of self inductances and serial resistances of the individual spirals used in fabricating the three sensors were measured using a SENCORE "Z-Meter" Inductor-Capacitor Analyzer Model LC 53 and a HP Model 34401A Multimeter and are displayed in Table 1. The inductance of each spiral in the SDIS (Fig. 7) was measured while the other spirals were in the open-circuit mode of operation.

Table 1. Inductance and serial resistance of the spiral windings made from fine magnet wires. The subscript numbers indicate the position of the spirals in the sensors layout, and the subscripts α and β indicate the spiral wining type as displayed in Fig. 11.

	SIS (Fig. 2)		LDIS (Fig. 5)			SDIS (Fig. 7)			
	$S_{1\alpha}$	$S_{2\alpha}$	$S_{1\alpha}$	$S_{2\alpha}$	$S_{3\alpha}$	$S_{1\beta}$	$S_{2\beta}$	$S_{3\beta}$	$S_{4\beta}$
Inductance (μH)	126	135	154	155	151	83.8	83.4	82.2	83.4
Resistance (Ω)	17.52	18.75	20.73	21.16	20.7	16.47	16.75	16.88	16.78

Next we interconnected the spiral winding to implement the three sensor types, and measured the inductance changes during sensor operation (while stretching the sensors). These results are presented below.

Single inductive sensor (SIS, Fig. 2). Fig. 13 and 14 show the results for the SIS, measured by decreasing overlapping areas between the two spirals by increments of 1mm along the x-axis. Fig. 13 shows the inductance variances along the sensor extension under different vertical spacing (z-axis) between the two spirals. The z-axis spaces between the spirals was created using the substrate material upon which the spirals were mounted (Evalon® 100gsm, thickness 0.40mm). Fig. 13(a) shows the inductance variance when the spirals are connected so that the current flows in the same direction in both. In Fig. 13(b), current in the spirals flows in opposite directions. Note that the relative sensitivity to the vertical distance (z-axis) and vertical deviation (y-axis deviation) is apparent in the graphs and that there is a linear sensing range in displacement if the vertical deviation between the two spirals is constant.

Fig. 14 demonstrates the effect of misalignment in the y-axis between the two SIS spirals of Fig. 2. Total inductance of the sensor was measured by shifting the top spiral two millimeter steps in the y-axis while the distance in z-axis between the two spirals was kept constant at a depth equal to the thickness of one nonwoven substrate. Misalignment causes and inductance increase in one inductor with a corresponding decrease in the other. Misalignment in the y-axis lowers sensibility while maintaining linearity. Hence, this sensing scheme is appropriate for displacements between 10 and 50 mm.

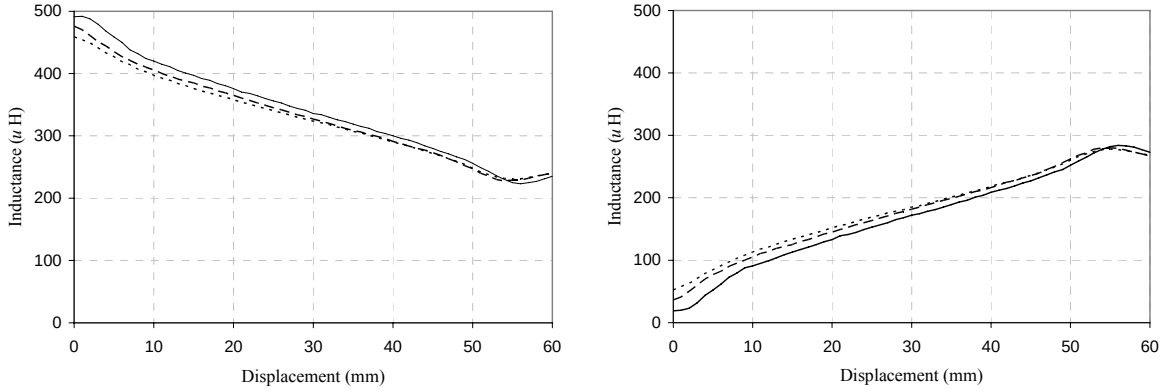

(a) (b)

Fig. 13. Inductance variances of the single inductive sensor. (A solid line (Gap 0) indicates the two spirals were adjacent without a gap. A dashed line (Gap 1) indicates there was one substrate between two spirals. A dotted line (Gap 2) indicates there were two substrates between two spirals.) (a) decreasing type (current in the same direction), (b) increasing type (current in opposite directions).

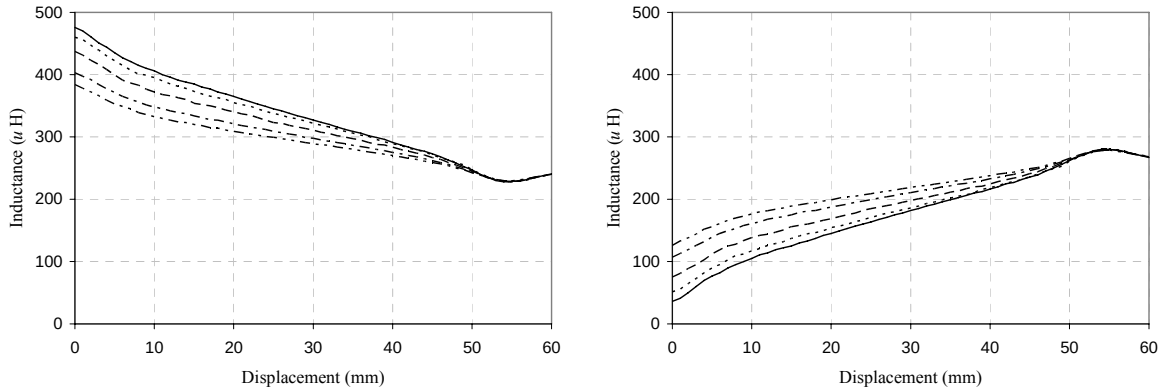

(a) (b)

Fig. 14. Inductance variances of the single inductive sensor. (From outside, each line indicates the inductance variance when the vertical misalignment is 0, 2, 4, 6, 8mm.) (a) decreasing type (current in the spirals is in the same direction), (b) increasing type (current in the spirals is in the opposite direction)

Lateral differential inductive sensor (LDIS, Fig. 5). To determine the relative mutual inductance variances between the primary coil and the two secondary coils in the LDIS during sensor extension, we measure induced voltages, e_{s1} and e_{s2}, in the secondary coils because these voltages are produced by the mutual inductances and current flow in the primary coil. For example, $M_{13} = e_{s1}/2\pi f i_p$, where M_{13} is mutual inductance between S_1 and S_3, e_s is the induced voltage in the secondary coil S_1, and i_p

is the current flow in the primary coil. During operation, the two lateral secondary spiral coils are one cm apart and the primary spiral coil is displaced 0.40 mm from the two secondary coils along the z-axis, separated by a nonwoven textile material.

Fig. 15 shows the production of the induced voltages in the two secondary coils when an ac voltage [sin ($2\pi ft$), f = 20 KHz] is applied to the primary coil. The primary coil S_3 is set up such that it overlaps one of the two spiral coils, S_2. In this position, the voltage e_{s2} is at its maximum and e_{s1} is at its near its minimum. When the primary coil moves away from S_2 towards spiral S_1, e_{s2} decreases and e_{s1} increases until the primary resides equally over both spirals. At this "balancing point" the two voltages e_{s2} and e_{s1} are equal. As the primary continues its movement away for S_2 towards S_1, voltage e_{s2} continues to decline while e_{s1} increases towards its maximum. So the x-axis of the graph represents the planar distance between S_3 and S_2. As expected, the experimental response of the induced voltages in the graph is very similar to the shape of mutual inductances in the LDIS simulation result of Fig. 6. The transition of the overall dominant magnetic coupling between the primary coil and the each of the two secondary coils from positive to negative and vice versa in Fig. 6 results in the phase conversion in the induced voltages. That is, each induced voltage has become 180˚ out of phase at the deviation of 21 mm (for e_{s1}) and 50 mm (for e_{s2}) in Fig. 15. Therefore, the actual effective differential sensing range is limited to the interval between these two points. Over the effective range, a maximum of approximately 12% of the applied voltage is transferred to the secondary spirals.

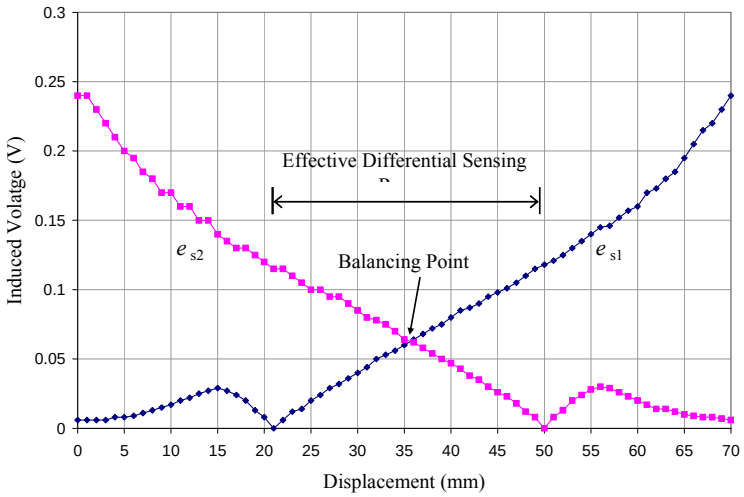

Fig. 15. LDIS experimental results. Voltages e_{s1} and e_{s2} are induced in secondary spiral S_1 and S_2, respectively.

Symmetric differential inductive sensor (SDIS, Fig. 7). Inductance variances along displacement variations in the three xy and z directions of the two sets of the two interleaved spirals were measured in a similar manner to that of the single inductive sensor after the four spirals were configured using wound coils as shown in Fig. 11 (b). Fig. 16 shows the inductance variances as the relative displacement in x-axis of the two interleaved spirals is increase in 1 mm increments. Each inductor increases and decreases by nearly the same amount. The top flat line indicates the total inductance of the sensor. Regardless of the displacement, the total inductance is nearly uniform. There is a balancing point where the two variable inductors have same inductances. Note that this balancing point differs from the LDIS whose balancing point is in the middle of its liner differential sensing range. For the SDIS the balancing point is near on end of its useful dynamic range. That is, the balancing point determines the maximum point of its linear differential sensing range.

Fig. 17 shows the inductance variances of the two inductors at different vertical variations in the z-axis (a) and misalignments in the y-axis (b) of the two sets of two interleaved spirals. As shown in Fig. 17, the inductances of the two variable inductors depend on both the misalignment and vertical distance along the y-axis. The balancing point is distance-in-z-axis-invariant but misalignment-in-y-

axis-variant. That means misalignment reduces the linear sensing range. Regardless of the misalignments in y-axis or vertical gaps in the z-axis between the two substrates, we can visually verify that there is a quasi linear sensing range in the middle of the displacement range.

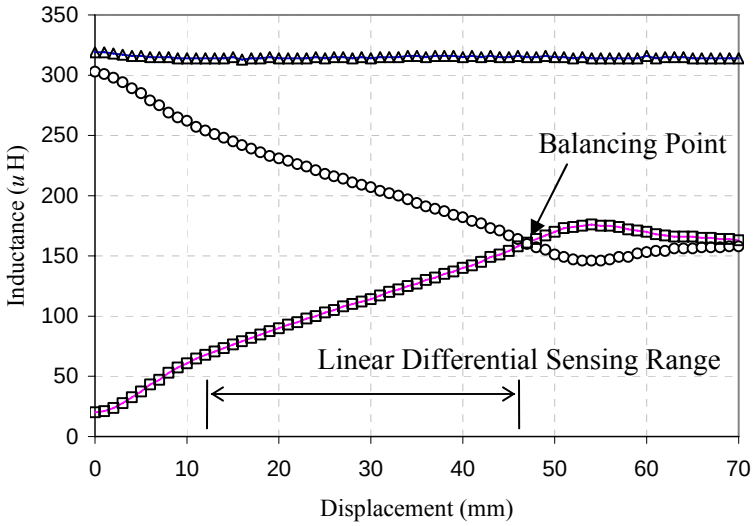

Fig. 16. Experimental inductance measurements of the symmetric differential inductive sensor. The two sloping lines show the inductances of the two variable inductors (each a pair of spirals as shown in Fig. 7), increasing and decreasing, respectively. Inductor L_1 consists of spirals S_1 and S_3 serially connected; L_2, of S_2 and S_4. The inductances of L_1 and L_2 were each measured independently with the other inductor in an open-circuit mode of operation. The top flat line indicates the total inductance of the sensor with L_1 and L_2 connected in series.

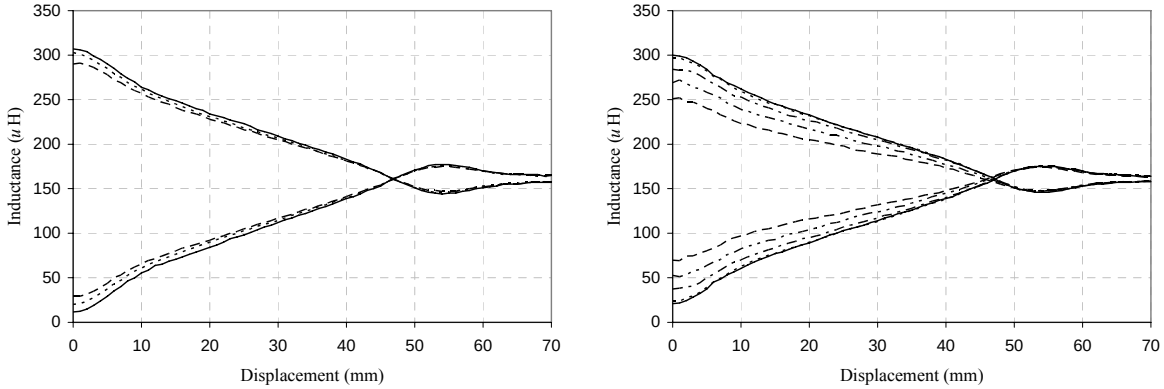

(a) (b)

Fig. 17. Experimental inductance measurements of the symmetric differential inductive sensor with different gaps and misalignments. As in Fig. 16, the inductance of each sensor was measured while its counterpart is open-circuited. (a) Inductance variances at the different vertical gaps between the two spirals. (A solid line indicates Gap 0. A dotted line indicates Gap 1. A dashed line indicates Gap 2.) (b) Inductance variance at different misalignments along the y-axis. From the outside, each line indicates the inductance variance when the y-axis misalignments are 0, 1, 3, 5, and 7 mm, respectively.

C. Position Detection Circuitry

Three different circuit configurations were designed, a LC tank, a differential transformer, and an autotransformer, one for each of the three sensor types.

Single inductive sensor (SIS, Fig. 2). For the SIS, we employed a Colpitts oscillator in which variations in sensor inductance generates a frequency shift. The resonant frequency of the Colpitts oscillator as shown in Fig. 18 is determined by

$$f_{osc} = \left(2\pi \sqrt{L\left(\frac{C_1 C_2}{C_1 + C_2} \right)} \right)^{-1} \tag{11}$$

For frequency stability, relatively high capacitance is required to ensure that parasitic capacitance changes have minimal impact. The output of the oscillator drives a buffer to isolate the oscillator from the load to improve stability. Then, the frequency shift is detected by a FM demodulator implemented using a phased-locked loop.

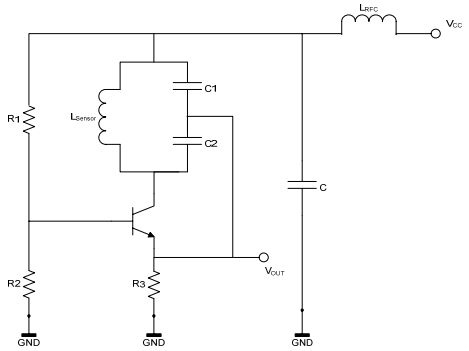

Fig. 18. The Colpitts oscillator circuit for the SIS.

Lateral differential inductive sensor (LDIS, Fig. 5). For the LDIS, the inductors S_1, S_2, and S_3 are connected to a monolithic LVDT signal conditioner (Analog Devices® model AD598) as shown in Fig. 19. This chip includes the necessary circuit elements for a differential transformer configuration such as a sine wave oscillator, a filter, and amplifiers. Only few extra passive components are

required to obtain a scaled DC output. For better performance, the conditioner requires that the sum of the secondary voltages across S_1 and S_2 remains constant regardless of displacement. The LDIS approximates this requirement because the sum is nearly constant in its designed differential sensing range. However, strictly speaking, the sum is not constant. Rather its response is convex having its highest value in the middle and the lowest values on the both ends of its effective different sensing range. The DC voltage output of the AD598 is determined by

$$v_o = \alpha \frac{e_{s2} - e_{s1}}{e_{s2} + e_{s1}} \tag{12}$$

where α is the gain.

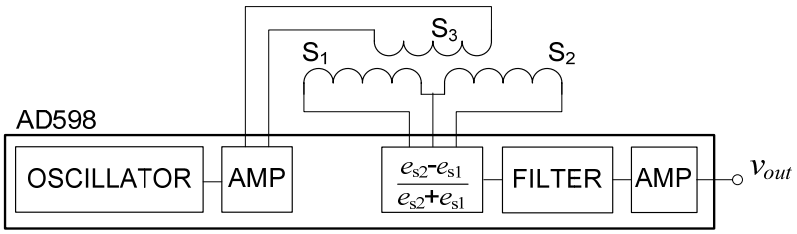

Fig. 19. LDIS sensing circuit schematic.

Symmetric differential inductive sensor (SDIS, Fig. 9). The linear ac bridge circuit (Fig. 9b) is employed with the SDIS. The SDIS is connected into a bridge circuit whose output is fed into a differential amplifier. The output of the amplifier is then supplied to the circuit of Fig. 20. Here, a chopping diode, D, and a capacitor to ground, C, serve as an envelop detector (a half wave rectifier) to extract the envelop of the ac signal being generated in the bridge. In the detector, an increasing v_{in} charges the capacitor, C, whose voltage is discharged through a resistor, R, when the signal v_{in} is decreasing.

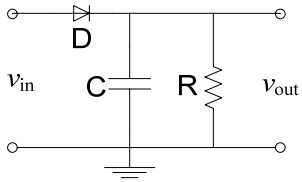

Fig. 20. Envelope detector based on half wave rectifier for SDIS.

The detected envelop may be distorted from 5% to 10% due to ripple and negative peak clipping effects and the diode's voltage-current characteristics. The negative clipping effect limits the accuracy of the detector when the changes of displacement are fast. To complete the detection circuitry for the SDIS, v_{out} is smoothed through a low pass filter. If precise measurement is required, a more accurate AM demodulation technique can be used to detect envelop of the signal.

Measured DC voltage outputs for the SIS, the LDIS, and the SDIS sensors with their respective sensing circuitry are displayed in Fig. 21. All the DC outputs were observed while the z-axis spaces between the spirals was filled with a nonwoven substrate upon which the spirals were mounted and hence the distance in z-axis between the two spirals was kept constant at a depth equal to the thickness of one nonwoven substrate (about 0.4 mm). Single 5V for the SIS and SDIS or dual ±5V for the LDIS were supplied to the respective sensing circuitry. For the Colpitts oscillator (Fig. 18) in the SIS circuitry, 0.01 uF capacitor was selected for C1 and C2 so that the oscillator generates sine waves having between about 125 and 165 KHz frequencies along with inductances of the sensor. To pickup displacement variance signal from the modulated oscillating signal, a CD74HC7046A high speed CMOS logic PLL chip of Texas Instruments was used. Fig. 21 (a) shows measured outputs of the FM demodulator along a unit displacement change in the x-axis between two spirals.

Fig. 21 (b) displays observed DC voltage outputs in the LDIS circuitry. To set up necessary parameters and peripheral components for the LVDT conditioner chip (see the datasheet for details), we used the measured data shown in Fig. 15. Then, the gain was adjusted for the DC output to be not saturated within a designed effective linear sensing range while achieving better sensitivity at 20 KHz in which the conditioner can generate maximally. With these settings, we changed the excitation frequency and measured the outputs as shown in Fig. 21(b). At a low excitation frequency, for example 2.095 KHz, the output was saturated in the output minima. To avoid this saturation, the gain

factor might be lowered, resulting in a degraded sensitivity. Note that in the given gain factor the slop of the DC outputs in a valid linear sensing range may be kept constant regardless of the excitation frequency.

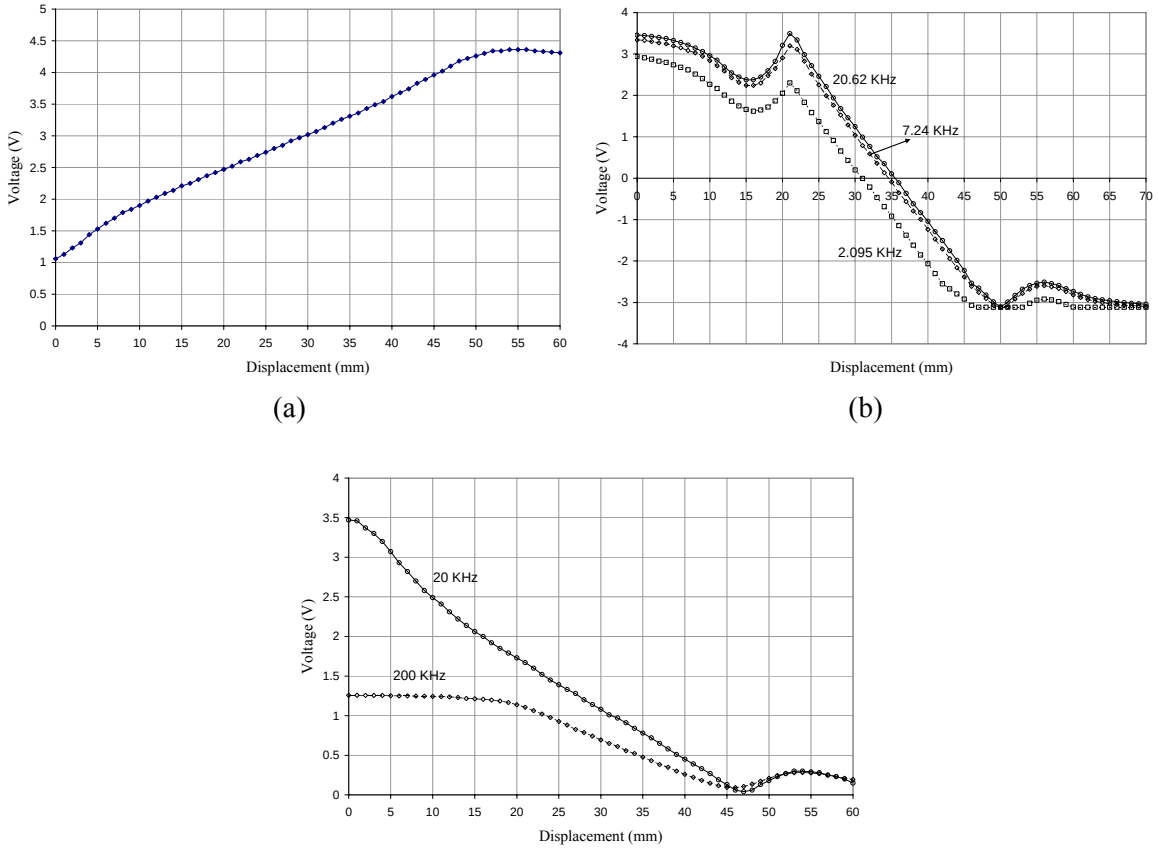

Fig. 21. The measured DC voltage outputs of the various circuits for (a) SIS, (b) LDIS, and (c) SDID, respectively.

In the AC bridge circuit of the SDIS sensing circuitry as shown in Fig. 9 (b), higher the modulating frequency, larger the differential output in a given inductance change and a fixed arm resistance. The reason is that inductor's impedance increases with the operating frequency. For example, magnitudes of the AC-bridge output at 200 KHz sinusoid input are definitely larger than that at 20 KHz sinusoid input. So a higher modulating frequency is preferred, but a following differential amplifier with a high gain is commonly narrow band-limited, resulting in altering shape of a sinusoid output of the ac

bridge circuit and generating a saturated DC output at the envelop detector as shown in Fig. 21 (c). The DC outputs at 200 KHz sinusoid input are saturated under 20mm deviation in the x-axis. To avoid the saturation, a very small gain in the differential amplifier and extra high gain amplifier is required. In Fig. 21 (c), the other DC outputs are measured at 20 KHz sinusoid input with 530 mV p-p and gain 50 of the differential amplifier while the arm resistor, R has 220 ohms.

D. Effective Linear Sensing Range (ELSR) and Linearity

To compare linear sensing ranges and linearity in the three planar inductive sensors, representative measured DC voltage outputs for the SIS, the LDIS, and the SDIS sensors in tandem with their respective sensing circuitry are displayed in Fig. 22. In the figure, we can visually notice that an effective linear sensing range (ELSR) is widest in the SIS and most narrow in the LDIS. Each effective linear sensing range for the SIS, LDIS, and SDIS is shown in Table 2. To quantify the linear relationship between the measured output voltages and x-axis displacements, a linear model was produced using simple linear regression and the data within the ELSR. We determined regression coefficients using the method of least squares such that the corresponding estimated line has the smallest possible sum of squared errors.

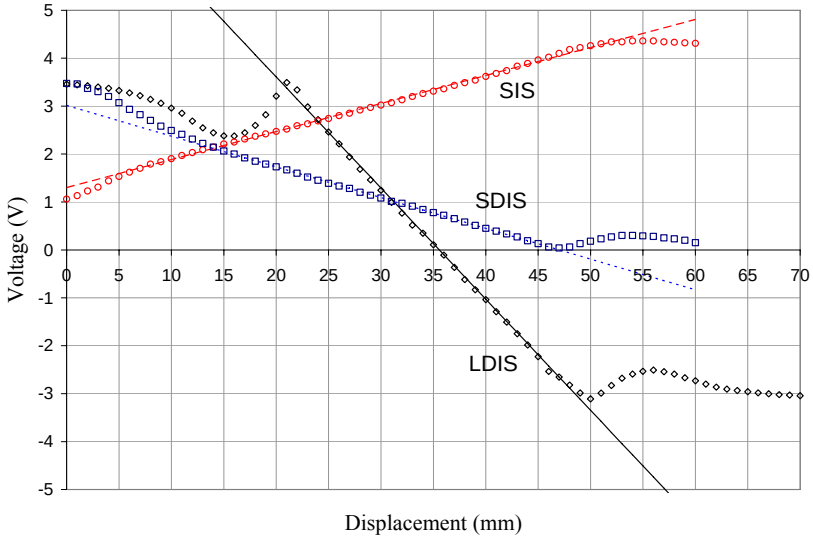

Fig. 22. The measured DC outputs and their estimated values using the simple linear regression. (The markers indicate the observed DC voltages and the lines indicate their estimated outputs.)

Table 2. The linearity, ELSR, and the regression coefficients of each sensor

	SIS	LDIS	SDIS
Effective Linear Sensing Range (ELSR)	8 mm – 52 mm (44 mm)	23 mm – 48 mm (25 mm)	13 mm – 45 mm (32 mm)
Slope, β_0	0.058457181	-0.2318703	-0.064140565
Y-intercept, β_1	1.300729029	8.245428995	3.014499618
Linearity	2.85 %	1.93 %	1.92 %

The linearity was obtained from the percentage of the most deviated distance from the estimated line over the full scale output. The resulting linearity parameters of the three sensor types are shown in Table 2, indicating good performance. The linearity of the SIS is lowest among the three sensor types. However, if we refine the effective linear sensing range of the SIS, for example by changing the farthest end of ELSR from 52mm point to 46mm point, then we can improve the linearity up to 2.03% which is close to the linearity of the LDIS and the SDIS, while still having the widest ELSR (38 mm).

In the LDIS system, even though the DC output levels are different with the three excitation frequencies, three output lines are parallel, that is, have a very similar slope within a valid linear sensing range that does not include saturated outputs. On the other hand, the output trends of the SDIS have different slopes depending on the operating frequencies and they cross around the balancing point in the x-axis with nearly zero magnitude. We can also notice this phenomenon when we measured DC output voltages by changing the distance in the y-axis between spirals while fixing a modulating frequency. In the LDIS system, the slops of the measured outputs at the different gaps are almost equal. In the SDIS system, the slopes of measured output voltages at the different distances differ from each other but cross near the balancing point.

VII. CONCLUSIONS

In this paper, we explored the feasibility of employing open-rectangular spiral windings for implementing planar position sensors on flexible nonwoven textile substrates. Several configurations of multiple spirals were introduced using a double substrate structure. Single and differential sensor schemes were explored. A single inductive sensor based on two spirals generates high self and mutual inductance compared to the differential sensor configurations. One of the differential inductive sensors obtains its sensitivity by changing its overlapping areas in opposite directions when the sensor is stretched. Another new differential inductive sensor was devised by utilizing both negative and positive mutual couplings while two differential inductors undergo the same overlapped area changes during sensor extension. Our test with respective sensing circuitry reveals that the three sensor types have good linear characteristics while having large sensing ranges.

Our conclusion is that this method of implementing displacement sensors on flexible nonwoven textile substrates shows great promise. Future work is planned to fabricate the spiral windings directly onto the nonwoven textile substrates using printing technologies. If this is successful, the cost of implementing these sensors will be greatly reduced and thus greatly increasing the number of applications that can be envisioned.

REFERENCES

[1] A. F. Vaz and R. Bravo, "Smart piezoelectric film sensors for structural control," *Instrumentation and Measurement, IEEE Transactions on*, vol. 53, pp. 472-484, 2004.

[2] H. Greenhouse, "Design of Planar Rectangular Microelectronic Inductors," *Parts, Hybrids, and Packaging, IEEE Transactions on*, vol. 10, pp. 101-109, 1974.

[3] S. S. Mohan, "The Design, Modeling, and Optimization of On-Chip Inductor and Transformer Circuits," Stanford University, December 1999.

[4] C. P. Yue and S. S. Wong, "On-chip spiral inductors with patterned ground shields for Si-based RF ICs," *Solid-State Circuits, IEEE Journal of*, vol. 33, pp. 743-752, 1998.

[5] S. S. Mohan, M. del Mar Hershenson, S. P. Boyd, and T. H. Lee, "Simple accurate expressions for planar spiral inductances," *Solid-State Circuits, IEEE Journal of*, vol. 34, pp. 1419-1424, 1999.
[6] A. Zolfaghari, A. Chan, and B. Razavi, "Stacked inductors and transformers in CMOS technology," *Solid-State Circuits, IEEE Journal of*, vol. 36, pp. 620-628, 2001.
[7] M. D. L. Bueno and A. K. T. Assis, *Inductance And Force Calculations In Electrical Circuits*: Nova Science Publishers, Inc., New York, 2001.
[8] S. C. Saxena and S. B. L. Seksena, "A self-compensated smart LVDT transducer," *Instrumentation and Measurement, IEEE Transactions on*, vol. 38, pp. 748-753, 1989.
[9] Y. Kano, S. Hasebe, C. Huang, and T. Yamada, "New type linear variable differential transformer position transducer," *Instrumentation and Measurement, IEEE Transactions on*, vol. 38, pp. 407-409, 1989.
[10] R. Pallas-Areny and J. G. Webster, *SENSORS AND SIGNAL CONDITIONING*: JOHN WILEY & SONS, INC., 1991.

Chapter 6

A WEARABLE PHYSIOLOGICAL MONITORING SYSTEM BASED ON TEXTILE-EMBEDDED SENSORS AND ITS APPLICATION IN SLEEP MONITORING

ABSTRACT

A wearable physiological monitoring system has been developed to monitor a wearer anywhere and anytime for health care, disease diagnosis, security, home rehabilitation, and/or surveillance. The system including biomedical sensors provides flexibility and comfort as well as robust signal sensing against noise interference and artifacts generated by body movement. Conventional wearable monitoring systems lack some of these desirable characteristics. For example, wearable monitoring systems based on knitting technology provide comport but their sensing capability for physiological signals, especially in EEG, EMG, and EOG, is limited even though sensors and interconnects are integrated into the garment in a textile form. In this paper, we described a wearable physiological monitoring system that achieves comfort as well as good signal sensing capability. The system includes textile-embedded sensors for ECG and respiration monitoring based on screen printing technology, a data acquisition module, and analysis software. In addition, we describe a sleep monitoring system as an application of the wearable monitoring system.

I. INTRODUCTION

In recent years, the demand for an unobtrusive, unconstrained, long-term, and continuous patient monitoring method for health care, disease diagnosis, and home rehabilitation has been sought by many research teams around the world [1-10]. A health monitoring system called SmartShirt® has been developed to monitor a wearer anywhere and anytime [1]. In monitoring systems of this type, biomedical sensors serve as front-end elements and, as such, are directly, indirectly, or invasively placed into contact with the human body to measure its physiological status, or to provide additional information like geo-location through the use of a GPS system and body posture through the use of

accelerometer. These monitoring systems require reliable and unobtrusive technologies to incorporate sensors and sensor networks into the everyday lives of medical patients. Commonly, the sensor system and its peripheral devices have been implemented as a body-worn apparatus or a surrounding apparatus like a bed, sofa, and an automobile [2]. A wearable sensor may be housed in body accessories such as a ring[3], a pendant [4], and a wrist watch [5], or integrated into a garment or a belt [5-12]. These examples of wearable health monitoring systems implement various hierarchical data-communication structures or signal interconnect methods.

In the ring sensor [3], a pulse oximetry sensor based on photoplethysmographic (PPG) techniques was developed for cardiovascular monitoring. All components including the sensor and a low power transceiver are integrated into the ring and it communicates with a remote server. In contrast, most of the other body-worn sensors and devices have a client-server architecture that forms a body area network (BAN); one or more sensors and devices (clients) communicate directly to a body-worn server via hard-wired or wireless connections. In [4], a passive wireless stethoscope system for health monitoring called "Smart Mole" was presented. A skin-attachable condenser microphone forms a resonant circuit with a coil. Then a detector circuit in the form of a pendant collects the sound using an inductive coupling technique. These body-accessory-type systems provide good long-term wearability, but the sensor's type and position are limited.

For wireless BANs, a sensor must be incorporated into a single unit that also contains a conditioning circuit, communication link, and power source. In [13], a wireless intelligent physiological sensor (WISE) is described that includes an ultra low-power microcontroller for ECG/EEG monitoring, physical rehabilitation, and long-term respiratory monitoring. These WISEs communicate with a body-worn server that interacts with a remote host system. For example, a body-worn personal server implementing a wireless heart rate monitor (WHRM) collects heart rate variability data from a commercial chest belt sensor to evaluate stress resistance during intensive physical training. A

wireless BAN-based monitoring system is highly desirable for wearers who require free body movement such as war fighters.

The LifeShirt System™ is an example using a BAN in which the sensors and wired interconnections are hidden in a garment of the user [11]. The system, which consists of LifeShirt Garment, LifeShirt Recorder, and VivoLogic software, is a well-publicized commercial wearable monitoring system for seamless detection of physiologic parameters during normal daily activities. Inductive plethysmography (IP) sensors are embedded into the LifeShirt Garment by sewing at abdominal and chest levels for respiration monitoring. Electrodes for ECG as well as these IP sensors are wired to the HandSpring Visor™ (LifeShirt Recorder) to store physiological data on a compact flash memory card. Other optional sensors for measuring blood pressure, blood oxygen saturation and end tidal CO_2 are attached to the shirt using secure connectors. VivoLog Digital Patient Diary software in the PDA allows recording time/date-stamped text information like symptoms. Finally VivoLogic software can process and analyz the physiological data to report sleep status.

Another example of a wired-BAN-based wearable monitoring system is SmartShirt™ [1, 12]. The SmartShirt™ is different from LifeShirt™ in that wired connections are embedded onto fabrics using textile-processing technology. The textile substrate is designed as a wearable motherboard upon which sensors can be placed anywhere using their interconnection technology. The system can record heart rate, respiration rate, and body temperature using off-the-shelf sensors.

Even though the wired systems described above enhance wearability by hiding sensors and/or connections into the clothing, the bulky, off-the-shelf sensors are still obtrusive. In recent work, there has been progress in integrating sensors and connections into garments in a textile form. WEALTHY (WEarable heALTH care sYstem) is a well known wearable health care system based on textile sensors [8]. Fabric electrodes were fabricated by knitting stainless-steel-based yarns (percentage of

metal is 30%) for ECG monitoring. For respiration monitoring, piezoresistive fabric sensors were realized using Lycra™ fabric coated with carbon-loaded rubber (CLR), while for activity monitoring, commercial conductive yarns were knitted onto other fabric clothing items. Interconnection was achieved with the conductive yarns by the tubular intarsia technique and sandwiched between two insulated textiles. Then, a body-worn server, called the Potable Patient Unit (PPU), processes the signals while communicating with the remote server via a cellular phone (GPRS-based) and the TCP/IP protocol.

The Respibelt™ and Textrode™ are fabric sensors fashioned by a knitting fabrication process [9]. The Respibelt for respiration monitoring is on a Lycra™ substrate within which the sensing element is formed by incorporating a stainless steel yarn. The Lycra™ provides compliance and the stainless steel provides the variation in electrical properties. Extending and contracting the knitting structure alters both the impedance and inductance characteristics simultaneously. The Textrode™ is used for ECG monitoring. Its transducer area is achieved by knitting stainless steel yarn into a 3 x 3 cm electrode.

Though these knitted fabric sensors provide a comfortable textile interface for wearability, they have limited capability for sensing physiological signals due to their knitted structure. Knitted fabric transducers used as ECG electrodes have high skin contact impedance due to their irregular surfaces and hence are susceptible to high frequency noise. The irregular surfaces can also generate skin irritation. To mitigate high frequency noise and skin sensitivity for stainless-steel-yarn based electrodes, a wetting gel is commonly employed. Even with a wetting gel, stainless steel knitted electrodes still possess a high input impedance that makes them susceptible to power line interference and motion artifact. Knitted stainless-steel and the carbon-loaded Lycra™ respiratory sensors express diverse hysteresis characteristics when the sensors are stretched or restored. That is, the knitted

patterns of the sensors, even when knitted into a Lycra™ belt, do not behave in a repeatable fashion, even under identical conditions.

II. NONWOVEN TEXTILE-EMBEDDED SENSORS

To achieve a comfortable textile interface as well as a high signal-to-noise ratio, several textile-embedded sensors are developed to monitor vitals signs by silk-screen printing Ag or AgCl inks onto nonwoven substrates. For ECG, EOG, and EMG monitoring, a transducer with a voltage follower circuit is embedded on nonwovens to form fabric active electrodes. For respiration monitoring, we have developed an area-variable capacitor based on multiple rectangular plates and an area-variable inductor based on open rectangular spirals using double nonwoven substrates for each. These fabric sensors could be integrated directly into normal clothes that sense multiple physiological parameters by just wearing it while allowing normal life activity like sleep, walking, sitting, running and so on.

A. Fabric Active Electrode [14]

Active electrodes consist of a transducer and, in very close proximity, a buffer amplifier to capture a biopotential signal. The buffer amplifier transforms a high impedance input into low impedance output. The active electrodes are robust against the electrically and mechanically induced noise such as 60 Hz power line interference and motion artifact, respectively. This noise immunity is exhibited even in use under the setting of dry electrodes and without traditional anti-noise methods like shielding and guarding.

As shown in Fig. 1, a nonwoven fabric substrate accommodates a transducer electrode layer on the top and a buffer circuit layer on the bottom. The circuit layer includes signal and power paths as well as electrical components. Printing is used to form the transducer area using AgCl ink and the signal and power lines using Ag ink. Prototype devices are displayed in Fig. 2. AgCl ink is desirable for the transducer because it forms a nonpolarizable electrochemical interface with the human body [15].

Adhesive conductive ink (CMI 119-05, Creative Materials Inc.) and conductive silver epoxy were used to fix the electrical components and external wires into their desired position, respectively. Electrical component and conductive lines are insulated and mechanically protected by another continuous nonconducting nonwoven textile substrate. These textile active electrodes are primarily for ECG, but are also suitable for EOG and EMG applications.

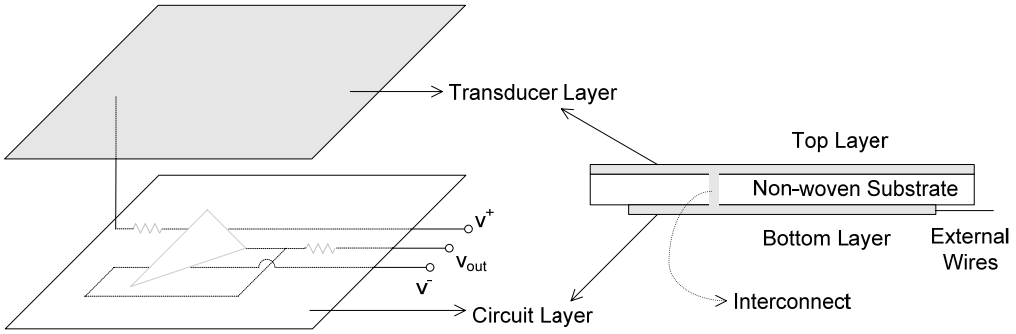

Fig. 1. Two-layered basic non-woven active electrodes on a single substrate. On the right a via is depicted to interconnect a point on the transducer layer and a point on the circuit layer. Line The crossover between the ground (v^-) line and op-amp feedback line in the circuit layer is avoided due to the pinout configuration on the op-amp circuit surface-mount package.

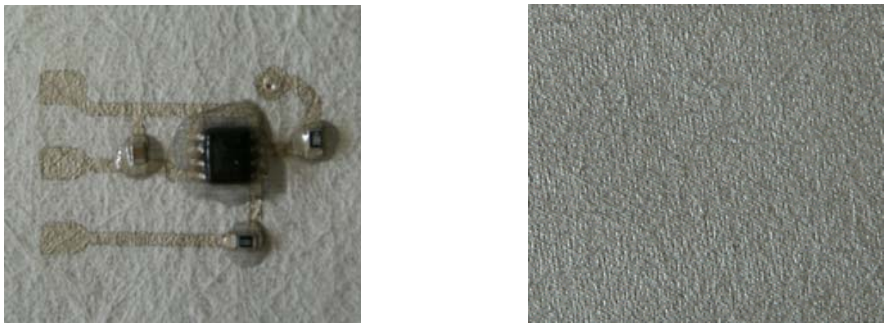

(a) (b)

Fig. 2. Screen-printed active electrodes. a) The circuit layer with signal and power paths and components attached, b) The transducer layer filled with silver ink by screen printing.

B. Double-Layered Fabric Sensor Structure [16, 17]

Fig. 3 shows a fabric sensor structure based on double substrates for respiration monitoring. Stretchable and non-stretchable segments of nonwoven fabrics are laterally attached by, for example,

ultra sonic bonding. The stretchable fabrics are employed to respond to breathing effort resulting in a changing sensor length in the horizontal direction. Rectangular plates for a capacitive sensor or open rectangular spirals for an inductive sensor are deposited on the non-stretchable fabrics by printing silver ink. Their relative positions change when the stretchable portion activates. Each plate is initially placed so that the conducting areas minimally overlap. As the stretchable portions of the device are exercised, the two plates slide in opposite directions, changing the effective area and hence the capacitance or inductance values.

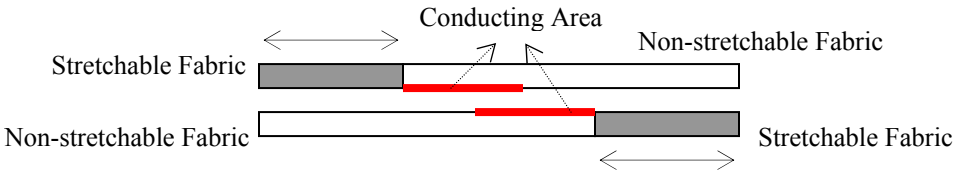

Fig. 3. Functional diagram of the textile-based displacement sensor.

For respiration monitoring, we can also utilize the variation in stretched length as well as distance between two substrates. Breathing will stretch this sensor as a function of the air volume change in the chest cavity, and compress the distance between the electrodes at the same time. By utilizing the variation in the stretched length along with the variation in the distance between the electrodes, which are both caused by breathing, we can double the variation in capacitance or inductance.

C. Capacitive Sensors [16]

To form an area-variable parallel plate capacitor, multiple rectangular plates as shown in Fig. 4 are placed on the flexible non-stretchable nonwoven substrates in the fabric sensor structure of Fig. 3. A single capacitive sensor (a) and a differential sensor (b) were designed and implemented to have linear sensing range along the horizontal sensor extension axis. The designed conductive patterns generate capacitance variance by sliding electrodes over each other along the sensor's extension axis. The sensitivity is doubled while the sensing range is halved compared to the simple rectangular plate-

based capacitive sensor. The design also allows misalignment in keeping the overlapped areas unchanged.

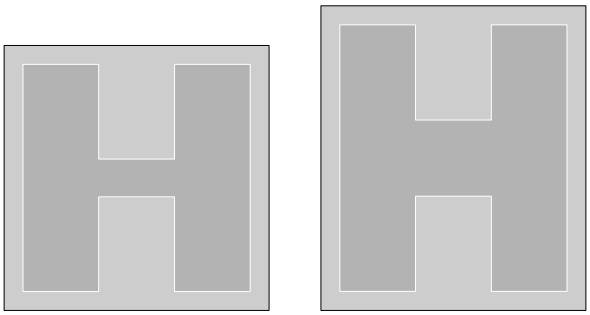

(a) Top (left) and bottom (right) electrodes in the single capacitive sensor

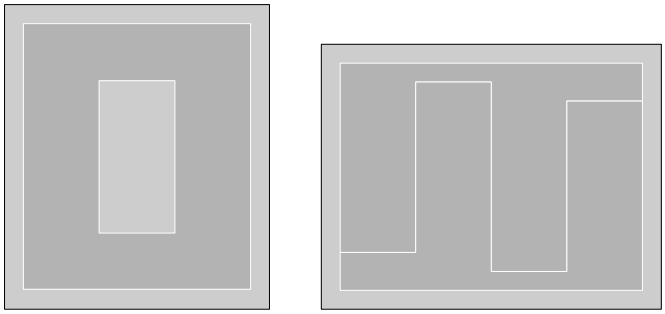

(b) The top pickup electrode (left) and two bottom electrodes (right) in the differential capacitive sensor

Fig. 4. The electrode patterns for capacitive sensors. Dark and light gray rectangles indicate electrodes and shield to minimize the back-plane effect, respectively.

D. Inductive Sensors [17]

New planar inductive displacement sensors based on the fabric sensor structure of Fig. 3 have been developed. Open-rectangular spirals are printed on the non-stretchable fabrics and connected to form area-variable-like, single or differential inductive sensors as shown in Fig. 5. We have developed a single inductive sensor (SIS), a transformer-type lateral differential inductive sensor (LDIS), and an autotransformer-type symmetric differential inductive sensor (SDIS). In the SIS of Fig 5(a), an inductor is created by having two rectangular spiral windings slide one relative to the other, thereby changing their overlapping area and generating quasi-linear mutual inductance variances. The LDIS is achieved employing three spirals, one (primary coil) of top of the other two (secondary coils) as

shown in Fig. 5(b). The overlapping areas change in equal amounts but in opposite directions (increasing and decreasing).

Finally the SDIS includes two inductors that were formed by two sets of two interleaved spirals, each set on a different substrate. This arrangement achieves simultaneously negative and positive mutual coupling between each spiral. The two inductors undergo the same overlapping area changes as the displacement takes place while keeping their layout symmetrical. In the two inductors, one inductance increases and the other inductance decreases by the same amount, while the total inductance of the sensor remains constant regardless of lateral displacement changes.

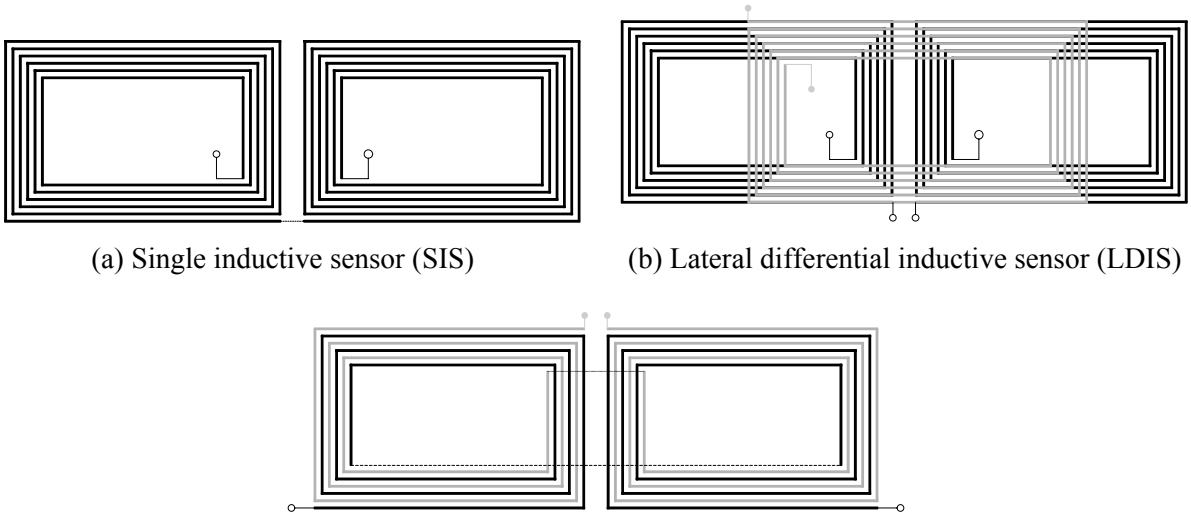

(a) Single inductive sensor (SIS)

(b) Lateral differential inductive sensor (LDIS)

(c) Symmetric differential inductive sensor

Fig. 5. Schematic diagram of open rectangular spirals and their connections.

III. A WEARABLE PHYSIOLOGICAL MONITORING SYSTEM

In this section, a wearable physiological monitoring system (WPMS) is designed with the textile-embedded sensors which can be incorporated into garments. For a wide range of applications, two main vital signs, respiration rate and heart rate, during normal daily activities are needed.

Fig. 6 illustrates a general concept for a wearable physiological data acquisition system. Bioelectrodes and respiration sensors are incorporated into the structure of the textile garment. Specific sets of fabric sensors can be selected for each specific application. The selected sensors must generate specific physiological parameters necessary to assess the wearer's health status. Wiring and/or wireless interconnections provide power and control signals as appropriate to the sensors and return information to a body-worn embedded data-gathering unit. Here the analog data are converted to digital form and are processed and stored into a local flash memory data module. The collected raw and/or processed data can be transmitted or transferred to a local information logger, such as a personal data assistant (PDA). This transfer of data can be on-line for real-time display, locally and/or remotely as dictated by the availability of appropriate computing power and automated software. Real-time local display of analyzed data may assist an expert in assessing the wearer's status. A software-implemented expert system in a PDA would also be valuable for many point-of-care or home healthcare applications. From this point, the data can be transferred back to a master database in a physician's office or a remote hospital data network for comprehensive analysis and diagnosis or validation of medical decisions made at the point-of-care. The system consists of three modules: a sensor belt, a PDA-based data acquisition system, and analysis software.

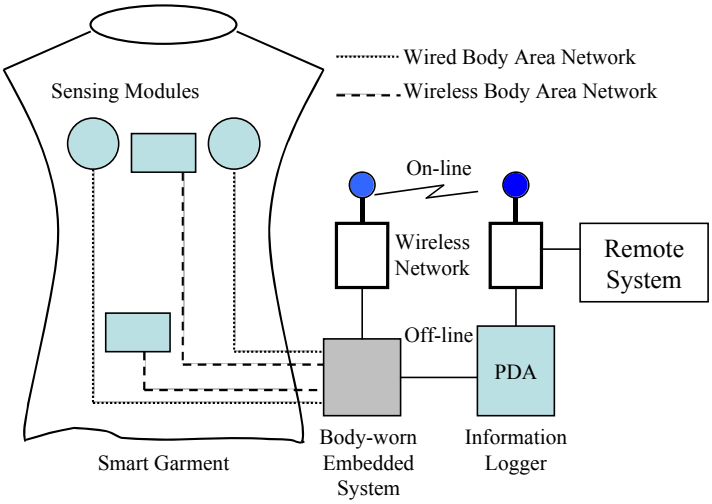

Fig. 6. Concept for a wearable physiological monitoring system.

A. Sensor Belts

A straight-forward implementation of the system in Fig. 6 can be achieved using two textile-based belts as shown in Fig. 7, one around the chest and a second around the abdomen. Three dry fabric electrodes, two active electrodes on the chest band and a single passive electrode on the abdominal band, are used for long-term ECG monitoring. Dry fabric electrodes require a special mechanical configuration to firmly contact to the subject's skin. These belts provide pressure to stabilize the position of the dry electrodes on the body.

The body-worn systems in Figs. 6 and 7 must be durable and washable. The critical components that must be protected are the electronic devices in the active electrodes of Figs. 1 and 2. For maintainability, the active electrodes can be divided into two parts: a separate removable (perhaps disposable) patch and a permanent module integrated into the garment. The removable patch and integrated permanent module can be connected using conventional textile accessories like metal snaps or conductive Velcro®. For a disposable patch, separately screen-printed plates on textiles or any commercial passive electrodes can be chosen. In heavy body movement situations, adhesive gels or glued electrodes can be selected. The permanent module includes the circuit elements of Fig. 2 with an adapter to interface the disposable patch with wires embedded into the garment. The circuit layer also can be included in the removable patch if the washability of the electronics is a concern.

In addition to ECG sensing, each belt contains a stretch sensor to measure respiration rate. The stretch sensors are implemented by placing capacitive or inductive sensors on the front-center of the belts. For better sensitivity, multiple sensors can be placed in each belt, for example on both sides. If multiple stretch sensors are employed, various combinations of the capacitive and inductive designs can be used.

The relative location of the two belts is important so the configuration of Fig. 7 includes belt loops in the garment to fix the belts' positions. This will keep the belts from shifting up or down during long-term monitoring. Since the ECG electrodes must contact the subject's skin, portions of each belt must reside on the inside of the garment (the shaded areas of Fig. 7). The unshaded areas can reside on the exterior of the garment.

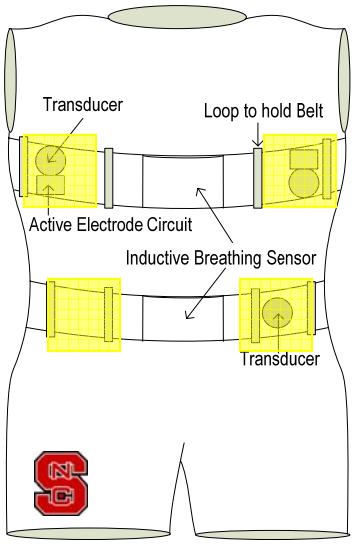

Fig. 7. Garment with two sensor belts at the level of the abdomen and the thorax.

B. Interconnects

To transport electrical commands to and physiological signals from the sensors in Fig. 7 to the body-worn embedded system of Fig. 6, wireless or wired connections must be made. However, for the deliver of electrical power to the active components in the sensors, a wired connection is highly desirable. Below we review several possible methods for implementing these connections.

Flexible textile ribbon cable [18]. Stretchable textile ribbon cables, Textro-interconnects™, are available from Textronics Inc. This technology can be attached to garments by sewing to provide signal paths and power lines. The cables can be washed. The interconnect density is six conductive lines per inch of width.

Conductive signal paths with conductive yarns. Conventional technologies such as sewing, embroidering, and knitting of conductive yarns are effective to form conductive paths on textile substrates. Various conductive yarns can be utilized from composite stainless steel threads to carbon rubber loaded yarns. In the WEALTHY system [8], knitting was used to interconnect sensors to a data-acquisition system. Knitting by the tubular intarsia technique was done using composite stainless steel yarns (30% metal) in a textile substrate sandwiched between two additional insulated textile layers.

Printed conductive lines with silver ink. Conductive lines can be achieved by printing or painting conductive inks onto textile substrates. Screen printed lines are suitable for forming foot prints for attaching surface-mount-technology (SMT) components and for implementing relatively short signal lines. As reported in [14], screen printed conductive lines of up to one cm can transport ECG signals of under 10 mv. This technology allows the printing of electrical conductors with constant geometric shape and hence reproducible electrical characteristics. However, in [14], it was noted that the screen-printed lines are could be easily damaged during flexion so a method to protect the lines, for example lamination, should be incorporated.

Wired connectors. An important challenge in producing reliable textile-based electronic systems is the problem of connecting circuit elements to embedded conducting lines. One of the early reports of success used embroidering technology [19].

Passive wireless connector. Robust methods for interconnecting signal lines between two textile substrates are also needed. For example, based on a resonant circuit [4], passive wireless connections can be used to interface a capacitive stretch sensor to the body-worn embedded system as shown in Fig. 8. The screen-printed single capacitive sensor based on the double layered fabric structure has

been designed in [16] to use this wireless connection. This same technique can be used for inductive stretch sensors of [17].

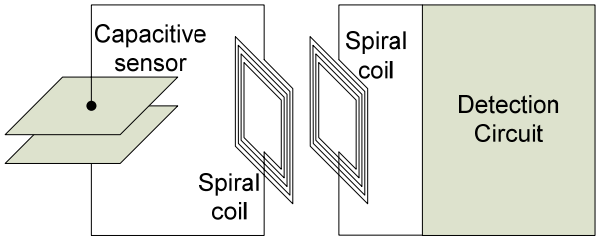

Fig. 8. Concept of passive wireless connection based on resonant circuit.

As shown in Fig. 8, the capacitor and spiral inductor form a serial LC resonant circuit (see the left side of the diagram). The detection circuit drives an excitation signal into spiral coils producing magnetic fields that induce current flow into the resonant circuit. The oscillations begin when power is supplied to the circuit. Since the inductance of the two spiral-coupling coils is fixed, variations in the capacitive sensor due to breathing change the resonant frequency. These changes in frequency can be used to determine breathing rate. A detection circuit for Fig. 8 can be made using a Colpitts oscillator.

C. Data Acquisition System

To collect various data on-site in real-time from body-worn sensors, a battery-powered portable data acquisition system is required. The data-acquisition system as shown in Fig. 6 includes a body-worn embedded device and a PDA. In our prototype system, we used a Palm Pilot® (model M505). The body-worn embedded device consists of an analog conditioning circuit for each sensor, digital circuit for A/D conversion (ADC) and data communications, and a power unit. An analog circuit interfaces directly with each body-worn sensor to monitor desired physiological signals and provides oscillating signals for modulating sensors. In the digital circuit, a micro controller (Atmel® ATmeg128L)

converts the analog physiological signals into digital form, stores the data to a local storage unit, and communicates with the Palm Pilot®. The Atmel® controller has extensive on-chip peripheral functions such as an ADC, a timer, a digital to analog converter (DAC), serial ports, and input-output (IO) ports. A 16 MB local flash-memory storage module (Atmel® AT45DB161B) was employed to temporarily record the data files. A serial IO port in the Atmel® processor was used to communicate with the flash memory module. To move the data from data flash memory, a Palm Pilot® or other computing machine can command the unit to download physiological data to other storage devices. This body-worn embedded system can be controlled externally by the PalmPilot® as well as operate in stand-alone-mode.

The Palm Pilot® M505 controlling the unit includes an expansion memory slot to accommodate MMC or Secure Digital (SD) flash memory cards. The sensed data in the body-worn device can be sent to the Palm Pilot® for display and storage. The user can verify the proper operation of the data acquisition system through real-time display of captured data. The Palm Pilot selects the place to store the data: body-worn embedded system, Palm Pilot®, or both. The device can display while saving the data into MMC storage. Fig. 9 gives and example of an ECG being displayed during data capture and transfer to permanent storage on a MMC.

Fig. 9. Palm Pilot® displaying ECG signals in real-time.

D. Analysis Software

ECG and respiration signals can be analyzed to obtain vital signs. For example, respiration and heart rates are the underlying bases for the analysis of sleep disorders, exercise stress, and subject activity. For vital signs extraction, the analysis software includes two modules, one for the detection of the QRS complex in the ECG waveform and the other for the detection of transition from expiration to inspiration, and vice versa. Only the first module for QRS complex detection is discussed in this paper. From QRS complexes, the R-R interval gives instantaneous heart rate and, over time, or heart-rate variability (HRV). This module uses algorithms that are based on the shape of the QRS complex. For long-term wearable heart-monitoring systems, the detection algorithms adapt to variations in the amplitude of the ECG signals due to changes in skin contact impedance and geometrical variation of transducer location caused by body movement and body posture. The algorithm for detecting the QRS complex needs to be fast enough to analyze long segments ECG signals, from hours to days. Real-time algorithms in the body-worn embedded system and/or portable PDA may provide information of physiological status and provide alerts for unusual conditions.

IV. DETECTION OF QRS COMPLEXES

In this section, we present a method for detecting QRS complexes that employs a decision stage with an adjustable threshold against feature parameters. For feature signals, the sampled ECG signal is band-pass filtered and then subjected to a non-linear energy operator (NLEO. A simple method to determine parameter thresholds is suggested to speed up and reduce computational complexity. The simplified method was tested using ECG signals from the MIT-BIH Arrhythmia Database [20].

A. Preprocessing and Feature Extraction

To suppress the P- and T-waves and to remove noise such as 60 Hz interference and baseline drift, we used a zero-phase 6th-order Butterworth band-pass filter with cutoff frequencies of 10 and 25 Hz. For feature extraction, a NLEO (Ψ) was applied to the filtered input signal $x(n)$ as follows [21, 22]:

$$E(n) = \Psi[x(n)] = x^2(n) - x(n-1)x(n+1) \quad (1)$$

where $E(n)$ represents feature being extracted at time instance n. Since the NLEO generates the frequency-weighted energy of the signal, it is appropriate to highlight the spike-like QRS complex [22]. In addition, the NLEO is computationally simple and temporally localizable.

B. The Adaptive Threshold Algorithm

A QRS complex is generally identified by comparing feature signals against a threshold function in the decision stage [23]. For better performance, we suggest that the threshold needs to be adjusted as the NLEO of the filtered ECG signal changes over long-term interval as well as beat-to-beat time interval, thus creating an adaptive threshold. For simplicity we explain only an off-line algorithm. At the beginning, the threshold at every sampling instance is initialized to zero. In the forward direction, if the NLEO output at the n-th time instance $\Psi(n)$, the feature value, is equal or larger than the current threshold at the n-th time instance $Th(n)$, and $\Psi(n)$ is equal or greater than $\Psi(n+1)$, then change the surrounding thresholds as follows:

$$\begin{cases} Th(p) = \Psi(n) \times h_1 & \text{if } Th(p) < \Psi(n) \times h_1 \quad \text{where } p = n, \ldots, n + w_1/2 \\ Th(q) = \Psi(n) \times h_2 & \text{if } Th(q) < \Psi(n) \times h_2 \quad \text{where } q = n + w_1/2 + 1, \ldots, n + w_2/2 \\ Th(r) = \Psi(n) \times h_3 & \text{if } Th(r) < \Psi(n) \times h_3 \quad \text{where } r = n + w_2/2 + 1, \ldots, n + w_3/2 \end{cases} \quad (2)$$

where w_1, w_2, and w_3 is a number of sampling sequence and h_1, h_2, and h_3 indicate the ratio to the feature parameters where these values form a three-step function as shown in Fig. 10. These parameters are determined such that when they combine with true R-peaks, the resulting thresholds suppress the other non-QRS waves and noise while do not affect to detect the two neighbor QRS peaks. For example, by setting h_1=1, thresholds are automatically set to be equal to the feature parameters where QRS complexes are expected.

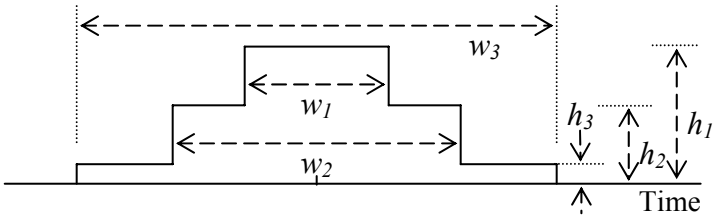

Fig. 10. The three-stepwise function.

Similar procedures are repeated in the reverse direction. If the NLEO output at the n-th time instance $\Psi(n)$ is equal or larger than the current threshold at the n-th time instance $Th(n)$, and $\Psi(n)$ is equal or greater than Ψ(n-1), then change the current threshold as follows:

$$\begin{cases} Th(p) = \Psi(n) \times h_1 & \text{if } Th(p) < \Psi(n) \times h_1 \quad \text{where } p = n - w_1/2, ..., n \\ Th(q) = \Psi(n) \times h_2 & \text{if } Th(q) < \Psi(n) \times h_2 \quad \text{where } q = n - w_2/2, ..., n - w_1/2 - 1 \\ Th(r) = \Psi(n) \times h_3 & \text{if } Th(r) < \Psi(n) \times h_3 \quad \text{where } r = n - w_3/2, ..., n - w_2/2 - 1 \end{cases} \tag{3}$$

Finally, if the threshold is still zero or less than a preset minimum threshold $Th_{\min}$, then change the surrounding thresholds as follows:

$$Th(n) = \max\left[Th_{\min}, \frac{\max\{\Psi(n - 1.5w_3 : n + 1.5w_3)\}}{K} \right] \tag{4}$$

In this method, a feature signal that has local peak only contributes to the determination of the surrounding thresholds within at least $2w_1$ or at most $2w_3$ intervals while the resulting thresholds due to the R-peak suppress the other non-QRS complexes and noise. Feature signals at the n-th time instance do not affect to determine thresholds at other positions if they are less than the current threshold at that point in time. Thereby the thresholds rise as feature parameters of QRS complexes go up to suppress other non-QRS beats or noise, and the thresholds fall down as the feature parameters go down to detect true beats whose feature parameters are comparatively low than that of normal QRS complex.

C. Detection of QRS Complexes

The threshold function determined by the proposed method has to be equal to the magnitude of the feature signal where an R-peak is expected. Thus, we detect QRS complexes where thresholds are

equal to the magnitude of the feature signal. However, a detected QRS complex may be displaced slightly due to application of the band-pass filter and the frequency-weighted feature extractor like the NLEO. The locations of those QRS complexes are adjusted with the gradient decent method except for QRS complexes detected close to the downward peaks.

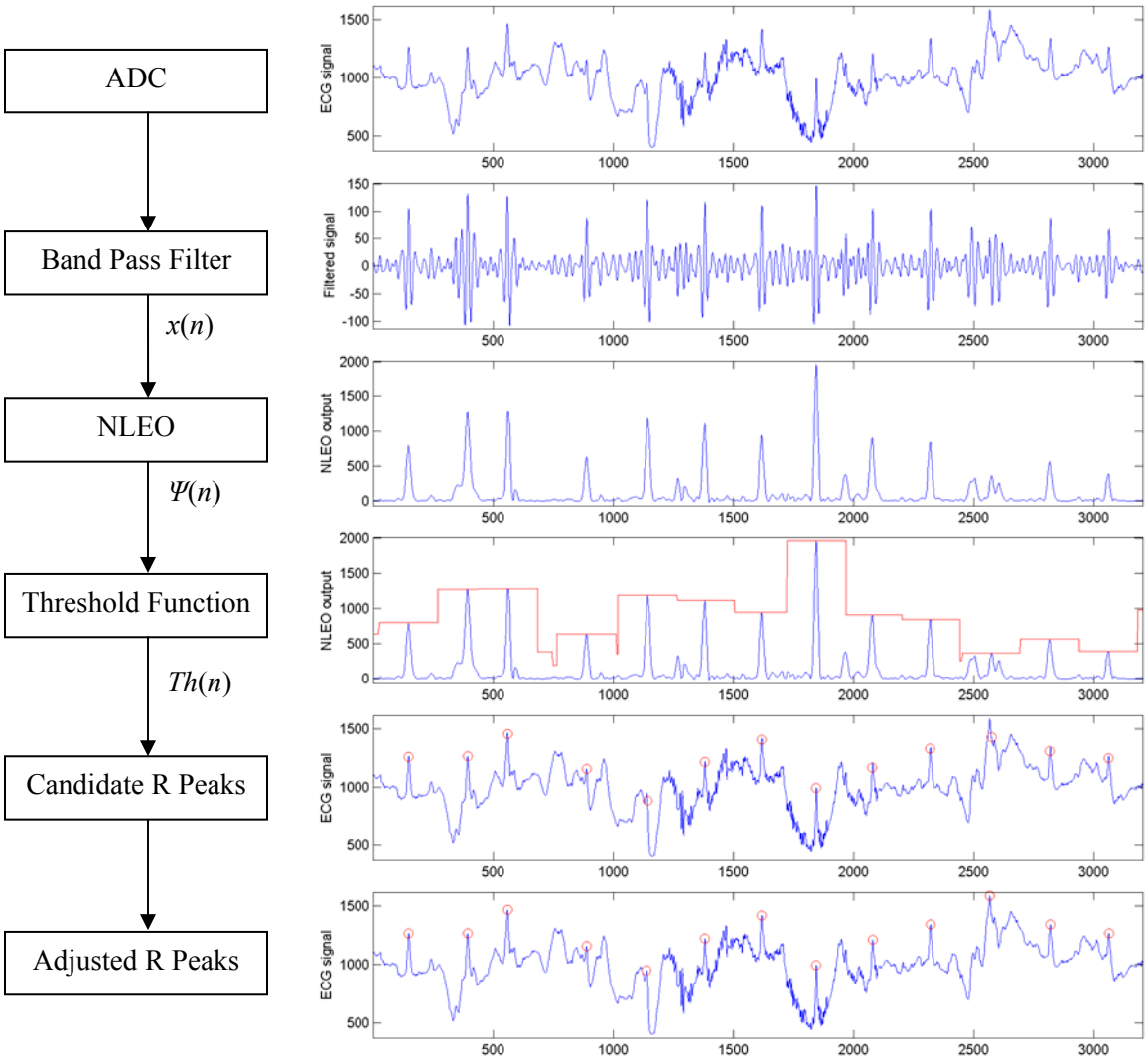

Fig. 11. Demonstration of the QRS detection algorithm. The left flow chart shows steps to detect QRS complexes and the right images displays results of the steps. ECG signals are partly excerpted from the record 105 of MIT-BIH Arrhythmia database [20].

Fig. 11 shows QRS complex detected with adaptable thresholds on the NLEO output signal. For detection of QRS complex, w_1=123, w_2=185, w_3=247, h_1=1, h_2=0.3, and h_3=0.1429 were used as the parameters of the three-step function in Fig. 10.

By trial and error, the parameters for a three-step function are selected as follows. Within the interval w_1, the extractor blocks detect other QRS complexes. That is, the width w_1 should be limited to detect an abnormal ECG complex within the period so the width w_1 is set as two times the minimum *R-R* interval expected in the given signal. The height h_2 can be determined to suppress other waves and noise while allowing the detection of abnormal QRS complexes in time and/or in shape within w_2 periods. The width w_3 is a constraint that limits the influence of the current peak in determining the threshold related to upcoming QRS complexes; a current peak contributes to the threshold of the next two upcoming peaks only. Since some QRS complexes may be missed by the algorithm, two times the mean of the R-R intervals is preferred as the w_3 value. The height h_3 should allow detecting QRS peaks that generate comparatively small feature parameters due to variation in signal shape and level. In general, QRS complexes are expected to be regular in time and to surpass the noise level.

V. A WEARABLE SLEEP MONITORING SYSTEM

Sleep, a basic necessity of life, can be fragmented and of poor quality in patients with sleep disorders like sleep apnea, heavy snoring and narcolepsy [24]. Sleep apnea, a common disorder among adults, is characterized by brief interruptions of breathing during sleep. If no air flows in or out for at least ten seconds, then the interruption is called an apnea. There are three categories of apnea: obstructive, central, and mixed. An obstructive apnea is induced by the local obstruction or structural deformation of the upper airways. If the throat collapses when the sleeper tries to breathe, no air movement occurs. A central apnea is caused by abnormalities of the central motoneural system. In these cases, the sleeper's brain does not signal the muscles to create a breath. There is no physical blockage of the throat and no attempt to breathe. Sometimes a physical blockage does in fact occur when a central

apnea episode ends and the patient tries to breathe again, compounding the problem. These compound cases are classified as mixed apnea. When airflow falls markedly but does not stop completely, the conditions of apnea are not met. These reduced airflow cases are called hypopnea.

Each apnea episode causes a fall in blood oxygen level, which is followed by increased sympathetic nervous activity, producing increased heart rate and blood pressure and finally inducing micro-awakens (arousals). The patient with untreated sleep apnea, especially obstructive apnea, may repeatedly wake up enough to activate the muscles of the upper airway and remove the obstruction. Even though it is not a total wakening, or the awakening is too short to be remembered, sleep can be of poor quality. Sleep quality is an important factor in performance of the professional workforce around the world. The pressures one encounters in daily life can adversely affect one's ability to get a good night's sleep.

Two categories of sleep have been defined: rapid eye movement (REM) and non-rapid eye movement (NREM) [24]. They are as distinct from one another as each is from wakefulness. NREM sleep consists of four stages, number simply as 1, 2, 3, and 4, each of which parallels a depth of sleep continuum. Stage 1 is associated with a low arousal threshold while stage 4 has a high one. Therefore, sleep in stage 1, which acts as an initial transition from wakefulness to sleep, is more vulnerable to disruptions than the others. Sleep stages have been related to a variety changes in the autonomic nervous system. REM sleep has been associated with increased sympathetic activity, and non-REM sleep with a predominance of parasympathetic [25].

Sleep disorders and sleep staging are frequently diagnosed by performing an overnight polysomnogram in a sleep facility at a clinic or hospital. These sleep tests are quite expensive, but comprehensive. One drawback is that a sleep lab cannot replicate the normal environment in which a subject sleeps. Hence, an in-home preliminary sleep assessment could help identify undiagnosed

sleep disorders at a fraction of the cost of over-night hospital and clinic polysomnograms. To evaluate a patient's sleep quality outside a clinic or hospital, reliable and unobtrusive technologies must be found to incorporate sensors and sensing systems into the everyday lives of those being tested. The wearable health monitoring system presented in the previous section provides a possible mechanism to detect sleep disorders, especially sleep apnea and hypopnea. Those sleep disorders may be identified by respiratory signals [26-29] or by heart rate variability or R-R intervals through ECG signals [30].

A. Detection of Sleep Apnea Based on Respiratory Signal

The process for detecting sleep apnea from sensor data may be segmented into three stages: preprocessing, feature extraction and pattern classification. Several studies have documented automated sleep apnea detection and classification methods employing a respiratory signal [26-29]. Most of these studies used an adaptive or non-adaptive process in the preprocessing stage to remove the base line drift [26, 29, 31]. To eliminate unwanted variations of the respiratory signal due to artifacts and noise, several techniques were employed to extract useful features from the raw respiratory signal [26-29, 31]. Piecewise linear approximation (PLA) was used to filter out minor fluctuations and noise from the respiration signals and to locate local extremes [27, 28]. Deterministic templates may also be employed in feature selection to filter out minor fluctuations and noise. Three templates, matched to signal waveforms for normal breathing, hypopnea and apnea, were generated using the Haar wavelet transform [26]. The Haar wavelet coefficients were used as the extracted signal features. Yet a different method has been employed in [29]. There, parameters for instantaneous respiration amplitude (IRA) and instantaneous respiration interval (IRI) were calculated from the incoming preprocessed sensor data.

The extracted features described above are then used for pattern classification. Several kinds of classifiers have been employed to detect sleep apnea. The Haar wavelet coefficients of the input

signal were compared in [26] with the reference signal of each template pattern of normal breathing, hpopnea, and apnea by a χ^2-like test. It can be expected that only the template-like patterns in the signal under test respond well. For the best performance, it is important to select template signals that are as representative as possible of the class being sought. A multi-layer neural network was used in [29] to detect sleep apnea and hypopnea. Four different neural networks were compared to test the efficiency of different inputs and networks for apnea detection. The authors showed that a neural network with IRA and IRI as inputs had better performance than the network utilizing the normalized original respiratory signal. That means the derived information like IRA and IRI absorb the variations of breathing and eliminate unwanted signal spikes including noise.

Reference [31] reports another artificial neural network algorithm to detect the onset of expiration and inspiration. A neural network using normalized breathing signals was used to locate the onset of expiration, and another for inspiration, in the presence of baseline drift, noise, artifacts and body movement. After post processing with heuristic information, the onset of each respiration was located with a degree of precision comparable to that of human experts.

The above classification methods require extensive signal preprocessing (signal normalization, re-sampling, fixed data processing interval) and prior information such as templates. In addition, some of the methods lack signal localizability, require prior training, and are computationally complex. Hence these algorithms are not appropriate to embed into a portable system for real-time detection of breathing and sleep apnea for clinical point of care or home use. On-line detection of breathing and sleep apnea is very important for real-time diagnosis and treatment. By detecting the sleep apnea syndrome on the fly, the system can initiate medical treatments such as Continuous Positive Airway Pressure (CPAP) after the onset of apnea episodes. In addition, real-time technology reduces the burden of mass storage to archive physiological data for post-processing in the laboratory while providing accessibility to diagnosis results on the spot.

B. Sleep Staging and Apnea Detection Based on Heart-Rate Variability

Traditionally, sleep staging has been performed by technicians using electroencephalogram (EEG), electromyogram (EMG), and electrooculogram (EOG) monitors. These signal possess different characteristics in each sleep stage [24]. REM sleep is commonly identified with muscle atonia, *i.e.*, suppression of EMG activity and episodic bursts of rapid eye movement in the EOG. In REM sleep, EEG signals have relatively low amplitudes and are of mixed frequency. Usually each stage in NREM sleep is identified by characteristic waveforms such as sleep spindles, K complexes, and high amplitude slow waves in the EEG. Eye movements do not occur in stage 3 and 4 sleep. Several methods been reported in the literature for extracting features such as the k-complex [32] and for sleep staging [33]. For sleep staging based on EEG, EMG, and EOG monitoring, multiple electrodes on the head are used. These are placed by technicians and are connected by wiring cables to data acquisition units located at the bedside. Thus, this method sleep staging can not be used for the wearable monitoring system we designed until a wearable sensorized cap that includes all electrodes for EEG, EMG and EOG is available.

On other hand, it was known that variations in heart rate due to changes in autonomic function are correlated with sleep state [25]. Through spectral and time domain analysis of heart period variability from healthy men, the authors showed that average heart rate decrease during sleep compared to resting wakefulness and beat-to-beat variations increase in stage 2 and REM sleep. Power spectra for each 128-beat epoch were divided into 4 classes; low frequency band (0.0 - 0.04 Hz), medium frequency band (0.04 – 0.12 Hz), high frequency band (0.2 – 0.4 Hz), and very high frequency band (0.4 – 0.5 Hz). These parameters are affected by sympathetic and parasympathetic activities. They revealed that 1) REM sleep and wakefulness demonstrate most power in the frequency band of 0.0 - 0.04 Hz, 2) significant differences of power in the medium frequency band (0.04 – 0.12 Hz) and high frequency band (0.2 – 0.4 Hz) were seen across sleep stages, and 3) in most cases, very high frequency variability (0.4 – 0.5) is low in all stages of sleep.

In [34], sleep staging in subjects with obstructive sleep apnea was performed based on three types fo signals: 1) R-R intervals from the ECG, 2) demodulated respiration signals from the ECG, and 3) respiratory effort signals from inductive sensors mounted on the on the ribcage. The authors classified into three categories (wakefulness, REM sleep, and NREM sleep) with moderate accuracy (67% - 79%). In [35], heart-rate variability was used for staging sleep and for sleep apnea detection, using "detrended fluctuation analysis" and spectral analysis for each. They classified sleep into four categories: light sleep (stage 1 and 2), deep sleep (stage 3 and 4), REM sleep, and wakefulness.

Sleep apnea also influences the autonomic nervous system and can cause heart-rate changes. In [30], the changes in R-R intervals during sleep were compared in healthy control and patients with obstructive sleep apnea (OSA). Spectral analysis showed that the R-R interval was apparently shortened in patients with moderate-to-severe obstructive sleep apnea than in the normal subjects. The variance of the R-R intervals was reduced significantly in both patients with mild OSA and patients with moderate-to-severe OSA.

VI. CONCLUSIONS

A wearable physiological monitoring system introduces many benefits for health care and fitness applications. For these systems, various technologies are available to implement sensors, interconnects, electronic circuits, and software for analyzing physiological signals. In this work, textile-embedded biomedical sensors for ECG and respiration monitoring were introduced. We designed a sensor belt on which these sensors can be directly integrated. We described a prototype data acquisition unit that can serve as a body-worn device. Any hand-held computing device, such as a Palm Pilot®, can directly link to the body-worn unit though off-line or on-line connections. For connecting sensors to the body-worn device, we described interconnect. A simple QRS detection algorithm was presented to analyze ECG signals, especially R-R intervals and heart rate variability. For an application of the system, we survey sleep apnea and sleep staging system that requires long-

term, unobtrusive wearable monitoring system. The results described in this work suggest that textile-based electronic systems show great promise for health monitoring applications such a sleep apnea detection and treatment.

REFERENCES

[1] S. Park and S. Jayaraman, "Enhancing the quality of life through wearable technology," *Engineering in Medicine and Biology Magazine, IEEE*, vol. 22, pp. 41-48, 2003.

[2] I. Korhonen, J. Parkka, and M. Van Gils, "Health monitoring in the home of the future," *Engineering in Medicine and Biology Magazine, IEEE*, vol. 22, pp. 66-73, 2003.

[3] H. H. Asada, P. Shaltis, A. Reisner, S. Rhee, and R. C. Hutchinson, "Mobile monitoring with wearable photoplethysmographic biosensors," *Engineering in Medicine and Biology Magazine, IEEE*, vol. 22, pp. 28-40, 2003.

[4] K. J. Cho and H. H. Asada, "Wireless, battery-less stethoscope for wearable health monitoring," presented at Bioengineering Conference, 2002. Proceedings of the IEEE 28th Annual Northeast, 2002.

[5] F. Axisa, P. M. Schmitt, C. Gehin, G. Delhomme, E. McAdams, and A. Dittmar, "Flexible technologies and smart clothing for citizen medicine, home healthcare, and disease prevention," *Information Technology in Biomedicine, IEEE Transactions on*, vol. 9, pp. 325-336, 2005.

[6] N. Taccini, G. Loriga, A. Dittmar, and R. Paradiso, "Knitted includes for health monitoring," presented at Engineering in Medicine and Biology Society, 2004. EMBC 2004. Conference Proceedings. 26th Annual International Conference of the, 2004.

[7] E. P. Scilingo, A. Gemignani, R. Paradiso, N. Taccini, B. Ghelarducci, and D. De Rossi, "Performance evaluation of sensing fabrics for monitoring physiological and biomechanical variables," *Information Technology in Biomedicine, IEEE Transactions on*, vol. 9, pp. 345-352, 2005.

[8] R. Paradiso, G. Loriga, and N. Taccini, "A wearable health care system based on knitted integrated sensors," *Information Technology in Biomedicine, IEEE Transactions on*, vol. 9, pp. 337-344, 2005.

[9] M. Catrysse, R. Puers, C. Hertleer, L. Van Langenhove, H. van Egmond, and D. Matthys, "Towards the integration of textile sensors in a wireless monitoring suit," *Sensors and Actuators A: Physical*, vol. 114, pp. 302-311, 2004.

[10] F. Carpi and D. De Rossi, "Electroactive polymer-based devices for e-textiles in biomedicine," *Information Technology in Biomedicine, IEEE Transactions on*, vol. 9, pp. 295-318, 2005.

[11] M. Coyle, "Ambulatory cardiopulmonary data capture," presented at Microtechnologies in Medicine & Biology 2nd Annual International IEEE-EMB Special Topic Conference on, 2002.

[12] D. Marculescu, R. Marculescu, Zamora, Stanley-Marbell, K. Park, J. Jung, L. Weber, K. Cottet, Grzyb, Troster, Jones, Martin, and Nakad, "Electronic textiles: a platform for pervasive computing," *Proceedings of the IEEE*, vol. 91, pp. 1993-1994, 2003.

[13] E. Jovanov, A. O'Donnell Lords, D. Raskovic, P. G. Cox, R. Adhami, and F. Andrasik, "Stress monitoring using a distributed wireless intelligent sensor system," *Engineering in Medicine and Biology Magazine, IEEE*, vol. 22, pp. 49-55, 2003.

[14] T.-H. Kang, "Chapter 2. NONWOVEN FABRIC ACTIVE ELECTRODES FOR BIOPOTENTIAL MEASUREMENT DURING NORMAL DAILY ACTIVITY," in *this thesis*.
[15] M. R. Neuman, "5. BIOPOTENTIAL ELECTRODES," in *Medical Instrumentation: Application and Design*, J. G. Webster, Ed., Third ed: John Wiley & Sons, Inc., 1997.
[16] T.-H. Kang, "Chapter 3. CAPACITIVE NONWOVEN FABRIC SENSORS FOR RESPIRATION MONITORING," in *this thesis*.
[17] T.-H. Kang, "Chapter 5. PLANAR INDUCTIVE DISPLACEMENT SENSORS BASED ON SPIRALS AND DOUBLE-SUBSTRATE DESIGNS," in *this thesis*.
[18] Textronics™ Inc. [Online]. Available: http://www.textronicsinc.com/.
[19] E. R. Post, M. Orth, P. R. Russo, and N. Gershenfeld, "E-broidery: Design and fabrication of textile-based computing," *IBM Systems Journal*, vol. 39, pp. 840 - 860, 2000.
[20] G. B. Moody, R. G. Mark, and A. L. Goldberger, "PhysioNet: a Web-based resource for the study of physiologic signals," *Engineering in Medicine and Biology Magazine, IEEE*, vol. 20, pp. 70-75, 2001.
[21] J. F. Kaiser, "On a simple algorithm to calculate the `energy' of a signal," presented at Acoustics, Speech, and Signal Processing, 1990. ICASSP-90., 1990 International Conference on, 1990.
[22] S. Mukhopadhyay and G. C. Ray, "A new interpretation of nonlinear energy operator and its efficacy in spike detection," *Biomedical Engineering, IEEE Transactions on*, vol. 45, pp. 180-187, 1998.
[23] B.-U. Kohler, C. Hennig, and R. Orglmeister, "The principles of software QRS detection," *Engineering in Medicine and Biology Magazine, IEEE*, vol. 21, pp. 42-57, 2002.
[24] M. H. Kryger, T. Roth, and W. C. Dement, *Principles and practices of Sleep Medicine*, Third ed. Philadelphia, PA: WB Saunders, 2000.
[25] B. V. Vaughn, S. R. Quint, J. A. Messenheimer, and K. R. Robertson, "Heart period variability in sleep," *Electroencephalography and Clinical Neurophysiology*, vol. 94, pp. 155-162, 1995.
[26] M. Kermit, g. J. Eide, T. Linblad, and K. Waldemark, "Treatment of obstructive sleep apnea syndrome by monitoring patients airflow signals," *Pattern Recognition Letter*, vol. 21, pp. 277-281, 2000.
[27] P. Varady and S. Bongar, "Detection of airway obstruction and sleep apnea by analyzing the phase relation of respiration movement signals," presented at Instrumentation and Measurement Technology Conference, 2001. IMTC 2001. Proceedings of the 18th IEEE, 2001.
[28] P. Varady, S. Bongar, and Z. Benyo, "Detection of airway obstructions and sleep apnea by analyzing the phase relation of respiration movement signals," *Instrumentation and Measurement, IEEE Transactions on*, vol. 52, pp. 2-6, 2003.
[29] P. Varady, T. Micsik, S. Benedek, and Z. Benyo, "A novel method for the detection of apnea and hypopnea events in respiration signals," *Biomedical Engineering, IEEE Transactions on*, vol. 49, pp. 936-942, 2002.
[30] K. Narkiewicz, N. Montano, C. Cogliati, P. J. H. van de Borne, M. E. Dyken, and V. K. Somers, "Altered Cardiovascular Variability in Obstructive Sleep Apnea," *Circulation*, vol. 98, pp. 1071-1077, 1998.
[31] R. C. Sa and Y. Verbandt, "Automated breath detection on long-duration signals using feedforward backpropagation artificial neural networks," *Biomedical Engineering, IEEE Transactions on*, vol. 49, pp. 1130-1141, 2002.
[32] T. Shimada, T. Shiina, and Y. Saito, "Detection of characteristic waves of sleep EEG by neural network analysis," *Biomedical Engineering, IEEE Transactions on*, vol. 47, pp. 369-379, 2000.

[33] R. Agarwal and J. Gotman, "Computer-assisted sleep staging," *Biomedical Engineering, IEEE Transactions on*, vol. 48, pp. 1412-1423, 2001.

[34] S. J. Redmond and C. Heneghan, "Cardiorespiratory-based sleep staging in subjects with obstructive sleep apnea," *Biomedical Engineering, IEEE Transactions on*, vol. 53, pp. 485-496, 2006.

[35] T. Penzel, J. W. Kantelhardt, L. Grote, J. H. Peter, and A. Bunde, "Comparison of detrended fluctuation analysis and spectral analysis for heart rate variability in sleep and sleep apnea," *Biomedical Engineering, IEEE Transactions on*, vol. 50, pp. 1143-1151, 2003.

Chapter 7

CONCLUSIONS AND FUTURE STUDY

I. CONTRIBUTIONS

In the dissertation, textile-embedded biomedical sensors that provide both a comfortable textile interface and robustness against noise and motion artifacts were developed. These sensors are intended to be unobtrusively integrated into an article of clothing for a long-term, reliable, wearable physiological monitoring system. These sensors include fabric active electrodes and fabric respiratory sensors for ECG and respiration monitoring, respectively.

For ECG monitoring, active electrodes that capture biopotential while changing high input impedance signals into low impedance ones were implemented by printing silver ink on nonwoven textiles for signal paths, power lines, and transducers. Nonwovens are employed as a flexible substrate for electric circuit conductors and components. Test results showed that the nonwoven textile active electrodes have robustness against 50/60 Hz hum and body motion artifact even under the operational setting of dry electrodes.

For respiration monitoring, we developed new fabric sensor structures to utilize capacitive and inductive coupling. The sensor structures use double substrates. Each substrate consists of stretchable and non-stretchable segments of nonwoven fabrics, which are laterally attached by, for example, ultra sonic bonding. The concept of the structure can be extended for other new sensor structures; for example, triple substrates may be used. The sensor structures provide a valuable textile platform for various area-variable capacitive and inductive sensors.

New electrode designs for area-variable capacitive sensor were suggested for both single and differential modes of operation. The sensor utilizes vertical pressure on the planar surface and lateral

in-plane strain to maximize capacitance variance. The electrode designs allow misalignment of two electrodes in the orthogonal direction of an applied strain without changing capacitance values.

Fabric inductive displacement sensors were also developed. Three kinds of inductive sensors based on quasi area-variable inductance were presented; a single inductor sensor (SIS), a lateral differential inductive sensor (LDIS), and a symmetric differential inductive sensor (LDIS). The LDIS and the SDIS are transformer- and autotransformer-type differential sensors, respectively. The SDIS includes two inductors that keep their layout fully symmetrical during use. One inductor increases and the other decreases by the same amount while the total inductance of the sensor remains constant, regardless of lateral displacement changes.

In addition to the design based on double substrates, we demonstrate a respiratory inductive sensor based on a single substrate. This sensor is an improvement over traditional designs because it avoids using textile folds or wrinkles to accommodate sensor extension. To form an inductive sensing area, fine magnet wires were stitched on a stretchable nonwoven substrate. The textile substrates supporting the conducting materials were then laminated to stabilize the geometric structure relationships and mechanically protect the sensor.

Finally, we transformed these textile-embedded sensors into a wearable human physiology monitoring system. The various elements of the system were described. Then we discussed the possibility as an application of the system in sleep apnea detection and sleep staging.

II. RECOMMANDATIONS FOR FUTURE RESEARCH

In the dissertation, a basic active electrode circuit (voltage follower) was employed to demonstrate the fabric active electrodes. These fabric active electrodes show robustness against motion artifact. For better performance, we need to adopt an amplifier gain stage in the fabric active electrode system.

For the amplifier gain, a scheme to remove DC offset is required. In addition, since the basic fabric active electrodes are not washable, the electrode sensors may malfunction due to sweat and other water sources. Therefore, further research to protect the screen-printed lines and components is needed.

The fabric capacitive sensors presented herein may not generate enough capacitance and variance to suppress stray capacitance or outside interference in severe environments. Electric field sensors that measure electric potential by capacitive coupling may void this problem. The fabric sensor structure based on double textile substrates can be used for electric field sensors.

For the inductive respiratory sensors based on double substrates, we demonstrated proof of the concept using fine magnet wires. For incorporating the sensors on textile in a manufacturing environment, screen-printing technology should be investigated as a method to enhance flexibility and washability. However, screen printing technology may dramatically reduce the inductance due to geometric limitations of screen printed lines on rough textile substrates. That is, the line width and spacing of the open rectangular spirals must be greater than a specific limit to avoid broken lines or shorts between neighboring lines. Increasing the line widths and spacing degrades the inductance as well as the linear sensing range. To improve these parameters, multi-layered designs and careful use of screen printing technology is required.

For the respiratory inductive sensors based on a single substrate, sewing technology with conductive yarns such as composite stainless steel yarns as well as screen-printing technology may be an appropriate manufacturing method. Using sewing and screen printing to produce sensing elements ensures that the electrical properties of the sensors will be uniform, and that they can be produced cost-effectively and in volume.

Besides the fabric active electrodes and the inductive and capacitive respiratory sensors, we need to develop other types of sensors based on textile substrates and screen printing technology. For example, unobtrusive fabric body temperature sensors are required to be implemented for a fully developed wearable physiological monitoring system.